PERMANENT MAGNET ASSISTED SYNCHRONOUS RELUCTANCE MOTOR DESIGN AND PERFORMANCE IMPROVEMENT

A Dissertation

by

PEYMAN NIAZI

Submitted to the Office of Graduate Studies of
Texas A&M University
in partial fulfillment of the requirements for the degree of

DOCTOR OF PHILOSOPHY

December 2005

Major Subject: Electrical Engineering

PERMANENT MAGNET ASSISTED SYNCHRONOUS RELUCTANCE MOTOR DESIGN AND PERFORMANCE IMPROVEMENT

A Dissertation

by

PEYMAN NIAZI

Submitted to the Office of Graduate Studies of
Texas A&M University
in partial fulfillment of the requirements for the degree of

DOCTOR OF PHILOSOPHY

Approved by:

Chair of Committee,	Hamid A. Toliyat
Committee Members,	Prasad Enjeti
	Shankar. P. Bhattacharyya
	Reza Langari
Head of Department,	Costas Georghiades

December 2005

Major Subject: Electrical Engineering

ABSTRACT

Permanent Magnet Assisted Synchronous Reluctance Motor

Design and Performance Improvement. (December 2005)

Peyman Niazi, B.S., Isfahan University of Technology (IUT), Isfahan, Iran;

M.S., Khaje Nassir Toosi University of Technology, Tehran, Iran

Chair of Advisory Committee: Dr. Hamid A. Toliyat

Recently, permanent magnet assisted (PMa)-synchronous reluctance motors (SynRM) have been considered as a possible alternative motor drive for high performance applications. In order to have an efficient motor drive, performing of three steps in design of the overall drive is not avoidable. These steps are design optimization of the motor, identification of the motor parameter and implementation of an advanced control system to ensure optimum operation.

Therefore, this dissertation first deals with the design optimization of the Permanent Magnet Assisted Synchronous Reluctance Motor (PMa-SynRM). Various key points in the rotor design of a low cost PMa-SynRM are introduced and their effects are studied. Finite element approach has been utilized to show the effects of these parameters on the developed average electromagnetic torque and the total d-q inductances. As it can be inferred from the name of the motor, there are some permanent magnets mounted in the rotor core. One of the features considered in the design of this motor is the magnetization of the permanent magnets mounted in the rotor core using the stator windings to reduce the manufacturing cost.

At the next step, identification of the motor parameters is discussed. Variation of motor parameters due to temperature and airgap flux has been reported in the literatures. Use of off-line models for estimating the motor parameters is known as a computationally intensive method, especially when the models include the effect of cross saturation. Therefore in practical applications, on-line parameter estimation is favored to achieve a high performance control system. In this dissertation, a simple practical method for parameter estimation of the PMa-SynRM is introduced.

Last part of the dissertation presents one advanced control strategy which utilized the introduced parameter estimator. A practical Maximum Torque Per Ampere (MTPA) control scheme along with a simple parameter estimator for PMa-SynRM is introduced. This method is capable of maintaining the MTPA condition and stays robust against the variations of motor parameters.

Effectiveness of the motor design procedure and the control strategy is validated by presenting simulation and experimental results of a 1.5 kW prototype PMa-SynRM, designed and manufactured through the introduced design method.

To my dear dad and mom for their continuous support and devotion.

To Shermin for her priceless love.

Peyman Niazi

ACKNOWLEDGMENTS

My deep appreciation is first given to almighty God for blessing me with success in my efforts and blessing me with the erudition of several people whose advice, assistance and encouragement helped me throughout the completion of this thesis.

I would like to express my heartfelt appreciation to my advisor, Prof. Hamid A. Toliyat, for his support and continuous help. His knowledge, invaluable guidance, understanding and patience inspired the completion of this thesis. I am very grateful to work with such an insightful and caring professor.

My sincere gratitude also goes to the members of my graduate study committee: Prof. Prasad Enjeti, Prof. Shankar Bhattacharyya, and Prof. Reza Langari for their valuable advice and help through the years I spent at Texas A&M University.

I would like to acknowledge the Department of Electrical and Computer Engineering at Texas A&M University for providing an excellent academic environment. Special thanks go to Ms. Tammy Carda, Ms. Linda Currin, Ms. Gayle Travis and Prof. Huang for all their efforts.

Grateful acknowledgment is extended to LG Electronics Co. for their cooperation during this work and providing us with part of the experimental setup.

I would like to extend my sincere appreciation to my fellow colleagues and friends at Advanced Electric Machine and Power Electronics Laboratory, past and present: Dr. Mehdi Abolhasani, Dr. S. M. Madani, Dr. Leila Parsa, Dr. Masuod Hajiaghajani, Dr. Sang-Shin Kwak, Salih Baris Ozturk, Sheab Ahmed, Steven Campbell, Salman Talebi, Rahul Khopkar, Bilal Akin, Dr. Namhun Kim, Dr. Lei Hao and Dr. Tilak

Gopalarathnam. I honor their friendship and so many good memories throughout my time at Texas A&M University.

Last but certainly not the least; I would like to thank my parents and my beloved Shermin, for their patience, care and endless devotion. I am very grateful to my dad for supporting me and teaching me to be strong. Also, I am deeply indebted to my mom for her patience and her prayers. I believe without them I would have been lost. I do not have the words to express my gratitude to Shermin for her emotional support and priceless love she has brought into my life through these years. During these years, whenever I was exhausted, hopeless and tired of struggling with the obstacles in my work, my prayers to God and the encouraging words of my loved ones were the only relief for me. No words can express my heartfelt gratitude to them for their endless love, care and sacrifice.

TABLE OF CONTENTS

TABLE OF CONTENTS (Continued)

TABLE OF CONTENTS (Continued)

LIST OF FIGURES

LIST OF FIGURES (Continued)

LIST OF FIGURES (Continued)

LIST OF FIGURES (Continued)

LIST OF FIGURES (Continued)

LIST OF TABLES

CHAPTER I

INTRODUCTION

A. OVERVIEW

This study is primarily concerned with the optimum design and robust maximum torque per ampere vector control of inverter fed permanent magnet assisted synchronous reluctance motors (PMa-SynRM) with a simple motor parameter estimator. The PM assisted synchronous reluctance machine is mainly a type of synchronous reluctance motors (SynRM) which is a family member of brushless AC machines consisting of the conventional dc permanent magnet machine, the permanent magnet synchronous machine and the cage induction machine. The members of this family have a standard three phase stator of induction machine with spatial sine wave rotating field. Generated torque is relatively smooth and as a result, the operation is quiet. A conventional three phase inverter can be used to drive the motors of this family if electronically controlled drive is desired.

Most of the early work on the SynRM in 1960's and 1970's was related to the line-start machine. The requirement of a squirrel cage for line-start, along with some other manufacturing factors, compromised the rotor design and led to relatively poor performance compared to an induction machine. Because of this poor performance, SynRM was mainly ignored until late 1980's.

With the development of power transistor technology and vector control theory over

---

This dissertation follows the style and format of *IEEE Transactions on Industry Applications.*

the past decays, the performance of SynRM has been drastically improved and this motor started to be seriously considered as a possible alternative to the other brushless machines (particularly an induction motor) in the variable speed industrial applications.

By controlling the machine via a transistor voltage inverter, line-start feature was no longer necessary for SynRM. Therefore, the starting cage was removed from the rotor and it was designed such that gives the maximum saliency ratio. The main motivations for the renewed interest in the SynRM are:

1. Improved saliency ratio makes the SynRM competitive with an induction machine, particularly in terms of power factor and inverter kVA requirement.
2. Small to medium size high performance drives may have simpler control using the SynRM as compared to the field oriented controlled induction machine.
3. It can be operated stably down to zero speed at full load unlike an induction motor which may suffer overheating problems. In addition, SynRM appears to be more efficient at low speed than an induction machine.
4. By adding appropriate amount of magnet into the rotor core, efficiency improves without having significant back-EMF and without necessary change in the stator design. Because of the existence of flux barriers, demagnetization is hard to occur if strong magnets are used. Demagnetization due to the machine over-loading and high ambient temperature is a significant problem in IPMs.

Before summarizing the main motivations for the work presented in this thesis, presenting the historical development of the machine can help the readers to have an

insight on the trend of SynRM evolution. Creating this background can highlight the major contribution of presented work in this thesis.

The earliest reference on SynRM's that could be found was published in 1923 [1]. Since then, various machine designs have been proposed in the literature by a number of authors. The main purpose of the previous works on the design of SynRM was to improve the overall efficiency of the motor. These designs are classified into several distinctive categories.

The second part of this chapter attempts to give an overview of the machine evolution in chronological order. Each of the machine categories are separately discussed emphasizing important design aspects, main features, and performance limitations. This section finally merges to the state of the art PMa-SynRM drive and its numerous advantages over the other members of the brushless family. These merits are considered in more detail and represent the main motivations for studying this machine.

Besides having an optimum design for the motor, having an optimal controller is also necessary to improve the performance of overall drive. The third section of this chapter reviews the trend of the modern SynRM drives and emphasizes the pros and cons of different industrial drives.

Finally the fourth and fifth sections of the Chapter I present the objectives of this research and outline the thesis structure.

B. EVOLUTION OF SYNCHRONOUS RELUCTANCE MOTOR

The principle of using the differences of reluctances to produce the torque has been known for over 160 years. Before the discovery of the rotating magnetic field by Tesla in 1887, the first reluctance motor was similar to the doubly salient synchronous reluctance motor, nowadays known as the switched reluctance motor. The first rotating-magnetic-field synchronous motor was, however, introduced by Kostko not earlier than in 1923 (Kostko 1923).

There are different designations for singly salient synchronous reluctance motors in the literature. The most popular names for this motor are: Reluctance motor (RM), Synchronous Reluctance Motor (SRM, Synchrel, SynRM) and Reluctance Synchronous Motor (RSM). In this thesis, Synchronous Reluctance Motor (SynRM) is used as the name and abbreviation for this motor. Figure 1-1 shows a cross-sectional view of a single saliency RM consisting of a non-salient stator and a two-pole salient rotor, both made of high-permeability magnetic material. This figure shows a three-phase stator winding although any number of phases is possible. Figure 1-2 shows the cross-sectional view of a three-phase double saliency RM.

In principle, the SynRM is similar to the traditional salient pole synchronous motor but does not have an excitation winding in its rotor. In this case only the rotor is constructed with salient poles. The stator inner surface is cylindrical and typically retains many of the benefits of variable reluctance motors and at the same time eliminates its several disadvantages. Before the development of today's AC motor drives, in a variable speed drive, motor was supplied from a fixed frequency power source. In this case, it

was necessary that the SynRM includes a squirrel cage on the rotor to provide the starting torque for line-start. Otherwise, the rotor could not accelerate and synchronize with the supplying network. The squirrel cage was also needed as a damper winding in order to maintain synchronism under sudden load torques. The presence of a cage for line starting in the rotor structure was interfering with the requirements of the optimum rotor design.

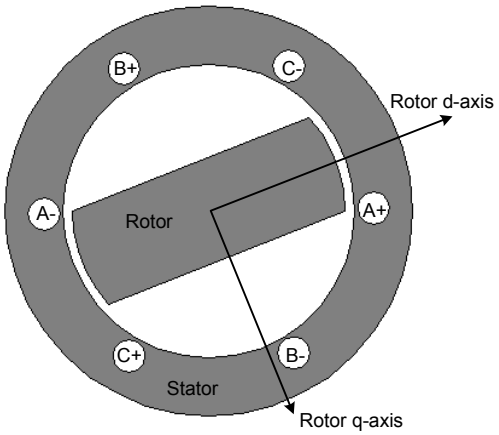

Figure 1- 1 Basic three phase, two pole reluctance variable motor, single saliency SynRM.

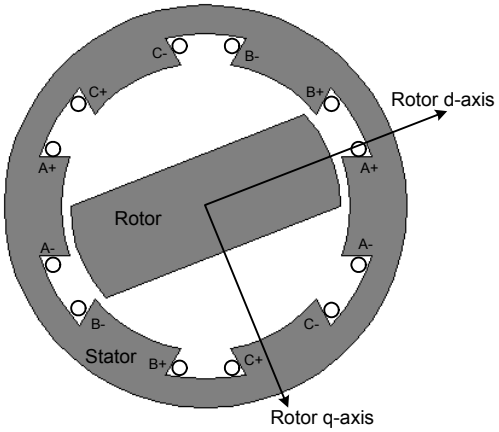

Figure 1- 2 Basic three phase, two pole reluctance variable motor, double saliency switch reluctance motor.

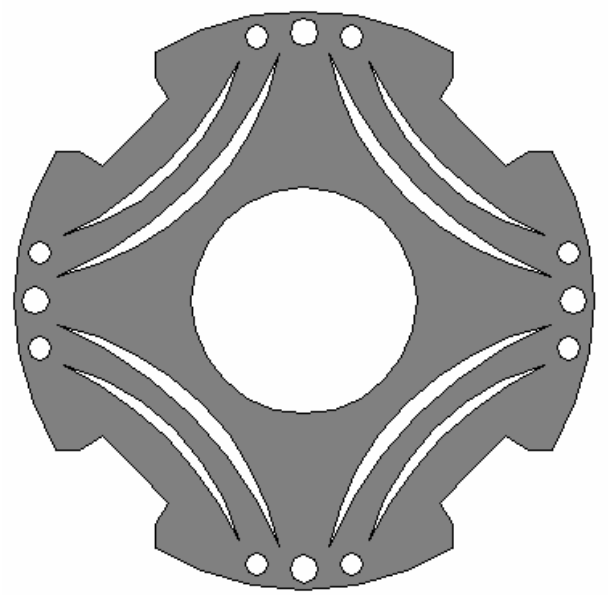

Figure 1- 3 Flux barrier type rotor of reluctance motor of the sixties.

Figure 1-3 shows a sketch of a typical machine of that era which utilized the flux barriers to form a difference in saliency between the polar axis (d-axis) and interpolar axis (q-axis). In most cases, inverters of these motors were not able to operate below 10Hz. Therefore, the motors were typically line started (asynchronously started) with the inverter frequency set at about 10Hz. After being synchronized with the supplied frequency, motor could continue its operation above 10Hz and proceed with the inverter frequency. Over the desired speed range, the inverter was controlled to supply a constant volt/hertz which approximately results in a constant air gap flux. Since the inverter frequency was not generally controlled such that damps the load oscillations, stability problems was occurred related to the "swing" of a synchronous machine operating from a fixed 60Hz supply. In fact, it has been shown that complete instability resulting in continuous speed oscillations around the nominal speed could occur without corrective

action. In addition, a “pull in” phenomenon was occurred when the motor was started up with a load. In this case, since starting torque is an inductive torque and is generated by an incomplete cage, as in Figure 1-3, synchronism with the inverter was not always achieved during the asynchronous start. Therefore, it resulted in continuous operation as an induction motor rather than a synchronous motor. In this case, generated torque had a large torque pulsation. Consequently, this large torque pulsation resulted in substantial speed oscillation. Finally, sudden change in loading of the machine resulted in loosing of synchronism with the power source frequency.

These problems were of course very detrimental to the application which demanded precise speed control. Moreover, ratio of the d axis inductance over q axis inductance (saliency ratio) of such machines could not exceed much more than 2:1. Because of the low saliency ratio, frame size of this motor was larger than an equivalent induction motor. Nonetheless, such machines were used for many years and continued to be manufactured. However, they have been largely replaced by permanent magnet synchronous motors in the fiber spinning application.

Developments in machine design and power electronics allowed the machine designers to remove the starting cage from the rotor and achieve a better performance by using field oriented (vector) control. In vector controlled drives, two crucial parameters are difference of d and q axes inductances (L_d-L_q), as in the line-start case, and the ratio of these two inductances (L_d/L_q) [2, 3, 4, 5, 6, 7]. A variety of vector controlled strategies have been introduced in literature and it turns out that the best performance for all of them is obtained if these two parameters are made as large as possible. In order to

fulfill this requirement, the rotor should be designed for maximum L_d and minimum L_q. Several attempts have been made on the design of the SynRM rotor and the evolution of the rotor configurations [5, 7] is an effort to accomplish this goal.

1. Conventional design

A starting point in the development of rotor designs was a simple salient pole or conventional arrangement (Figure 1-4). Most of the early works presented in the period of mid-1940's and mid-1960's were purely theoretical and investigated the various performance aspects of the fixed frequency operation of this type of machine in the presence of rotor cage. A brief review on these works can be found in the relevant papers of 1960's and 1970's [8, 9, 10]. Low saliency ratio and consequently poor performance of these machines was almost compromised by their simple and rigid structure and also their low manufacturing cost. They were commonly used in the line-start single-speed [9, 11, 12, 13] and two-speed applications [14, 15] during the mid-1960's and early 1970's. In the following 20 years, this machine lost its popularity. Only two applications were reported in the literature [16, 17] during this period. The reason mainly was its substantially inferior performance with respect to the other machines and an absence of the vector controllers. It resulted in gradually replacement of this motor with the vector controlled cageless salient pole machines in the variable speed [18] and spindle drives [4, 19, 20].

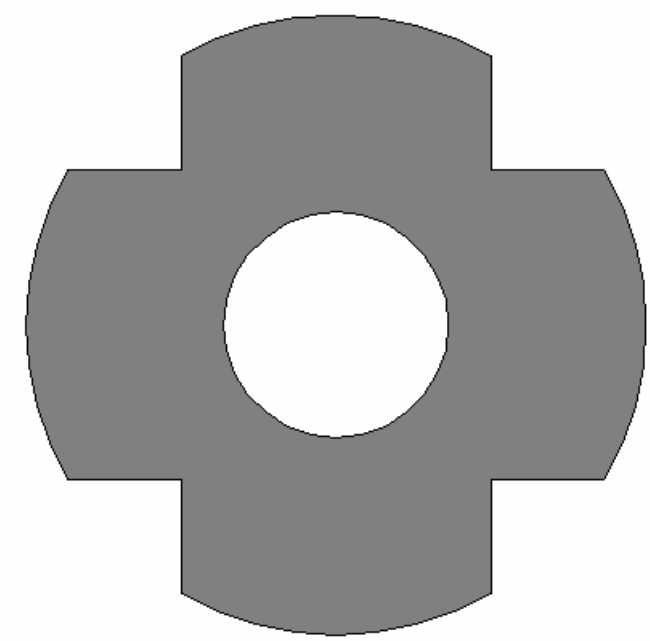

Figure 1- 4 Four-pole conventional salient pole design.

2. Segmental design

The rotor of a "second generation" type of synchronous reluctance motor which appeared somewhat later is shown in Figure 1-5. This rotor utilizes a segmental construction. In this design the rotor cage was not used in order to start the machine. The machine was started in synchronism with inverter frequency.

Saliencies of five or more were obtained with such machines. This saliency ratio could enable this machine to fit in the same frame size as its induction motor counterpart. Since 1963, Lawrenson and Agu [8, 21, 22] extensively developed the segmental rotor design (Figure 1-5). They built several low-inertia cage machine prototypes suitable for some applications where high torque/inertia ratio was required [22].

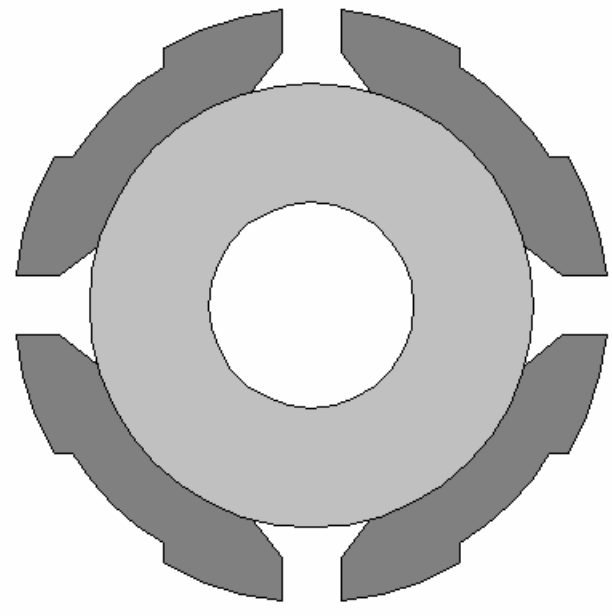

Figure 1- 5 Four-pole isolated segmental rotor design.

Four years later, Lawrenson improved his segmental rotors by introducing q-axis channels [23] and used them for both single-speed [23] and multi-speed [24] applications. Due to the larger saliency ratio, the obtained performance better than equivalent conventional machine designs. However, the complicated rotor construction and its high manufacturing cost were the main limits on development of this type of SynRM rotor. Segmental machines of this type were almost completely ignored in the period after 1960's with only a few references in the literature [16, 26, 27].

3. Double barrier design

Double barrier laminated machines with the rotor structure shown in Figure 1-6 appeared in the early 1970's in some works by Honsinger [10, 28, 29]. They had two barriers per pole and were fitted together with a starting cage. Unlike the conventional

and segmental machines, this type of SynRM was inverter driven with V/f controller. Similar single barrier rotor geometries for the line-start applications were developed in the same period [11, 12, 13].

The main advantage of this type of SynRM over the segmental constructions was the superior design of the flux barriers which allowed them to achieve better saliency ratio and performance. Of course the same as earlier designs, this one was also largely ignored in the later years and was only addressed by Klingshirn in 1978 [30] and Wung [31] and Kamper [32]. The latter authors obtained an output torque comparable to an induction machine with a cageless Honsinger type machine under vector control.

The single barrier rotor arrangement represents one of the latest generations of cageless rotor design. This rotor construction was proposed in 1986 [33] primarily for interior permanent magnet (IPM) machines [33, 34]. In the absence of magnets, an IPM machine becomes a pure SyncRM. These machines have been extensively studied and developed by Miller and Staton in the early 1990's [5, 35]. It was shown that this motor can be comparable with an induction machine in some performance aspects.

The rotor designs in Figures 1-5 and 1-6 were all an attempt to optimize the external magnetic asymmetry by appropriately shaping the radial laminations with the objective of decreasing L_q without reducing L_d. One of the key conclusions of the Kostko's work [1] which was not previously mentioned was that the anisotropy of the magnetic material is also an important optimization factor which should be considered in the design procedure. Anisotropy of the magnetic material directly affects the characteristics of d axis inductance L_d.

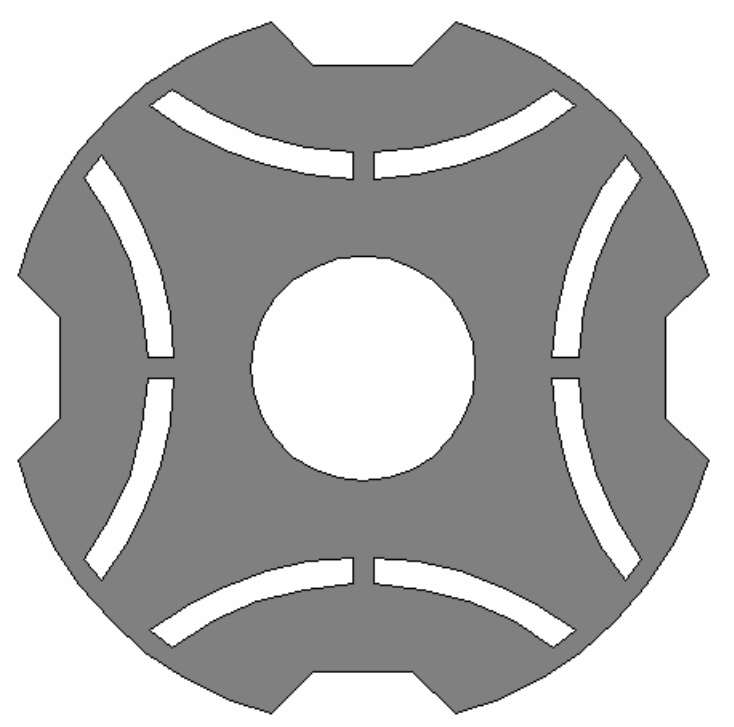

Figure 1- 6 Four-pole double-barrier rotor design.

4. Axially-laminated design

The axially-laminated anisotropic (ALA) rotor shown in Figure 1-7 is made of grain-oriented steel laminations, and implements the main principles of SynRM. In this type of SynRM, the rotor is constructed of axially laminated steel sheets bent into a "u" or "v" shape and then stacked in the radial direction. To describe the overall shape of the rotor, the analogy to four stacked piles of rain gutters on a solid shaft can be used. In this case, the permeance (inductance) in the direction of the gutters from the salient poles (d axis) is high and they form a flux path in the direction of the gutters.

The first ALA machine with a squirrel cage was built by Cruickshank and Menzies in Scotland in 1966 [36]. More developments were performed by the same inventors in

the early 1970's [9, 37, 38] and by Rao in the mid-1970's [26]. Due to the design constraints imposed by the presence of starting cage, the great potential of ALA machine in terms of saliency ratio was not fully utilized. Its performance was well below the performance of an equivalent induction machine. This resulted in a lack of interest in this machine in the following years. In the late 1980's the modern cageless ALA machines featured very high saliency ratio and presented an improved performance [5, 6, 39, 40, 41, 42, 43, 44]. On that time, this machine was considered as a possible alternative for the other electric machines.

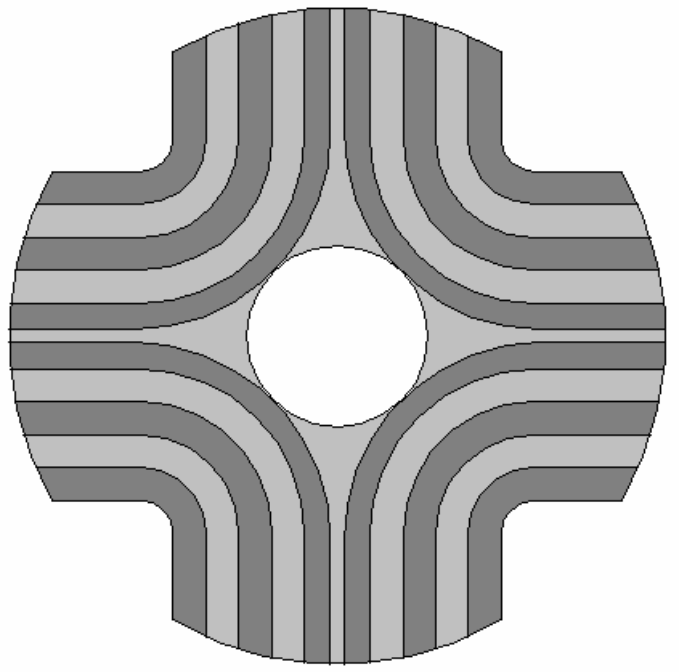

Figure 1- 7 Four-pole axially-laminated rotor design.

5. Transversally-laminated design

The next generation of the SynRM came when transversally laminated (TLA) rotors were introduced. This type of rotor is also called multiple-flux barrier rotor. Figure 1-8 shows a 4-pole transversally laminated rotor with two flux barriers per pole. Mechanical strength is guaranteed by the thin ribs, disposed at the airgap and also in the inner rotor laminations for large speed and/or large rotor diameters. The rotor laminations are made by traditional punching or wire cutting. As a result construction is easy and cheap. However, in compare with the ALA rotors, this type of rotor has more leakages, therefore, the produced torque and power factor is lower in transversally laminated SynRMs with respect to the SynRM with ALA rotor.

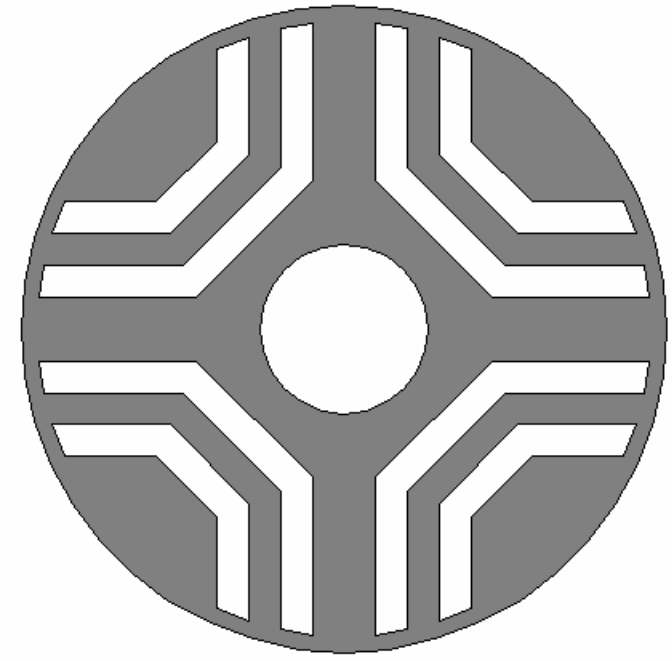

Figure 1- 8 Four-pole transversally-laminated rotor design.

In spite of this fact, TLA rotor has some advantages including suitability for rotor skewing and easy for mass production. Moreover, the transversally laminated type of rotor can be optimized by proper design, in order to minimize the airgap harmonics and their effect on torque ripple. This is obtained by both the proper shaping of the various flux-barriers and the proper choice of their access points at the airgap.

6. Permanent magnet assisted SynRM

When PMs are inserted into the rotor flux barriers of a synchronous reluctance motor, it becomes a permanent magnet assisted synchronous reluctance motor (PMa-SynRM). PMs can be mounted in the rotor core of the axially or transversally laminated structure. Figure 1-9 shows a transversally laminated PMa-SynRM. The polarity of magnets is chosen such that counteract the q-axis flux of the SynRM at rated load. Regardless of the different choice of d, q axes, in principle, the PMa-SynRM seems nothing more than a particular case of interior permanent magnet motor (IPM). However, a substantial difference is the high anisotropy rotor structure of PMa-SynRM and as a result, low value of the PM flux. The amount of PM flux is quite lower than the amount of rated flux. In contrast, in the usual IPM the most flux comes from the magnets and the flux produced by stator currents is considered as an unwanted reaction flux. In practice, because of the above mentioned difference between PMa-SynRM and IPM machines, they have different suitability to the large flux-weakening ranges.

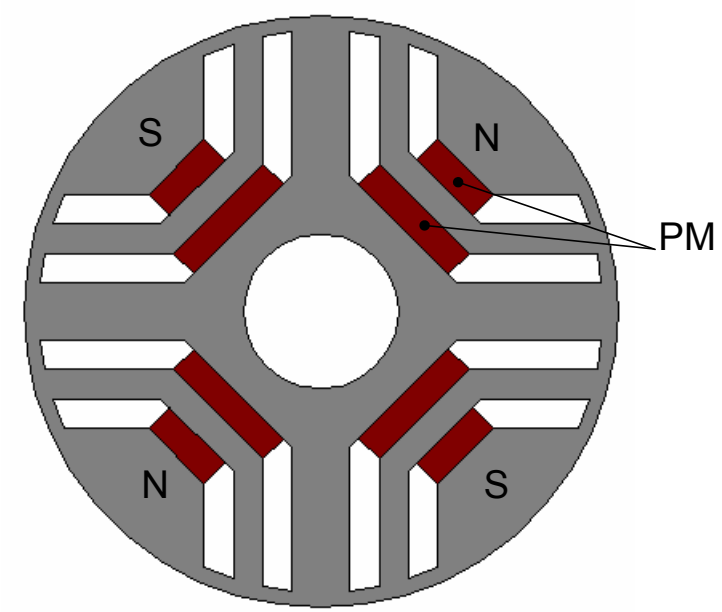

Figure 1- 9 Four-pole transversally-laminated PM assisted rotor design.

C. MODERN SYNCHRONOUS DRIVES

With the development of new technology, particularly in the areas of digital electronics and power semiconductor devices [34], performance of synchronous drives has drastically improved. Current controlled PWM inverters along with the field oriented (vector) control [45, 46, 47] have significantly contributed to the revival of interest in the SynRM over the last few years. Enhancement of drive performance and stable synchronous operation down to very low speeds including standstill has been possible by use of vector control [4, 48, 49, 50, 51, 52, 53, 54]. Achieving of this operation was difficult by use of conventional V/f control [9, 29, 46, 55, 56].

In order to have a high performance SynRM drive capable of competing with the other brushless drives [34, 35], design and optimum refinement of the rotor geometry is necessary. As it was presented, so much effort has been put on the optimization of the

SynRM rotor geometry in order to have a more efficient SynRM drive. More refinements in the design of the SynRM rotor geometry have been possible through the numerical magnetic analysis by use of finite element softwares [57, 58, 60].

Use of other materials such as composite powder metal rather than iron has been considered as an alternative for the rotor manufacturing [59]. By using of this type of materials, geometry of the rotor can be more flexible and manufacturing becomes easier.

Inserting magnet in the rotor flux barriers is another way to improve the performance of the motor [62, 63, 64] which changes the motor from SynRM to PMa-SynRM.

Beside the better design of the motor, the enhancement of the overall drive could be possible by using more advance control algorithms. By the advent of the high speed microprocessors implementation of the advanced control procedures has been possible.

Most of the modern control algorithms are model based and are parameter dependent. The main limitation of most of the works on the optimal control of SynRM is use of an ideal model in order to perform theoretical analysis [2, 3, 7] and practical implementation [49]. However, in a real machine the effects of saturation and iron losses result in deviation of the current angle from the optimal operating point. Variation of PMa-SynRM or SynRM parameters due to temperature and airgap flux has been reported in the literatures and also will be discussed in this dissertation. Knowledge of the motor parameters and also use of a more realistic model is crucial in order to implement an optimal control.

Several off-line models have been introduced for estimating the motor parameters and overcoming the problem of parameter variation in SynRM [65]. However, use of

off-line models for estimating the motor parameters is known as a computationally intensive method, especially when the effect of cross saturation is included in the models. Therefore in practical applications, on-line parameter estimation is favored to achieve a high performance control system. Several adaptive estimation methods have been proposed in the literature [57, 58, 59, 60]. Some of the estimation algorithms have utilized recursive least square (RLS) procedure. Having a persistence excitation condition is necessary in RLS based parameter estimator which is not a realistic condition for most of the practical application.

D. RESEARCH OBJECTIVES

The purpose of this research is to design and implement an efficient AC drive using a permanent magnet assisted SynRM with high reliability, adequate performance for high volume production. The proposed system consists of a voltage source inverter (VSI) plus a three-phase PMa-SynRM motor.

The first objective of this research is to develop a systematic procedure in order to optimize the geometry of the SynRM rotor. This design needs to be done through the magnetic analysis and by use of numerical methods. A finite element analysis on a transversally laminated SynRM is performed to investigate the effect of different rotor parameter on the motor performance in terms of output torque and saliency ratio. Limited amount of magnet is used to increase efficiency of motor by improving saliency ratio and also adding magnetic torque to overall output torque. Geometry of the rotor is designed to be suitable for magnetizing of the ferrite. Magnetization is performed after

manufacturing of the motor through its stator windings which makes the design very cost effective.

Parameters of this motor such as inductances and back-EMF vary due to change of operating point and temperature of the motor. These changes affect the optimum working point and cause a deviation from desirable operating condition. In this case estimation of these parameters is necessary to achieve the optimum operating condition. Therefore, the second objective of this research is to develop an effective on-line parameter estimation method in order to obtain the real value of parameters. This estimation also helps control system to operate at correct power angle which is very critical in this type of variable speed motor drive.

In an AC drive with a long steady state operating condition, maximum torque per ampere (MTPA) is considered one of the most desired optimal operating conditions. MTPA controller is a parameter dependent controller and its performance relies on the knowledge of motor parameters. The third objective of this research is to introduce a reliable and simple maximum torque per ampere controller for PMa-SynRM equipped with the introduced parameter estimator. This controller can guarantee the robustness of the operating condition against the variation of the parameters.

E. THESIS OUTLINE

In order to conduct the stated research objectives, this dissertation is outlined as following:

Chapter I covers some backgrounds on synchronous reluctance motor. In this chapter the evolution of this motor is discussed and the main goals of this research are introduced.

In Chapter II, some background information on synchronous reluctance motor are given and objectives of the rotor design in this motor are defined. Several important key parameters in SynRM rotor geometry are introduced and their effects on the motor performance are studied. Based on the predefined constrains on some motor specifications, one optimum geometry for the target SynRM is obtained. Some modification is enforced in the rotor geometry to make it suitable for PMa-SynRM motor. Effects and improvement of the designed PMa-SynRM is discussed through the simulation studies.

In Chapter III, variation of the motor parameters and their effects on the control system are discussed. A short survey on some parameter identification methods is done. PMa-SynRM model using high order harmonics are used to extract a simple and robust parameter estimator. The developed parameter estimator can be used in tuning of current control loops and also some high specific drive strategies such as maximum torque per ampere control. Some simulation results are presented to show the effectiveness of the introduced method.

In Chapter IV, one of the most desirable control methods, maximum torque per ampere (MTPA) control, for the PMa-SynRM is introduced and parameter dependency of this controller is discussed. In order to assure the robustness of MTPA control against the variation of the motor parameters, a simple on-line current-angle tuner is introduced. This tuner is equipped with the presented parameter estimator and guarantees the MTPA condition.

The implementation and laboratory measurement results on a 1.5 kW prototype PMa-SynRM are presented in these chapters. This prototype has been designed and manufactured based through the introduced design procedure in chapter II. The controller implements the maximum torque per ampere control strategy on TMPF2812 platform. A set of experimental results generated by executing the control algorithm has been presented to show the feasibility of the introduced parameter estimator and MTPA control and validate the proposed controller.

Chapter V is a summary of the relevant conclusions and possible extensions that can be drawn from the work presented in this thesis.

CHAPTER II

DESIGN OF A LOW COST PERMANENT MAGNET ASSISTED SYNCHRONOUS RELUCTANCE MOTOR

A. INTRODUCTION

In this chapter, various key points in the rotor design of a low cost permanent magnet assisted synchronous reluctance motor (PMa-SynRM) are introduced and their effects are studied. Figures 2-1 and 2-2 show two transversally and axially laminated SynRM rotors, respectively. An axially laminated rotor can present a high-anisotropy and provide a very high unsaturated saliency ratio [70, 71, 72]. However, from the mechanical stress point of view, this rotor has some drawbacks with respect to the transversally laminated one. The effective saliency ratio of transversally laminated rotors can be enhanced by proper placement, proper shape and the proper number of the flux barriers. To optimize the motor design, a reasonably good magnetic design can be obtained without using numerical techniques [73, 74]. However, the finite-element method must be used to consider the nonlinear magnetic behaviors of the materials which play a key role whenever overload performance prediction is essential [60].

Figure 2- 1 Modern transversally laminated rotor
for synchronous reluctance motors.

Figure 2- 2 Axially laminated rotor
for synchronous reluctance motors.

Adding the proper quantity of permanent magnets into the SynRM rotor core is another way to improve the operating performance of this motor. In this case, the motor is similar to an interior permanent magnet (IPM) motor. However, the amount of permanent magnets used and the permanent magnet flux-linkages are smaller with respect to the conventional IPM. Thus, the proposed motor can be called a Permanent Magnet Assisted Synchronous Reluctance Motor (PMa-SynRM) [75].

The main purpose of this chapter is to introduce a systematic approach in order to optimize the design of SynRM by performing a set of finite element analysis on a transversally laminated synchronous reluctance motor. In this procedure, different rotor parameters and their relative effects on the motor performance in terms of output torque and saliency ratio are studied.

Moreover, improvement of the motor performance due to the permanent magnets placed in the rotor core is investigated by studying their effect on developed torque and the d and q inductances. The amount of permanent magnets used in the motor is limited by the cost and flux barrier shapes.

In order to reduce the manufacturing cost, one of the design criteria is to achieve a rotor geometry that is suitable for magnetizing the ferromagnetic materials (such as Ferrite) placed in the rotor core. Ferrite is placed in the rotor core first and then is magnetized using the stator winding. Simulation and preliminary experimental results will be presented to support the validity of the proposed procedure.

Before going through the design procedure, mathematic model of the SynRM is introduced. Using this model, the effects of the motor parameters on the behavior of the

motor is investigated and the design criteria such as output torque and power factor are obtained. Knowledge of these effects helps the designer to achieve the optimum design. After that by introducing the computer aided design (CAD) in electric motor design and providing some background on finite element, design procedure is presented.

B. MATHEMATICAL MODEL OF SynRM

1. The d-q equation of synchronous reluctance machine

A 2-pole synchronous reluctance motor is shown in Figure 2-3. It has 3-phase stator winding and a salient rotor. The stator windings are identical winding and displaced 120° from each other with N_s equivalent turns and resistance of r_s. It is usually assumed that windings are distributed sinusoidally. Since the stator winding of the synchronous reluctance motor is sinusoidally distributed, flux harmonics in the air gap contribute only

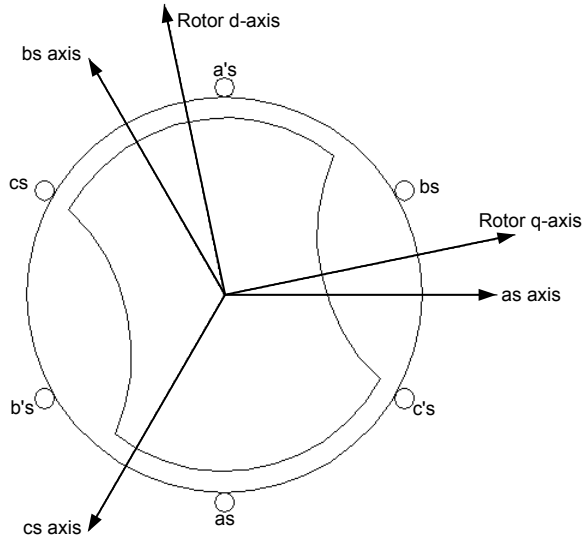

Figure 2- 3 Two-pole synchronous reluctance motor.

an additional term to the stator leakage inductance. Hence, the equations which present the behavior of the synchronous reluctance machine can be obtained from the conventional equations of a conventional wound field synchronous machine. In SynRM, the excitation (field) winding does not exist. Moreover, in machines typically employing a modern axially or transversally laminated rotor structure, a rotor cage is normally absent because the machine can be starting synchronously from zero speed by proper inverter control. Hence, eliminating both the field winding and damper winding equations from Park's equations, the basis for the d-q equations for a synchronous reluctance machine can be obtained. That is:

$$\begin{aligned} v_d &= r_s i_{ds} + \frac{d\lambda_{ds}}{dt} - \omega_r \lambda_{qs} \\ v_q &= r_s i_{qs} + \frac{d\lambda_{qs}}{dt} + \omega_r \lambda_{ds} \end{aligned} \tag{2-1}$$

where:

$$\begin{aligned} \lambda_{ds} &= L_{ls} i_{ds} + L_{md} i_{ds} = L_{ds} i_{ds} \\ \lambda_{qs} &= L_{ls} i_{qs} + L_{mq} i_{qs} = L_{qs} i_{qs} \end{aligned} \tag{2-2}$$

and L_{ls} , L_{md} and L_{mq} are the stator leakage inductance, direct axis magnetizing inductance and quadrature axis magnetizing inductance, respectively. The quantity r_s is the stator resistance per phase. In terms of the d-q variables, the electromagnetic torque is identical to that of a synchronous machine, namely,

$$T_e = \frac{3}{2}\frac{P}{2}\left(\lambda_{ds} i_{qs} - \lambda_{qs} i_{ds}\right) \tag{2-3}$$

where P is the number of poles.

2. The steady state equations for a synchronous reluctance motor

These d-q equations express the behavior of the physical stator and rotor currents in a reference frame which is rotating with the rotor of the machine in much the same manner as for wound field synchronous machine (rotor reference frame). When balanced three phase voltages are applied to the machine, these voltages form a constant amplitude rotating vector in the d-q plane. When the rotor rotates at the same angular velocity as the angular velocity of the rotating voltage vector (modified by the number of pole pairs), the voltage vector appears to be stationary at the rotor reference frame. In this case it is conventional to describe the angular relationship between the stator voltage vector and the d-q axes as the two components (Figure 2-4):

$$\begin{aligned} V_{qs} &= \widetilde{V}_s \cos\delta \\ V_{ds} &= -\widetilde{V}_s \sin\delta \end{aligned} \tag{2-4}$$

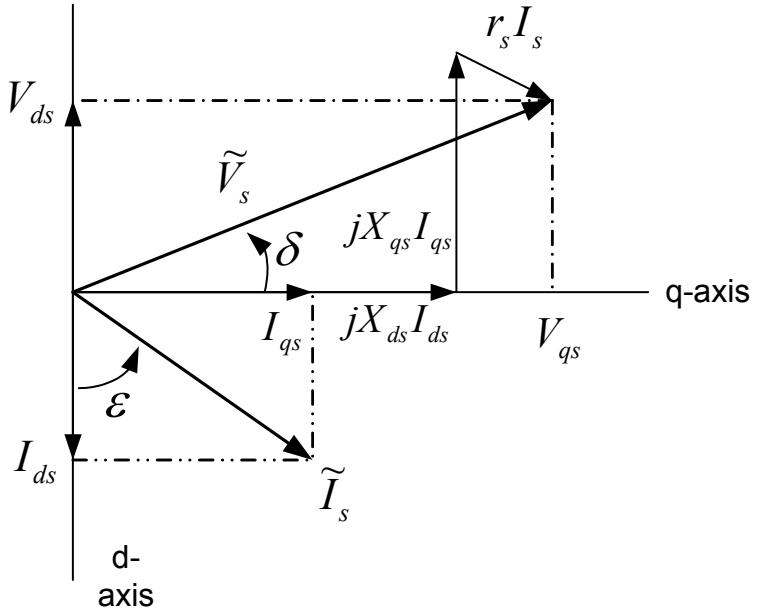

Figure 2- 4 Phasor diagram for synchronous reluctance machine.

The "variables" in the differential equation (2-1) also become constant in steady state. That is the $\frac{d}{dt}$ terms can be eliminated. The currents can then be solved in terms of the steady state voltages as:

$$I_{ds} = \frac{\omega_e L_{qs} V_{qs} + r_s V_{ds}}{r_s^2 + \omega_e^2 L_{ds} L_{qs}}$$
$$I_{qs} = \frac{-\omega_e L_{ds} V_{ds} + r_s V_{qs}}{r_s^2 + \omega_e^2 L_{ds} L_{qs}} \quad (2\text{-}5)$$

or, approximately, neglecting stator resistance as:

$$I_{ds} = \frac{V_{qs}}{\omega_e L_{ds}},\ I_{qs} = \frac{-V_{ds}}{\omega_e L_{qs}} \quad (2\text{-}6)$$

3. Phasor equations for a synchronous reluctance machine

Alternatively, we can create a single phasor equation from the steady state version of (2-1) by multiplying the first line of (2-1) by $-j\,(j = \sqrt{-1})$ and adding it to the second line. The result is:

$$v_{qs} - jv_{ds} = r_s(I_{qs} - jI_{ds}) + \omega_e(\lambda_{ds} + j\lambda_{qs}) \quad (2\text{-}7)$$

or, using (2-2) and (2-7):

$$v_{qs} - jv_{ds} = r_s(I_{qs} - jI_{ds}) + \omega_e(L_{ds} I_{ds} + jL_{qs} I_{qs}) \quad (2\text{-}8)$$

(2-8) can be manipulated to the form of:

$$V_{qs} - jV_{ds} = r_s(I_{qs} - jI_{ds}) + j\omega_e L_{ds}(-jI_{ds}) + j\omega_e L_{qs} I_{qs} \quad (2\text{-}9)$$

In phasor notation:

$$\widetilde{V}_s = r_s \widetilde{I}_s + jX_{ds}\widetilde{I}_{ds} + jX_{qs}\widetilde{I}_{qs} \tag{2-10}$$

Alternatively, the results of (2-5) can be obtained from these phasor equations. A phasor diagram of (2-10) is shown in Figure 2-4.

4. Torque expression for constant Volt/Hertz and constant current operation

Using (2-5), the torque equation can be solved in terms of voltage as:

$$T_e = \frac{3}{2}\frac{P}{2}(L_{ds} - L_{qs})\frac{-\omega_e L_{ds} r_s V_{ds}^2 + \omega_e L_{qs} r_s V_{qs}^2 + (r_s^2 - \omega_e^2 L_{ds} L_{qs})V_{ds} V_{qs}}{(r_s^2 + \omega_e^2 L_{ds} L_{qs})^2} \tag{2-11}$$

Except frequencies near zero, in all frequencies, (2-11) is well approximated by neglecting the stator resistance. In this case, (2-11) is reduced to:

$$T_e = -\frac{3}{2}\frac{P}{2}\frac{(L_{ds} - L_{qs})}{L_{ds} L_{qs}}(\frac{V_{ds}}{\omega_e})(\frac{V_{qs}}{\omega_e}) \tag{2-12}$$

Substituting (2-4) we obtain the torque in terms of the Volt per Hertz and "torque angle" δ as:

$$T_e = \frac{3}{2}\frac{P}{2}(\frac{1}{L_{qs}} - \frac{1}{L_{ds}})(\frac{V_s}{\omega_e})^2 \frac{\sin 2\delta}{2} \tag{2-13}$$

As it can be seen, the torque varies at the square of the Volt per Hertz and as the sine of twice of the angle δ. When the Volt per Hertz is fixed, the maximum torque is clearly reached when $\delta = 45^o$. Therefore the maximum torque for a fixed Volt per Hertz is:

$$T_{e(\max)} = \frac{3}{4}\frac{P}{2}(\frac{1}{L_{qs}} - \frac{1}{L_{ds}})(\frac{V_s}{\omega_e})^2 \tag{2-14}$$

If (2-2) is directly substituted into (2-3) the torque equation can also be written in terms of stator d-q current as:

$$T_e = \frac{3}{2}\frac{P}{2}(L_{ds} - L_{qs})I_{ds}I_{qs} \tag{2-15}$$

Clearly the currents as described by (2-5) also describe a constant amplitude vector of I_s on the d-q plane. If we write the solutions to these equations as:

$$\begin{aligned} I_{ds} &= I_s \cos\varepsilon \\ I_{qs} &= I_s \sin\varepsilon \end{aligned} \tag{2-16}$$

Then the electromagnetic torque can be expressed in terms of the stator current amplitude and "MMF angle" ε as:

$$T_e = \frac{3}{2}\frac{P}{2}(L_{ds} - L_{qs})I_s^2 \frac{\sin 2\varepsilon}{2} \tag{2-17}$$

5. Maximum power factor

A frequently used argument against the use of a synchronous reluctance motor is its poor power factor. It is useful to consider this issue more closely. Referring to Figure 2-4 the power factor of a synchronous reluctance motor, cosϕ, can be expressed as the ratio of the projection of the voltage vector on the current vector divided by the amplitude of the voltage vector. That is:

$$\cos\phi = \frac{V_{qs}\sin\varepsilon - V_{ds}\cos\varepsilon}{\sqrt{V_{qs}^2 + V_{ds}^2}} \tag{2-18}$$

Again it is convenient to neglect the stator resistance. Clearly, in this case, this is a pessimistic assumption since any resistive component will clearly raise power factor.

Hence, the result to be obtained is a minimum limit. From (2-6), this expression can be written as:

$$\cos\phi = \frac{\omega_e L_{ds} I_{ds} \sin\varepsilon - \omega_e L_{qs} I_{qs} \cos\varepsilon}{\sqrt{(\omega_e L_{ds} I_{ds})^2 + (\omega_e L_{qs} I_{qs})^2}} \tag{2-19}$$

utilizing (2-16):

$$\cos\phi = \frac{\omega_e L_{ds} I_s \cos\varepsilon \sin\varepsilon - \omega_e L_{qs} I_s \sin\varepsilon \cos\varepsilon}{\sqrt{(\omega_e L_{ds} I_s \cos\varepsilon)^2 + (\omega_e L_{qs} I_s \sin\varepsilon)^2}} \tag{2-20}$$

which reduces to

$$\cos\phi = \frac{(L_{ds} - L_{qs}) \sin\varepsilon \cos\varepsilon}{\sqrt{(L_{ds} \cos\varepsilon)^2 + (L_{qs} \sin\varepsilon)^2}} \tag{2-21}$$

or after some reduction:

$$\cos\phi = \frac{k-1}{\sqrt{k^2 \frac{1}{\sin^2\varepsilon} + \frac{1}{\cos^2\varepsilon}}} \tag{2-22}$$

where k denotes the saliency ratio.($k = \frac{L_{ds}}{L_{qs}}$)

(2-22) gives the power factor as a function of MMF angle ε for a machine with any saliency ratio, k. It is useful now to determine which value of MMF angle results in the maximum power factor. If this point is chosen as the rated value then the machine can be considered as optimally performing its energy conversion function.

By substituting $x = \sin^2\varepsilon$ into (2-22), the power factor cosϕ is expressed as a function of x as:

$$\cos\phi(x) = \frac{k-1}{\sqrt{k^2\frac{1}{x}+\frac{1}{1-x}}} \tag{2-23}$$

By differentiating cosϕ(x) in terms of x and solving, the value of x that gives the maximum value of cosϕ(x) can be determined. Thus,

$$\frac{d}{dx}\cos\phi(x) = \frac{k-1}{\left(k^2\frac{1}{x}+\frac{1}{1-x}\right)^{-3/2}}\left(\frac{-k^2}{x^2}+\frac{1}{(1-x)^2}\right) = 0 \tag{2-24}$$

Upon reducing the result, since k=1 is not a solution,

$$-k^2(1-x)^2 + x^2 = 0 \tag{2-25}$$

since x≠0 and k≠0 the solution is $x = k(1-x)$ or

$$\sin^2\varepsilon = k(1-\sin^2\varepsilon) = k\cos^2\varepsilon \tag{2-26}$$

that is $\tan\varepsilon = \sqrt{k}$ and thus:

$$\cos\phi_{\max} = \frac{k-1}{\sqrt{k^2\frac{1}{\frac{k}{1+k}}+\frac{1}{1-\frac{k}{1+k}}}} = \frac{k-1}{k+1} \tag{2-27}$$

The power factor therefore reaches a maximum value of $\cos\phi_{\max} = \frac{k-1}{k+1}$, when the MMF angle reaches ε, such that $\tan\varepsilon = \sqrt{k}$. The motor power factor versus saliency ratio k under maximum power factor scheme is plotted in Figure 2-5. Note that for machines with a saliency ratio of 7-8, the power factor is near 0.8 which is quite typical of class B induction machine rated about 10Hp.

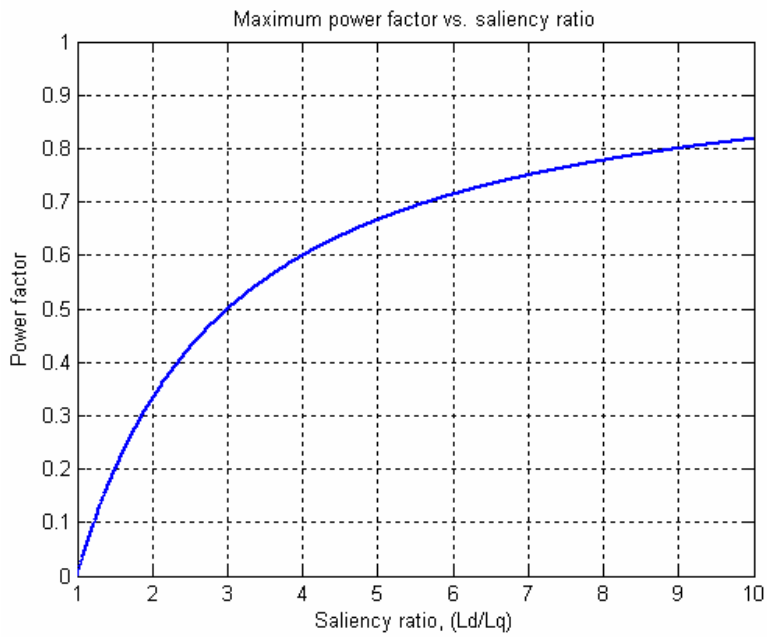

Figure 2- 5 Power factor vs. saliency ratio (K) of a synchronous reluctance motor when the motor is controlled with the maximum power factor control scheme.

The maximum power factor operation point is clearly an ideal operating condition for which to define rated torque. It is useful to consider how close this operating point is to the maximum torque condition at pull out. If the stator resistance is neglected the input power and output power can be equated. The input power for the maximum power factor condition is from (2-27):

$$P_{pf(\max)} = \frac{3}{2} V_s I_s \cos\phi = \frac{3}{2} V_s I_s \frac{L_{ds} - L_{qs}}{L_{ds} + L_{qs}} \tag{2-28}$$

When stator resistance is neglected:

$$\begin{aligned} V_{qs} &= V_s \cos\delta = X_{ds} I_{ds} = X_{ds} I_s \cos\varepsilon \\ V_{ds} &= V_s \sin\delta = X_{qs} I_{qs} = X_{qs} I_s \sin\varepsilon \end{aligned} \tag{2-29}$$

taking the ratio of these two equations,

$$\tan\delta = \frac{X_{qs}}{X_{ds}}\tan\varepsilon = \frac{L_{qs}}{L_{ds}}\tan\varepsilon \tag{2-30}$$

However, as we saw previously $\tan\varepsilon = \sqrt{k}$ or $\tan\varepsilon = \sqrt{\frac{L_{ds}}{L_{qs}}}$, so that the tangent of the torque angle δ at maximum power factor is:

$$\tan\delta = \sqrt{\frac{L_{qs}}{L_{ds}}} \tag{2-31}$$

From (2-30) and (2-31) we can easily establish that:

$$\cos\varepsilon = \sqrt{\frac{L_{qs}}{L_{ds}+L_{qs}}}$$
$$\cos\delta = \sqrt{\frac{L_{ds}}{L_{ds}+L_{qs}}} \tag{2-32}$$

Finally from (2-29) the current amplitude at the maximum power factor condition is:

$$I_s = \frac{V_s}{X_{ds}}\sqrt{\frac{L_{ds}}{L_{qs}}} \tag{2-33}$$

Combining (2-28) and (2-29) we can now express the input power solely in terms of the input voltage as:

$$P_{pf(\max)} = \frac{3}{2}\frac{V_s^2}{\omega_e}\frac{1}{\sqrt{L_{ds}L_{qs}}}\frac{L_{ds}-L_{qs}}{L_{ds}+L_{qs}} \tag{2-34}$$

from (2-14), the output torque is at pullout:

$$T_{e(po)} = \frac{3}{4}\frac{P}{2}\left(\frac{1}{L_{qs}}-\frac{1}{L_{ds}}\right)\left(\frac{V_s}{\omega_e}\right)^2 \tag{2-35}$$

Neglecting losses the input power is:

$$P_{po} = \frac{2\omega_e}{P} T_{e(po)} = \frac{3}{4}\left(\frac{1}{L_{qs}} - \frac{1}{L_{ds}}\right)\left(\frac{V_s^2}{\omega_e}\right) \tag{2-36}$$

taking the ratio of (2-36) to (2-34) results in:

$$\frac{P_{po}}{P_{pf(\max)}} = \frac{1}{2}\frac{L_{ds} + L_{qs}}{\sqrt{L_{ds} L_{qs}}} \tag{2-37}$$

Hence, if $\frac{L_{ds}}{L_{qs}} = 8.0$, then $\frac{P_{po}}{P_{pf(\max)}} = 1.59$ which is a very reasonable value of per unit pull out torque.

C. DESIGN CRITERIA

As it was mentioned before, the main aim of this chapter is to find a rotor design suitable for the transversally laminated PMa-SynRM. As it was shown in previous section, the two crucial parameters in drive of a SynRM and its performance are L_d-L_q and saliency ratio (L_d/L_q). Therefore, the criteria in the rotor design or the main target could be making these two parameters as large as possible. In order to fulfill this requirement, the rotor should be designed for maximum L_d and minimum L_q. Instead of using analytical approaches, computer aided design approach is selected to reach this goal.

1. Computer aided design

i. Why we need computer aided design

Techniques for designing, analyzing, and driving electric motors have been developed rapidly using fast computers and numerical techniques. Today we rely on numerical methods to understand the electromagnetic, thermal, and mechanical behavior of machines. Design is distinct from analysis. It requires imagination and judgment that go beyond the realm of mere computation. Most of the key tasks of electric machine design are software-based and can be categorized as following:

1. Basic electrical and mechanical design
2. Thermal analysis
3. Control and system performance analysis
4. Mechanical CAD
5. Mechanical analysis (dynamics, stress, noise)
6. Optimization
7. Database management of designs, manufacturing details, inventory, etc.

The most fundamental tasks are (1) and (2). These two tasks determine all the basic dimensions of the motor, the materials used to construct it, and its performance.

In the simplest cases, task (3) is a matter of ensuring that the motor will start when it is connected to energy source or stop when it is disconnected. Much more complex simulations may be required when the motor design is associated with the design of a complex system, such as an automotive electric power steering gear. Task (4) is a necessary part of the design for manufacturing and is frequently integrated with task (5).

Task (6) is for the refinement of the design, and its optimization depends on having a fast and reliable computer engine or model for task (1) and (2). Task (7) is not really motor design per se, but it is often important for motor design software (task 1) to interface closely with a company's database or catalog of design, characteristic info of the materials, and/or with its inventories of standard components and manufacturing limits such as punching, end-ring, dies, etc. Because of these reasons, software for task (1) may be required to calculate cost functions based on material weights and other parameters related to performance and manufacturing factors.

ii. The nature of the design process

A "design" is defined as a set of "design parameters." The design parameters include all dimensions of the laminations, windings, magnets, etc., together with the numbers of turns in the winding, layout of the windings, and many details of the supply. For motors that run from electronics drives, the design may include details of control parameters such as commutation angles and set-point values of controlled voltages or currents.

The design process is concerned with determining the design from a set of specified performance requirements. It also includes performance calculations to ensure that the design meets the performance requirements. Because there is no general procedure for synthesizing a design to meet a set of performance requirements, most designers rely on an iterative or recursive process in which the parameters are adjusted recursively until the performance calculations indicate that the design will meet the performance requirements. The final results are in a design sheet summarizing all the design parameters and many aspects of performance, including graphical data.

Even when a computer program is available to perform the performance calculations, the design engineer make all the decisions about parameter adjustments. In the other words, all the intelligence and creativity is contributed by the design engineer, while the computer does modeling of the current version of the design. Calculation of the performance might be complex and sophisticated, while the design decisions can be delicate and may involve difficult compromises and judgments. That's the boarder line of the responsibilities between the computer software and the design engineer during the design procedure.

The basic design process includes three enhancements:

1. the incorporation of finite-element analysis in the performance calculation
2. the automation of some or all of the manual repetition
3. the storage and management of the design in a database

Finite-element analysis is generally specialized to one technology such as electromagnetic field analysis or thermal analysis and is still relatively slow in spite of the advances made in computer processing speed. For these reasons it is not a trivial matter to integrate finite-element analysis into the design process.

Automation of the manual repetition is possible if a sensible algorithm is provided. Consider, for example, the automatic determination of the number of turns required in a winding by a search process. The search must follow the basic relationship between voltage and flux, expressed mathematically in the correct form for the particular type of motor. But it must also work within the practical constrains of discrete wire sizes, maximum slot-fill factor, etc. Once the process is automated, the designer's role

becomes one of supervision and evaluation, rather than of execution. Therefore, the automatic algorithm must be written carefully and efficiently to avoid hidden errors and produce reliable, practical results.

Design automation becomes extremely complex if the computer has the control of more than one or two design parameter. There is no serious interest in those software that automatically synthesize or optimize the design without having option of detailed programming by the user.

As it was mentioned, finite element method is the main core of the most electromagnetic computer aided design software. In the next step the main idea and the bases of the finite element approach is introduced.

2. Finite element approach

The magnetic circuit or permeance method described in the literature is a very useful method for calculating approximate magnetic field in devices of simple geometry. For more accurate calculation, however, finite element computer programs are necessary.

The main limitation of the magnetic circuit method is that it requires the assumption of magnetic flux paths. The lengths and cross-sectional areas of all the paths must be known. Usually the paths are assumed to consist of straight lines, which is erroneous to some extent. To calculate the effects of flux fringing, saturation and leakage flux usually empirical correction factors are used. If a motor or other magnetic device has had essentially the same type of design for many years, then the empirical factors are fairly well known. Nowadays, the motor designers are often involved with the new design

concepts for which the flux paths and empirical factors are unknown. Even if the design is a newer version of a well-understood older design concept, there is a great need for accurately determining the effects of geometric changes and saturation on the motor efficiency and other parameters related to the magnetic field.

The finite element method can be made readily available in the form of computer software called Maxwell® [76]. The software requires no assumption of flux paths or related empirical factors. This software can accurately calculate magnetic field and the related motor design parameter for motors of complicated geometry, with saturation and/or permanent magnets, with significant armature reaction, and with or without eddy currents.

i. Energy functional

The finite element method is based on energy conversion. The law of conversion of energy in electric motors may be derived from Maxwell's equations and can be expressed as [77]:

$$-\int_{v} \overline{E}.\overline{J}dV = \int_{v} \overline{H}.\frac{\partial \overline{B}}{\partial t}dV \qquad (2\text{-}38)$$

Where $\overline{B}$ is magnetic or flux density, $\overline{H}$ is field intensity, $\overline{J}$ is current density, $\overline{E}$ is electric field, and v is the volume enclosing the analyzed device.

The left-hand term of (2-38) is the net electrical power input P_E. It can be shown as voltage times current. The right-hand term can be written to give (2-39) [78]:

$$-\int_{v} \overline{E}.\overline{J}dV = \frac{\partial}{\partial t}\int_{v}\left(\int_{0}^{B} \overline{H}.d\overline{B}\right)dV \qquad (2\text{-}39)$$

The term on the right-hand side is the rate of increase of the stored magnetic energy:

$$W_m = \int_v \left(\int_0^B \overline{H}.d\overline{B} \right) dV \tag{2-40}$$

The input power P_E may be expressed in terms of magnetic vector potential $\overline{A}$ rather than $\overline{E}$ by using the definition of $\overline{A}$:

$$\overline{B} = \overline{\nabla} \times \overline{A} \tag{2-41}$$

in Faraday's law:

$$\overline{\nabla} \times \overline{E} = -\frac{\partial \overline{B}}{\partial t} \tag{2-42}$$

Hence:

$$\overline{\nabla} \times \overline{E} = -\frac{\partial}{\partial t}(\overline{\nabla} \times \overline{A}) \tag{2-43}$$

Neglecting the electrostatic potential, which is true if there are no power losses, then:

$$\overline{E} = -\frac{\partial}{\partial t}\overline{A} \tag{2-44}$$

Substituting the expression for $\overline{E}$ in (2-44) into (2-39) gives:

$$P_E = \int_v \overline{J}.\frac{\partial \overline{A}}{\partial t} dV \tag{2-45}$$

Which becomes:

$$P_E = \frac{\partial}{\partial t} \int_v \left(\int_0^A \overline{J}.d\overline{A} \right) dV \tag{2-46}$$

The integral is the net input electrical energy [78]:

$$W_E = \int_v \left(\int_0^A \overline{J}.d\overline{A} \right) dV \tag{2-47}$$

Then (2-44), (2-41) and (2-42) give:

$$\int_v \left(\int_0^B \overline{H}.d\overline{B} \right) dV = \int_v \left(\int_0^A \overline{J}.d\overline{A} \right) dV \tag{2-48}$$

That states that stored magnetic energy is equal to input electrical energy for lossless devices. Variational techniques such as finite element method obtain solution to field problem by minimizing the energy functional, F, that is the difference between the stored energy and the input (applied) energy in the system volume [79]. Thus, for magnetic systems, (2-40), (2-47) and (2-48) give

$$F = \int_v \left(\int_0^B \overline{H}.d\overline{B} - \int_0^A \overline{J}.d\overline{A} \right) dV \tag{2-49}$$

F is minimized when:

$$\frac{\partial F}{\partial A} = 0 \tag{2-50}$$

Thus: $$\int_v \left(\frac{\partial}{\partial A} \int_0^B \overline{H}.d\overline{B} - \overline{J} \right) dV = 0 \tag{2-51}$$

The functional F is changed from (2-49) if losses due to induced currents exist. In linear induction problems F becomes:

$$F = \int_v \left(\frac{B^2}{2\mu} - \overline{J}.\overline{A} + j\omega \frac{1}{2} \sigma \overline{A}^2 \right) dV \tag{2-52}$$

Where $\overline{J}$ is the applied current density of angular frequency ω, μ is permeability, and σ is conductivity.

ii. Finite element formulation

Minimization of the magnetic energy funcational over a set of finite elements leads to a matrix equation that can be solved for the potential $\bar{A}$ throughout the mesh. The assembly of this matrix equation is here derived for the case of planar induction problems.

Figure 2-6 shows the coordinate system for planar problems, along with part of a typical finite element mesh. The entire planar mesh may represent, for example, the stator and rotor laminations and air gap of a motor. Figure 2-7 shows an example for generated mesh in Maxwell® in order to formulate the problem. The analyzed device must be subdivided into triangles or quadrilaterals called finite elements. Each of these elements has three or four vertices called grid point. Given the motor geometry, this mesh can be automatically generated in the software for the best solution accuracy.

In such two-dimensional problems, $\bar{J}$ and $\bar{A}$ are assumed to be directed out of or into the page. Within each triangular finite element A is assumed to vary linearly according to:

$$A = \sum_{k=l,m,n} \frac{A_k}{2\Delta}(d_k + e_k X + f_k Y) \tag{2-53}$$

where Δ is the triangle area.

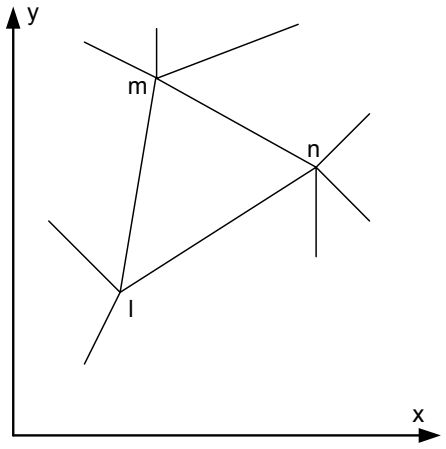

Figure 2- 6 Typical triangular finite element connected to other finite elements.

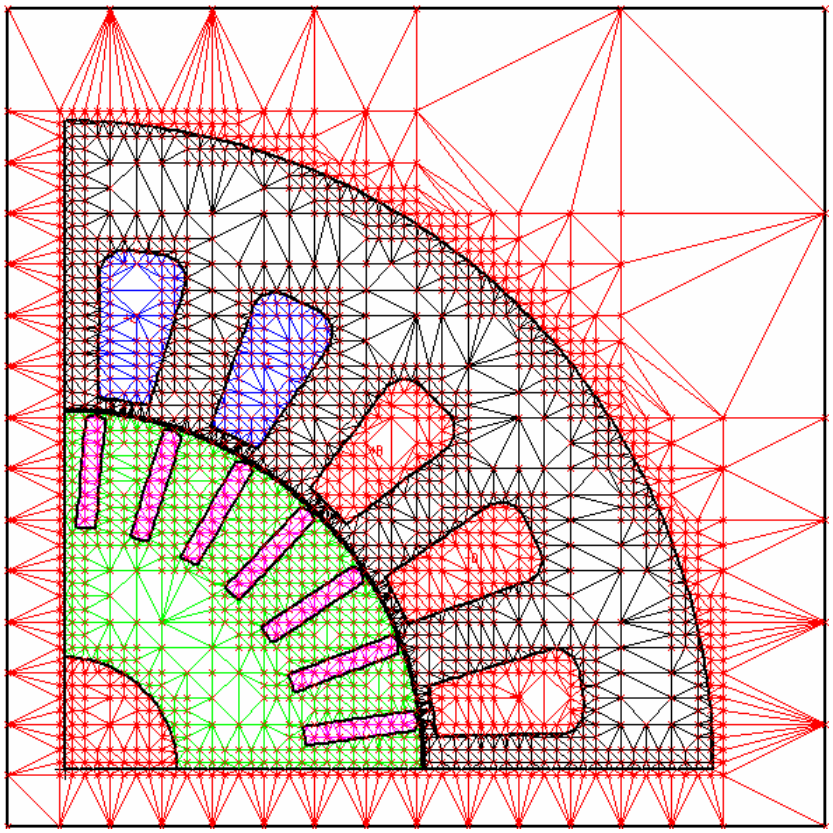

Figure 2- 7 Mesh generated by a Maxwell®.

Evaluating (2-53) at three vertices gives the solution for the *d, e, f* coefficient:

$$\begin{bmatrix} d_l & d_m & d_n \\ e_l & e_m & e_n \\ f_l & f_m & f_n \end{bmatrix} = 2\Delta \begin{bmatrix} 1 & x_l & y_l \\ 1 & x_m & y_m \\ 1 & x_n & y_n \end{bmatrix}^{-1} \tag{2-54}$$

The magnetic field in a triangle is:

$$\overline{B} = \overline{\nabla} \times \overline{A} = \overline{\nabla} \times A\overline{u}_z \tag{2-55}$$

$$\overline{B}(x,y) = -\frac{\partial A}{\partial y}\overline{u}_x + \frac{\partial A}{\partial x}\overline{u}_y \tag{2-56}$$

where $\overline{u}_x$, $\overline{u}_y$, and $\overline{u}_z$ are unit vectors. Substituting (2-53) into (2-56) gives:

$$\overline{B}(x,y) = \frac{1}{2\Delta}\sum_{k=l,m,n}\left[-f_k A_k \overline{u}_x + e_k A_j \overline{u}_y\right] \tag{2-57}$$

Thus the magnetic field is constant within a particular triangular finite element. Quadrilateral finite elements are composed of two or four triangles. The grid point potentials A_k can be found by minimizing the functional (2-52), which becomes for planar problems:

$$F = \int_s \left(\frac{B^2}{2\mu} - JA + j\omega\frac{1}{2}\sigma A^2 \right) dS \tag{2-58}$$

Where *dS=dx.dy*. Substituting (2-58) into (2-50) and considering one triangular finite element yields:

$$\int_s \frac{\partial}{\partial A_j}\left(\frac{B^2}{2\mu} - JA + \omega\sigma A^2 \right) dS = 0 \ , \ \ j = l,m,n \tag{2-59}$$

Integration over the triangle can be shown to yield the 3×3 matrix equation:

$$[R][A]+j[M][A]=[C] \tag{2-60}$$

Where:

$$[R]=\frac{v}{4\Delta}\begin{bmatrix}(e_l e_l+f_l f_l) & (e_l e_m+f_l f_m) & (e_l e_n+f_l f_n)\\ (e_m e_l+f_m f_l) & (e_m e_m+f_m f_m) & (e_m e_n+f_m f_n)\\ (e_n e_l+f_n f_l) & (e_n e_m+f_n f_m) & (e_n e_n+f_n f_n)\end{bmatrix} \tag{2-61}$$

$$[M]=\frac{\omega\sigma}{12}\begin{bmatrix}2 & 1 & 1\\ 1 & 2 & 1\\ 1 & 1 & 2\end{bmatrix} \tag{2-62}$$

$$[C]=\frac{J\Delta}{3}\begin{bmatrix}1\\ 1\\ 1\end{bmatrix} \tag{2-63}$$

(2-60) through (2-63) solve for the potential A in a region containing the one triangle with nodes *l, m,* and *n* in Figure 2-6. For practical problems with *N* nodes (grid points), the above process is repeated for each finite element, obtaining matrices [R] and [M] with *N* rows and columns. [C] and [A] are then column vectors containing N rows of complex terms.

iii. Boundary conditions

An *N*×*N* finite element matrix equation such as (2-60) can be solved for the grid point potential A using sparse matrix techniques. Generally, all interior grid points are unconstrained, while grid points on the exterior of the mesh are constrained in a manner dependent on the boundary conditions at the exterior of the region analyzed.

In two dimensional planar problems a flux line is a line of constant magnetic vector potential A. For most electrical machines with steel exterior surface, the flux is assumed

confined to the steel outer boundary. By using the boundary condition, A=0, flux lines are constrained to follow the boundary.

Absence of any constrain on an exterior grid point can be shown to cause the flux lines to be perpendicular to the finite element mesh boundary condition. In any electrical machine having identical poles, each pole boundary has periodic boundary condition. For rotary planar machines, periodic boundary conditions are expressed in polar (r,θ) coordinates as:

$$A(r,\theta_0 + p) = -A(r,\theta_0) \tag{2-64}$$

Where θ_0 is the angle of one radial boundary and p is the pole pitch angle. This is often called a NEGA boundary condition.

v. Solution techniques

Once the matrix equation has been assembled and A constrains have been enforced, solution for A at the unconstrained grid points may proceed. If the permeability μ, is known throughout the region, then (2-63) can be solved directly by Gauss-Jordan elimination. Grid renumbering to minimize the bandwidth of the sparse [R] matrix can be used to reduce computer storage and time. Usually, the computer time is proportional to the number of unknown grid point potentials taken to a power between 2 and 3. For most electrical machines models of one pole pitch, the time ranges from a few hours on a personal computer to a few minutes on a medium size computer.

If the permeability μ is not constant, then the [R] matrix depends on the magnitude of B (and J). An iterative procedure is developed by expanding (2-50) in a multidimensional Tylor series:

$$\left|\frac{\partial F}{\partial A_i}\right|_{A+\delta A} = \frac{\partial}{\partial A_i}\Big|_A - \sum_j \frac{\partial^2 F}{A_i A_j}\Big|_{A+\delta A} \delta A_j + \ldots \tag{2-65}$$

Where *i* and *j* are integers varying from 1 to N. substituting (2-65) in (2-50) gives the matrix equation:

$$A_j = -\left|\frac{\partial^2 F}{\partial A_i \partial A_j}\right|^{-1}_{A+\partial A} \frac{\partial F}{\partial A_i}\Big|_{A+\partial A} \tag{2-66}$$

This equation is based on Newton's iterative process used to solve for A in a saturable magnetic device. The Jacobian matrix in (2-66) is first estimated from an initial solution using approximate material permeabilities. Then (2-66) is solved repeatedly until the correction A_j is negligibly small. In each solution of (2-66) both the Jacobian matrix and the residual vector in its right-hand side are reevaluated based on the latest A values, enabling rapid convergence to the correct saturable potentials A throughout the device.

The exact expression for the Jacobian matrix and residual vector are derived elsewhere for planar [80] and for ax-symmetric [81] problems. The technique requires knowledge of reluctivity $v(=1/\mu)$ and of $\partial v/\partial B^2$ in each nonlinear material. In the FEM software these parameters are automatically computed from B-H curves supplied as input data.

vi. Parameter from field

While the distribution of magnetic vector potential A obtained above has little meaning to design engineers, many useful parameters can be calculated from it. For instance, Maxwell® postprocessor can obtain parameters of significant interest to electromagnetic device designers.

The flux density B is calculated in each finite element using the curl of A as defined in (2-41). Also, flux plots are obtained and displayed using the interactive preprocessor and postprocessor Maxwell®. Both monochromic flux line plots and color flux density plots are created. Flux densities and flux plots tell the designer where steel should be added and where it can be removed.

From A the flux flowing between any two points is easily obtained. The definition of flux φ is:

$$\varphi = \int \overline{B}.d\overline{S} \tag{2-67}$$

Substituting the definition of A from (2-66) gives:

$$\varphi = \int \overline{\nabla} \times \overline{A}.d\overline{S} \tag{2-68}$$

From Strokes' identity the surface integral may be replaced by a closed line integral around the surface:

$$\varphi = \oint \overline{A}.d\overline{l} \tag{2-69}$$

Thus, for two-dimensional problems the flux between any grid point 1 and 2 is simply:

$$\varphi_{12} = (A_1 - A_2).d \tag{2-70}$$

Where d is depth (stack) into the page.

Also the inductance or impedance seen by each current-carrying coil are obtained from distribution of A. The saturable inductance L is calculated from magnetostatic problems using:

$$\frac{L}{d} = \frac{J}{3I^2} \sum_{n=1}^{N_j} \left(S_n \sum_{k=1}^{3} A_k \right) \tag{2-71}$$

Where d is the depth (stack height) of planar devices, I is the coil current, N_j is the number of elements containing J, and S_n is finite element area.

The calculated impedance for the problems with induced currents contains both resistive and inductive components. For example, for ax-symmetric problems the impedance of a coil is:

$$\overline{Z} = \frac{j\omega \overline{A}_{ave} N}{I_s} 2\pi r_0 \tag{2-72}$$

Where r_0 is the average radius (distance to the axis of symmetry) of the source current, $\overline{A}_{ave}$ is the average phasor magnetic potential over the source current region, and N is the number of conductors carrying $I_s = J_s \times$ (the area of one conductor).

Other outputs by Maxwell® are the $\overline{J} \times \overline{B}$ forces acting on each current-carrying finite element and the total current in each element. The current distribution in each conductor can be calculated including skin effects in single or multiple conductors.

The magnetic energy W_m of (2-40) is also calculated both in every finite element as well as integrated over the volume of the entire finite element mesh. Another useful energy calculated is the magnetic co-energy which is very useful in calculating force and torque:

$$W_c = \int \left(\int_0^H \overline{B}.d\overline{H} \right) dV \tag{2-73}$$

Giving some background on the FEM, the design procedure of SynRM rotor can be presented.

D. DESIGN PROCEDURE

The main purpose of the presented design method is to follow a systematic numerical approach in order to optimize the geometry of SynRM rotor. To do so, some of rotor geometry specs are selected as the design variables. The variables investigated here are the width and location of the flux barriers, insulation ratio in each flux barrier and the width of the tangential and radial rotor ribs. Also, the width of the rotor q-axis cut-out is analyzed.

The design is carried out using the two-dimensional finite element method, 2D-FEM. The SynRM rotor structure must be designed in such a way that it is possible to achieve the maximum torque per current ratio. The calculation method used to evaluate the torque takes into account the effect of cross saturation between the d- and q-axis inductances, but the effect of the iron losses on torque production is ignored.

1. Design strategy

The design is based on a 24-slot stator with full pitched stator windings and 61 mm inner diameter. Figure 2-8 shows the stator used for the finite element analyses. Basically, the stator is similar to the stator of a conventional induction motor; therefore

stator design is not repeated here. In all of the digital computer simulations, the amount of the ampere per turn in stator windings is kept constant but the current angle is changed such that the maximum torque per ampere is delivered. The above mentioned mechanical specifications of the rotor are varied in each simulation.

With the variation of arc radius and flux barrier width, it is possible to investigate the effect of the flux barrier number as well as their locations and widths on the motor torque. In the transversally laminated rotor, usually the widths of the tangential and radial ribs are not zero due to mechanical reasons. These parameters have a negative effect on the electromechanical torque and efficiency of SynRM. The bore of the stator is fixed. The effect of rotor q-axis cut-out is studied by changing the d-axis pole span (τ) width. In order to achieve a low q-axis inductance, the ribs of the transversally laminated type rotor should be as thin as mechanically possible. Usually due to punching of the lamination, the rib width should not be less than the thickness of the laminations. Here the lamination thickness is 0.5 mm so the width of tangential ribs cannot be less than 0.5 mm.

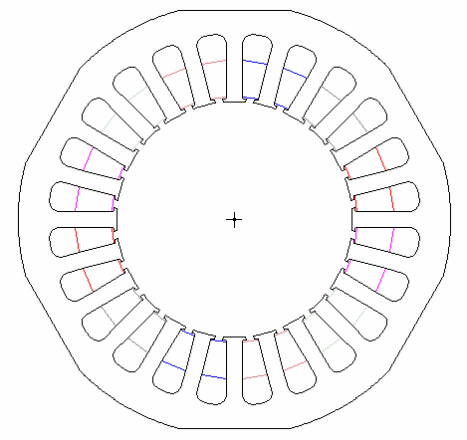

Figure 2- 8 Stator structure.

2. Design tool

The FEM solver used to analyze the different SynRM rotor designs is a non-linear, two dimensional, magneto-static solver. In this case, the effect of the end windings and flux scatterings at the both sides of the stator are ignored. The stator has 24 slots, 4 poles, and 61 mm inner diameter. So the slot pitch is 15 mechanical degrees. In the following investigations, the effects of different parameters on the torque production are studied with the aid of stepped calculations of finite element package with a constant ampere turn. Since the angular step for each simulation is one degree, totally 15 simulation steps are performed for one slot pitch rotation of the rotor.

By movement of the rotor over one slot pitch, all the torque ripples caused by permeance variations are taken into account during evaluation of the electromechanical torque. The torque waveform for the 15° interval along the air-gap is constructed of the torque values calculated for different rotor positions. The torque ripple is then calculated with respect to the mean value of the torque. Figure 2-9 shows the illustration of rotor design parameters.

With parameters number 2 and 5 it is possible to investigate the effect of the flux barrier number as well as the location and width on the motor torque. In the transversally laminated type the rotor tangential and radial ribs (parameters 3 and 4) must be set non-zero for mechanical reasons. These parameters have a strong negative effect on the SynRM motor properties. The effect of the air-gap length is studied by changing the rotor radius (parameter 1). The bore of the stator is fixed. The effect of rotor q-axis cut-out is studied by changing the d-axis pole span τ_p value. In order to achieve a low q-axis

inductance the ribs of the transverse laminated type rotor should be as thin as mechanically possible.

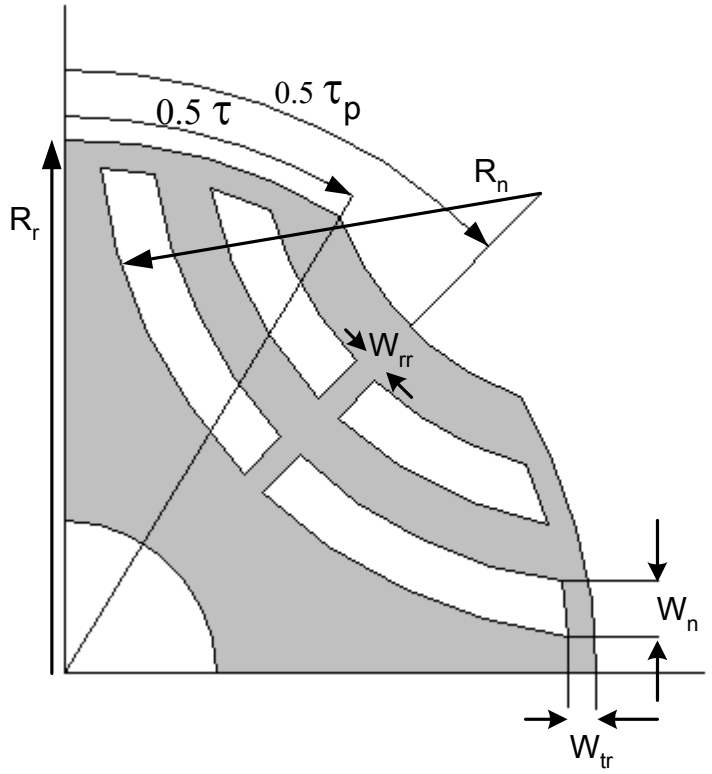

1. R_r - rotor radius
2. R_n - *n*th arc radius
3. W_{tr} - tangential rib width
4. W_{rr} - radial rib width
5. W_n - *n*th flux barrier width
6. τ_p - d-axis pole pitch
7. τ - d-axis pole span

Figure 2- 9 Illustration of design parameters.

i. Effect of the single flux barrier width

The effect of a single flux barrier width has been investigated by changing the width of the barrier as it is presented in Figure 2-10. At each step, the flux barrier width is increased by 2 mm. The calculated torques as functions of the rotor angles are shown in Figure 2-11 for different flux barrier widths. It may be assumed that by increasing the flux barrier width, the torque first increases from the initial value. The reason could be that the d-axis flux path reluctance does not change while the q-axis flux path reluctance increases rapidly. Of course after a certain value of flux barrier width, torque starts decreasing while the flux barrier width increases.

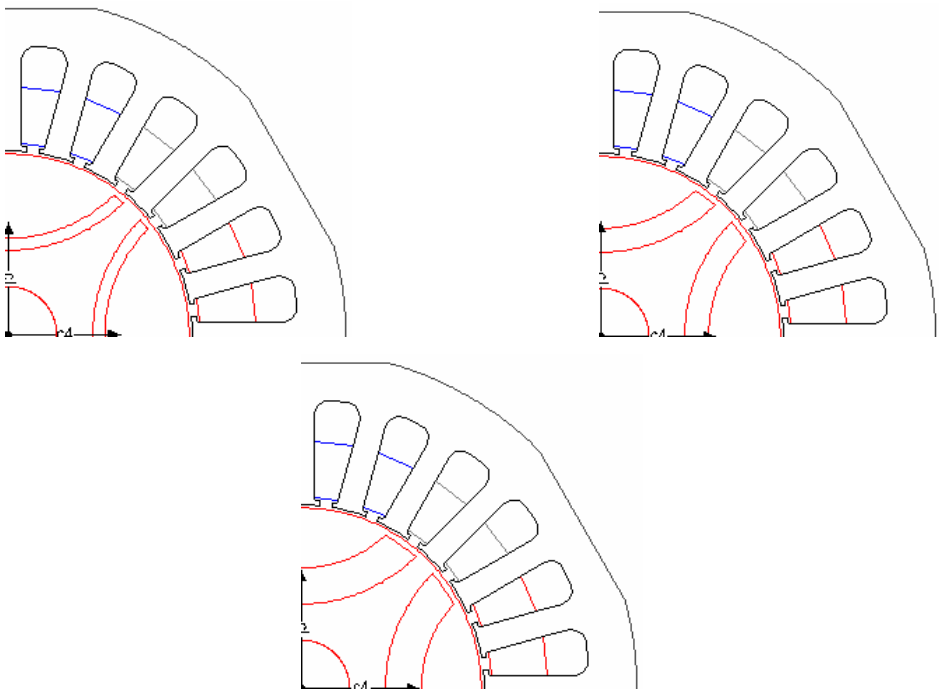

Figure 2- 10 Modification of one flux barrier width.

As it can be seen in Figure 2-11, the maximum and average level of the torque increase as a function of the barrier width, however, at the same time the torque ripple also increases. Because a constant current vector has been used, the air-gap flux varies due to the saturation effect in the stator teeth and tangential rib. Therefore, it reduces the smoothness of the flux distribution in the air gap. The distribution of the air gap flux and its smoothness is also a function of the ampere turn. Therefore the lower the amplitude of the current vector is, the lower the saturation levels in the stator teeth are, and consequently the lower the torque ripple is.

Figure 2-12 shows the average, maximum and minimum values of the torque shown in Figure 2-11. By increasing the single flux barrier width, the average torque first increases from 0.66 up to 0.8 at 5 mm width. After this point, the average value of torque does not change so much and seems to be constant.

Based on Figure 2-12, the absolute difference between the maximum and minimum torque, which means the torque ripple, drops to its minimum when the flux barrier width is equal to 7.5 mm. By increasing the flux barrier width while the q-axis inductance decreases, the d-axis inductance also decreases. This situation of flux linkages is illustrated in Figure 2-13. This figure shows the flux plots in the flux barriers with width of 2 mm and width of 8 mm.

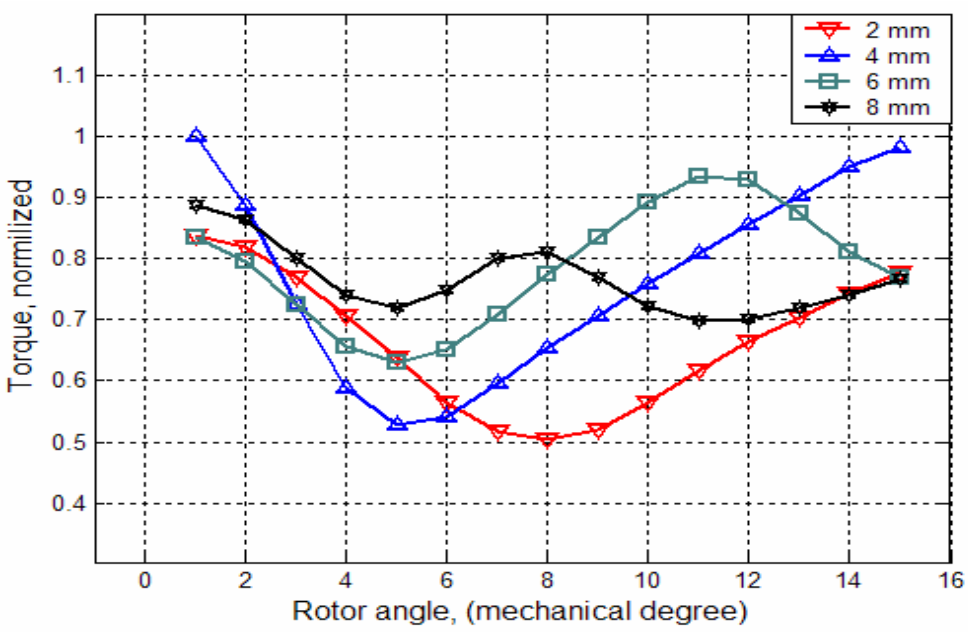

Figure 2- 11 The torque of a single flux barrier rotor as a function of the rotor angle barrier width.

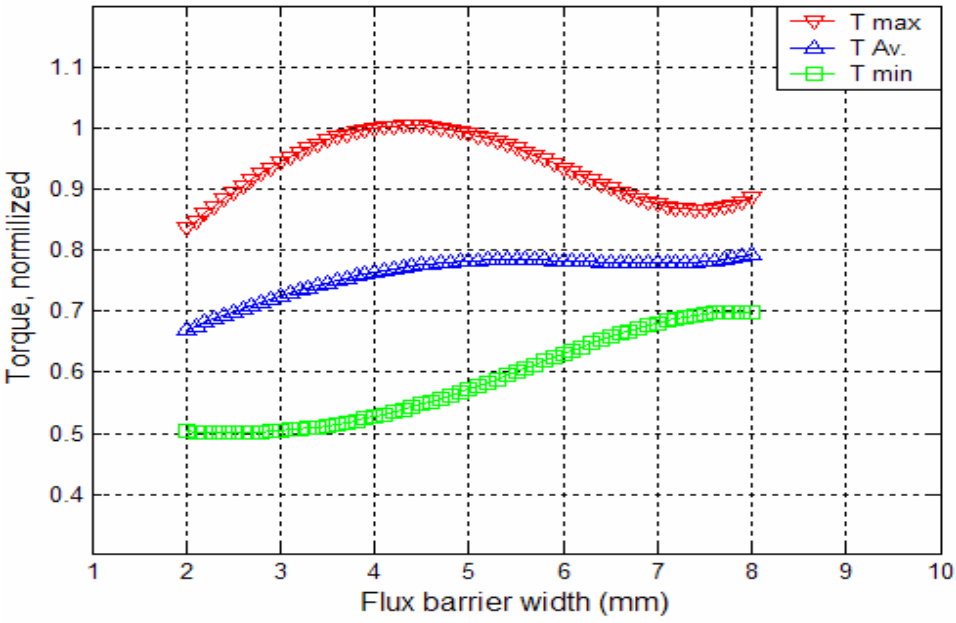

Figure 2- 12 The maximum, minimum and average normalized torque values as a function of flux barrier width.

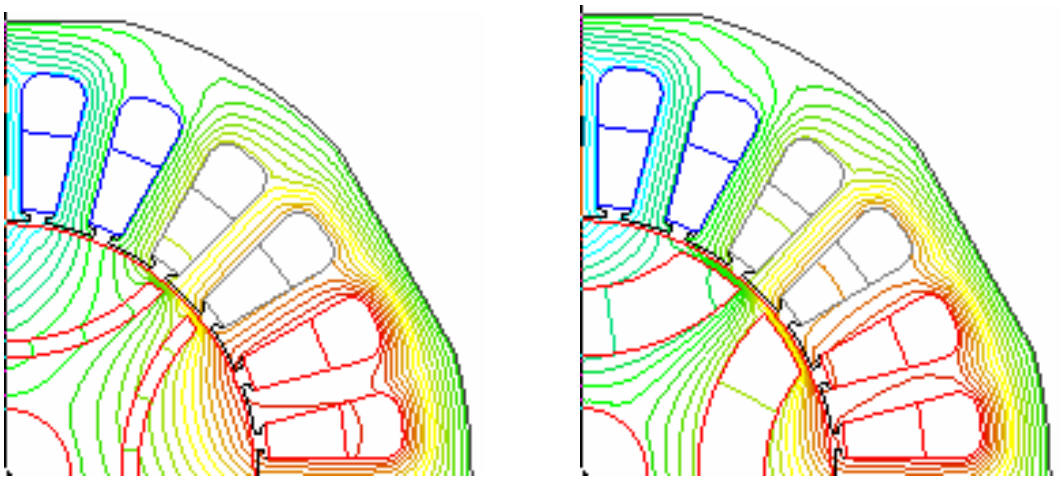

a) b)

Figure 2- 13 The flux plots with flux barrier widths of a) 2mm, b) 8mm.

By increasing the width of the flux barrier, the flux channels through the tangential rib will go back to the stator, using the shorter path. Even though the current vectors used in Figure 2-13 are equal, the position of the maximum flux has moved towards the d-axis direction. The same effect can also be noticed in Figure 2-11, where the location of the maximum torque versus rotor angle is moving as a function of the flux barrier width.

ii. Effect of the flux barrier location

The effect of the location of a single flux barrier with constant width is investigated by moving the barrier as shown in Figure 2-14. The replacement of the barrier is performed so that at each step the flux barrier moves 2 mm toward the flux barrier arc center point. The width of the flux barrier used here is set equal to the width given in previous step (4 mm).

The output torque of a single-flux-barrier-rotor is presented in Figure 2-15 as a function of the barrier location. In this figure, the lowest torque ripple over one slot pitch rotation is achieved using the barrier position 2 and 4. None of the flux barrier positions produce totally smooth torque. This means that in order to avoid a torque ripple when using several flux barriers the positions of the flux barriers should be selected such that the sum of torque ripples is minimized.

The data shown in Figure 2-15 are analyzed by calculating the average, minimum and maximum value of normalized torque over one slot pitch and are shown in Figure 2-16. According to this figure, in a rotor with one flux barrier, the torque ripple reaches to its minimum at the position 2. The reason is that in this position, the cogging torques at the both ends of the flux barrier cancel each other. The main flux variations are also minimized in this point.

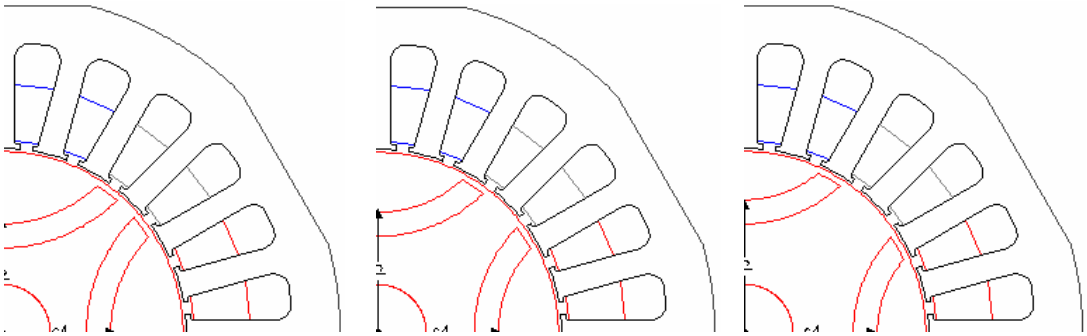

Position 1 Position 2 Position 3

Figure 2- 14 The direction of the flux barrier movement.

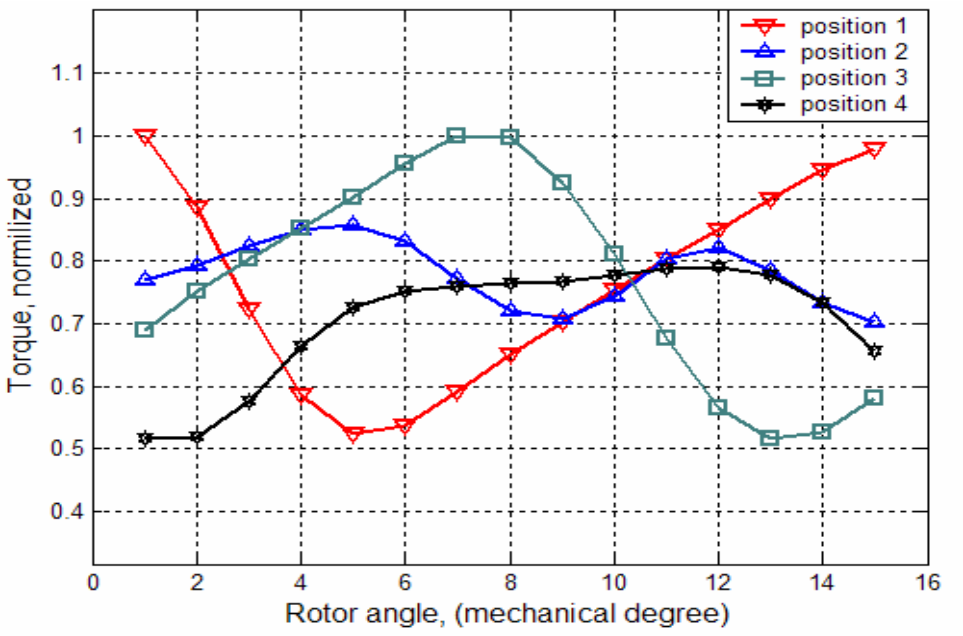

Figure 2- 15 The torque of a single flux barrier rotor as a function of the rotor angle.

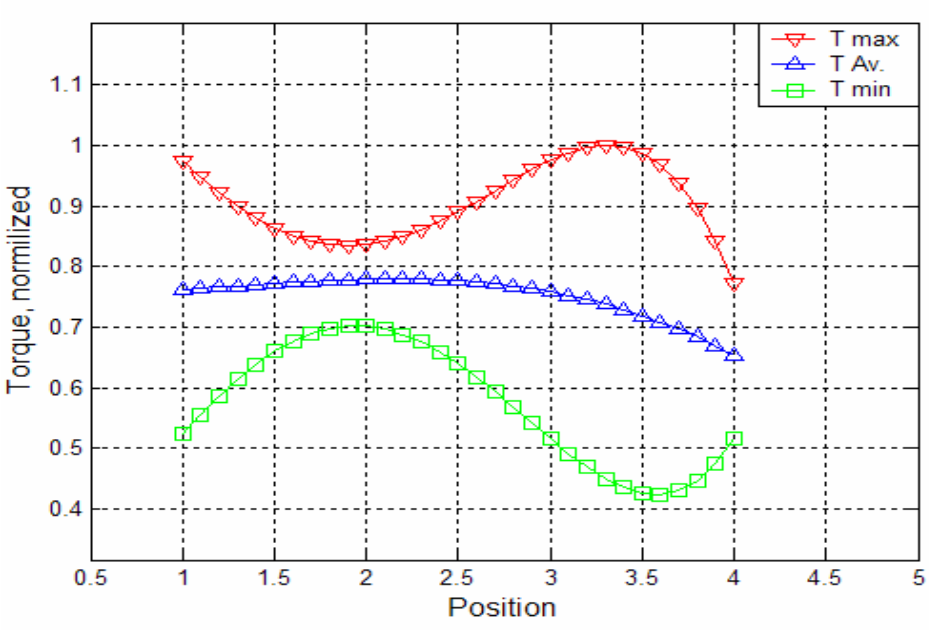

Figure 2- 16 The maximum, minimum and average torque as a function of the flux barrier location.

As the flux barrier starts moving from positions 1 to 2 the average torque increases slightly and then decreases. It can be inferred that after certain position, the d-axis flux does not increase significantly and mostly the q-axis inductance increases.

iii. Effect of the flux barrier insulation ratio

To investigate the effect of insulation ratio in the developed torque, a rotor with three flux barriers is considered. The sum of flux barrier width (insulation) and flux guide are kept constant in each simulation and just the ratio of their thickness is changed.

Figure 2-17 show the same rotor with 3 barriers and different insulation ratio. The insulation ratio is defined as:

$$W_{tot} = \frac{W_{ins}}{W_{ins} + W_{iron}}$$

where

W_{ins} - Sum of the widths of the flux barrier layers

W_{iron} - Sum of the widths of iron layers (flux guides).

Based on the results shown in Figure 2-18, the maximum torque is occurred at insulation ratio between 0.5 and 0.6.

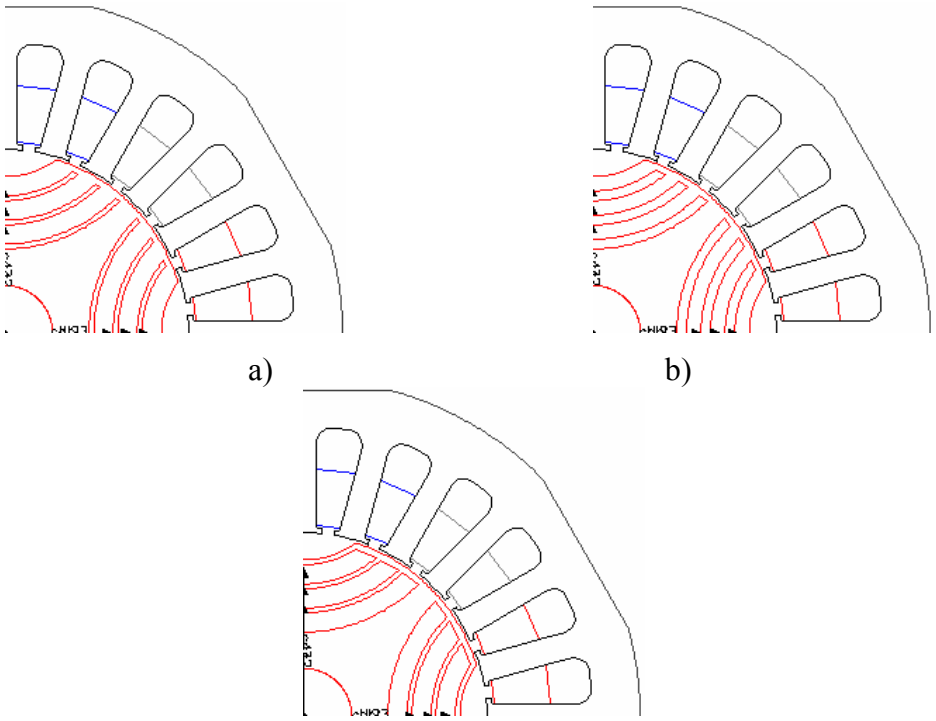

a) b)

c)

Figure 2- 17 Rotor with 3 barrier and different insulation ratio, a) W_{tot}=0.2, b) W_{tot}=0.4, c) W_{tot}=0.8.

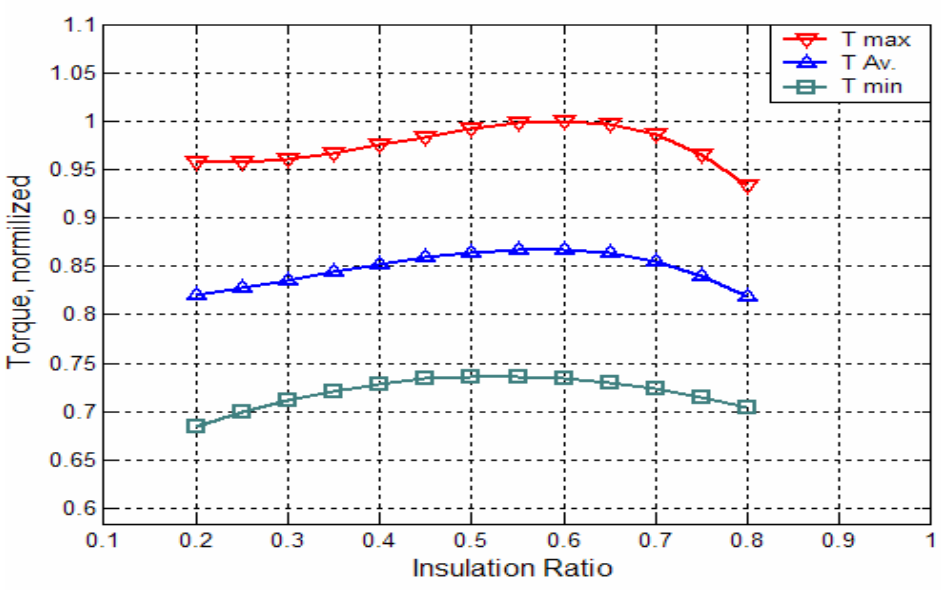

Figure 2- 18 The maximum, minimum and average torque as a function of the insulation ratio.

iv. Effect of the pole span on the pole pitch ratio

The torque to current ratio increases by increasing the air-gap width in the q-axis direction. In this case, a new parameter is introduced as the pole span over pole pitch ratio (τ/τ_p) and is defined in Figure 2-9. Figure 2-19 shows three salient pole rotor with different pole span on the pole pitch ratio. With this method, the d-axis flux path reluctance is kept quite stable as the q-axis reluctance increases. The limit for the pole span/pitch ratio is the value where the ratio between the d- and q-axes inductances starts decreasing. In this analysis, no flux barrier has been used in the rotor.

The electromechanical torque as a function of the pole span over pole pitch ratio is shown in Figure 2-20. According to this figure, the maximum torque per ampere condition is achieved using a pole span/pitch ratio of 0.55.

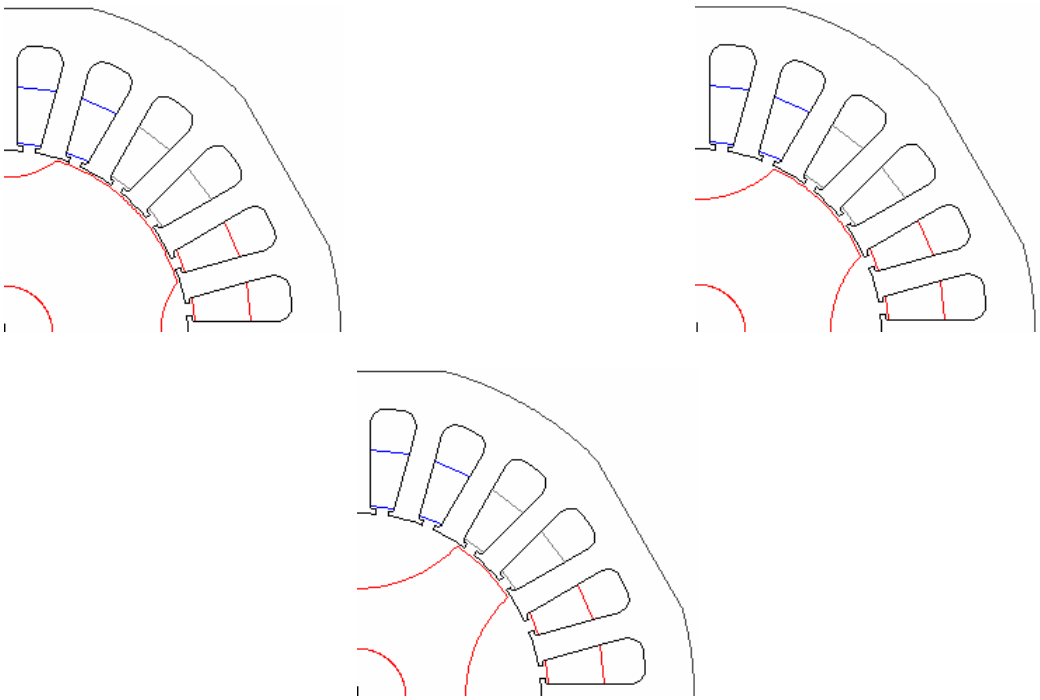

Figure 2- 19 The rotor structure with a pole span caused by the q-axis cut-out.

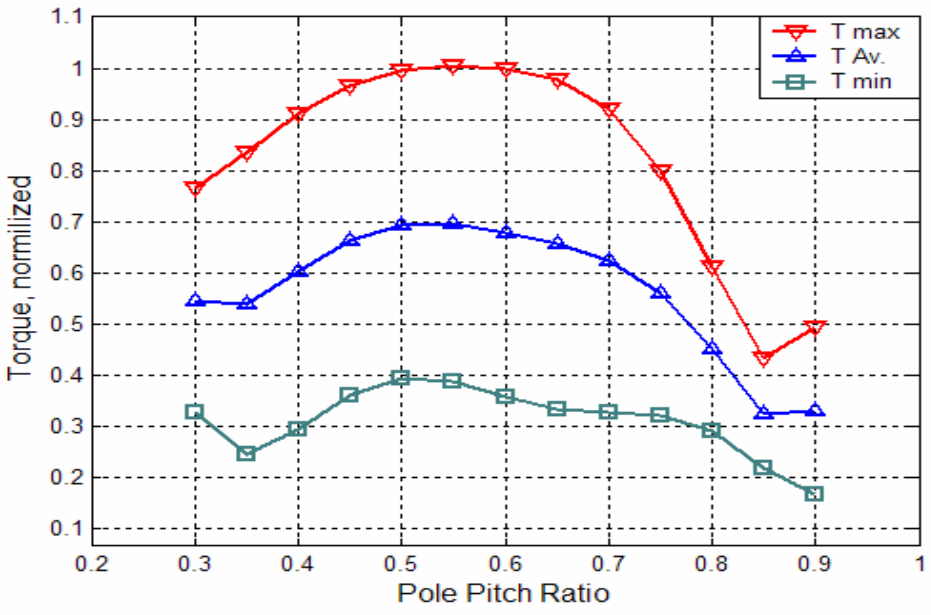

Figure 2- 20 The behavior of the torque as a function of the pole span ratio (τ_p/τ).

The minimum torque ripple is achieved at a higher pole span/pitch ratio than the corresponding maximum average torque. If the difference of the pole span/pitch ratio between these two extreme values is quite small it is recommended to select the pole span/pitch ratio correspondent to a lower torque ripple value. Higher pole span/pitch ratio brings a wider flux guide and more rigidity in the rotor structure.

v. Effect of the air-gap length

The air-gap length affects the direct axis inductance, the stator leakage flux inductance, the iron losses and the mechanical loss values. Decreasing the air-gap length increases effectively the d-axis inductance. The air-gap length effect on the q-axis inductance is minor because of its relatively large reluctance consisting of the rotor inner flux barriers.

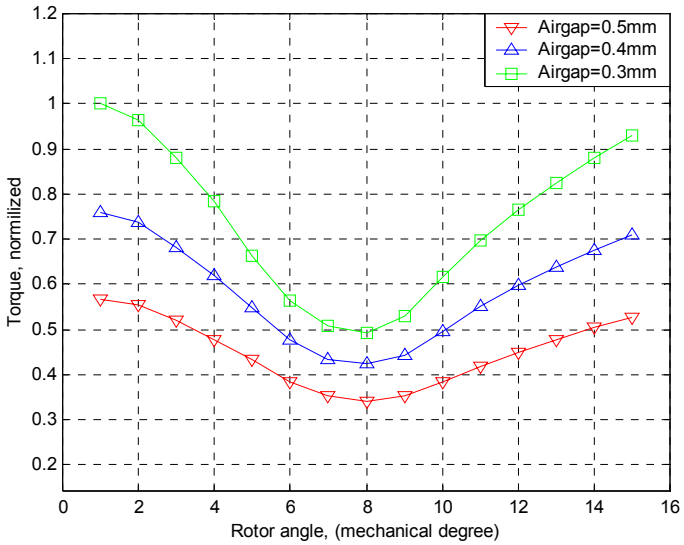

Figure 2- 21 Behavior of output torque as a function of the rotor angle and airgap.

Figure 2-21 illustrates the effect of the air-gap length on the output torque which can be inferred as an effect on d-axis self-inductance.

vi. Effect of the mechanical strutting

In the transversally laminated rotor, from mechanical forces point of view, the weakest parts are the tangential and the radial ribs. These ribs are shown in Figure 2-9. To have more rigidity in the rotor structure, it is desired to have wide flux guides and therefore the number and the width of the flux barriers are mechanically limited. Mechanical forces and stresses inside and on the surface of the rotor go up as the nominal power of the motor goes up. Therefore, the widths of the tangential and radial ribs must be increased in high power motors.

The q-axis flux path reluctance of the transversally laminated reluctance motor consist of the air-gap, the individual radial ribs, the tangential rib and the sum of the equal flux barrier reluctances.

(a) Radial rib

The effect of the width of the radial rib on the average torque and torque ripple is presented in Figure 2-22. The enlargement of the radial rib increases the q-axis inductance and decreases the average torque. The increase of the q-axis inductance decreases the saliency ratio and increases the effect of the cross saturation. In this case, use of small permanent magnet housed by radial ribs is recommended. These magnets saturate radial and tangential ribs such that the q-axis inductance is decreased. So drawbacks caused by radial and tangential ribs can be relatively eliminated.

(b) Tangential rib

Figure 2-23 presents the output torque as a function of the tangential rib widths. As it can be seen, an increase in the width of tangential ribs can reduce the output torque and performance of the SynRM dramatically.

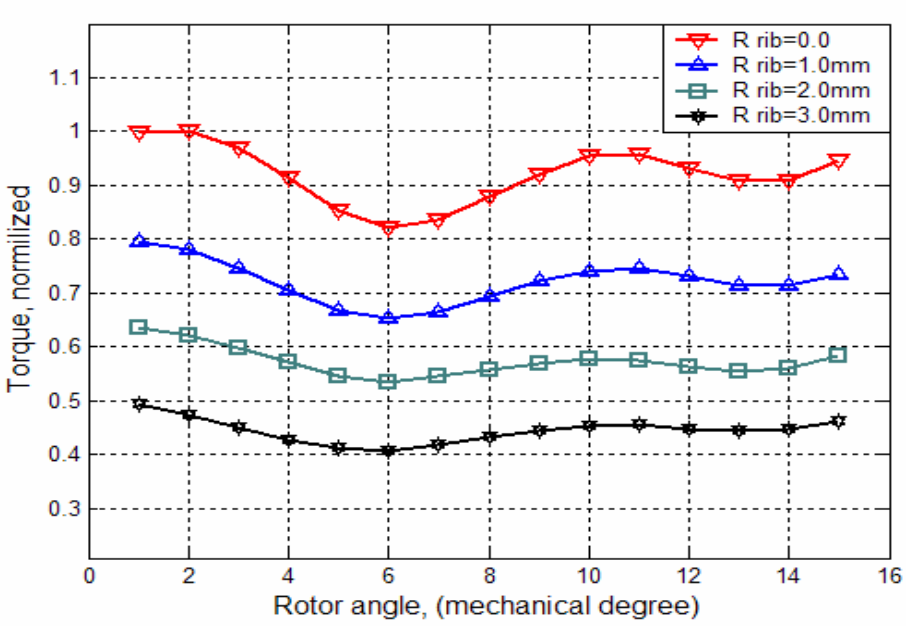

Figure 2- 22 Behavior of output torque as a function of the rotor angle and radial rib width.

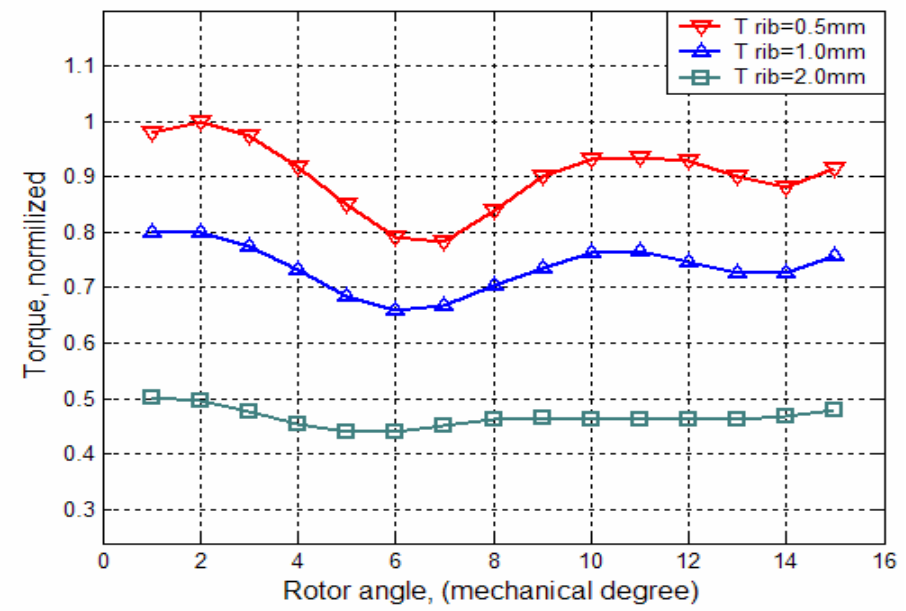

Figure 2- 23 Behavior of output torque as a function of the rotor angle and tangential rib width.

E. PROPOSED MOTOR

Based on the described design procedure, the rotor geometry can be obtained to meet the desired criteria and manufacturing limits such as minimum width of ribs and number of flux barriers. Figure 2-24 shows the geometry of the designed SynRM motor. As it was mentioned before, to improve the efficiency of the motor some Ferrite magnets are placed in the rotor. One of the features considered in the design of this motor is the magnetization of the Ferrites using stator windings. This feature will cause a reduction in cost and ease of manufacturing. To do so, the geometry of the rotor has been changed slightly to make it suitable for this purpose.

Figure 2-25 shows the same rotor with modified flux barriers and permanent magnets inside the core. The amount of the ferrite placed in the rotor core is limited by the geometry of the rotor and also the material cost. Also the permanent magnet flux in the air-gap and adjacent ribs is another factor to select the size of the ferrites. The amount of each permanent magnet is usually selected such that roughly 20% of its produced flux saturates the adjacent ribs.

Figure 2- 24 Rotor flux barriers geometry of optimized SynRM.

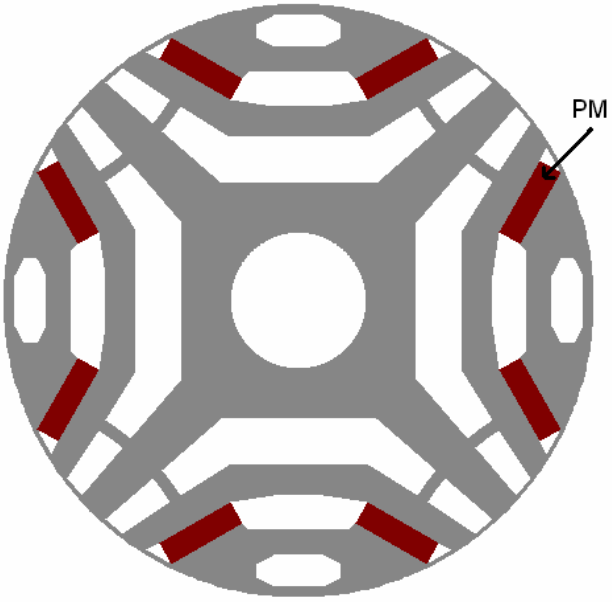

Figure 2- 25 Proposed PMaSynRM.

The magnetization of the ferrites is done through the stator windings. To do so, rotor q-axes is placed along the axis of the phase A. Then an avalanche current is applied to the star-connected stator winding while phase B and C are connected in parallel. This current can be obtained by discharging a capacitor in stator windings. In this case current is going though the phase A and coming out from phase B and C. Therefore, the stator flux vector is along with the phase A axis. It results in magnetizing the ferrite in a symmetric way. Figure 2-26 shows the stator and rotor in finite element software while magnetization current is applied to the stator winding to magnetize the ferrites mounted in rotor core. Generated flux and the flux density in the air gap due to the magnetized ferrites are shown in Figure 2-27.

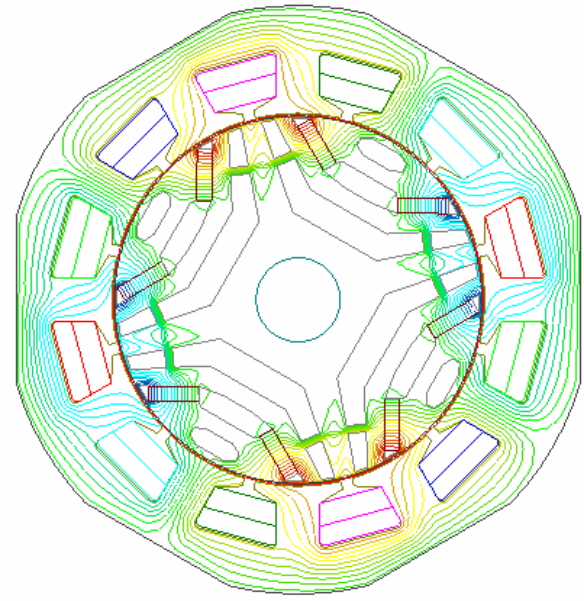

Figure 2- 26 Magnetization of PM through the stator windings.

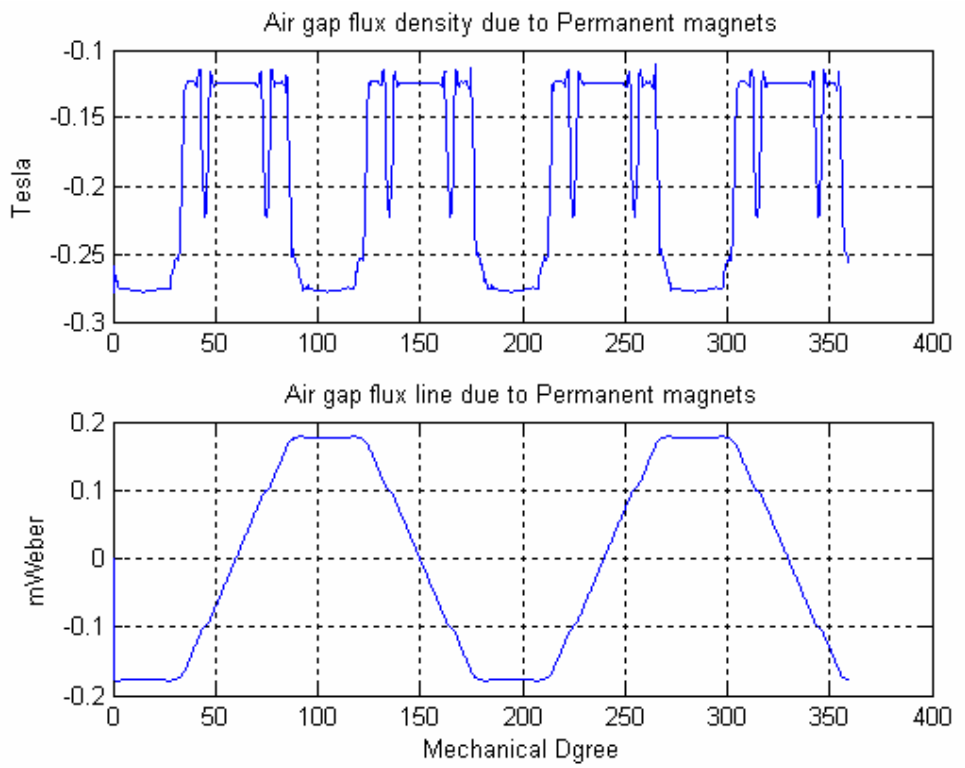

Figure 2- 27 Air gap flux density and PM flux while stator has one turn winding.

Figure 2-28 shows the stator of the proposed motor. Winding information is presented in Table 2-1. To calculate the d-q axes inductances, 3-phase stator flux is measured while rotor is placed on d- direction and on q-direction. Using the Park transformation, d and q axes fluxes can be obtained for different amount of stator current amplitude. Figure 2-29 shows the d and q axes flux while stator winding consisted of just one turn and magnets are placed in the rotor core.

Table 2- 1 Stator winding information

12 Slot *128 turn per phase, AWG17*					
Phase A		*Phase B*		*Phase C*	
In	*OUT*	*In*	*Out*	*In*	*Out*
1	*4*	*5*	*8*	*3*	*6*
1	*10*	*5*	*2*	*3*	*12*
7	*4*	*11*	*8*	*9*	*6*
7	*10*	*11*	*2*	*9*	*12*

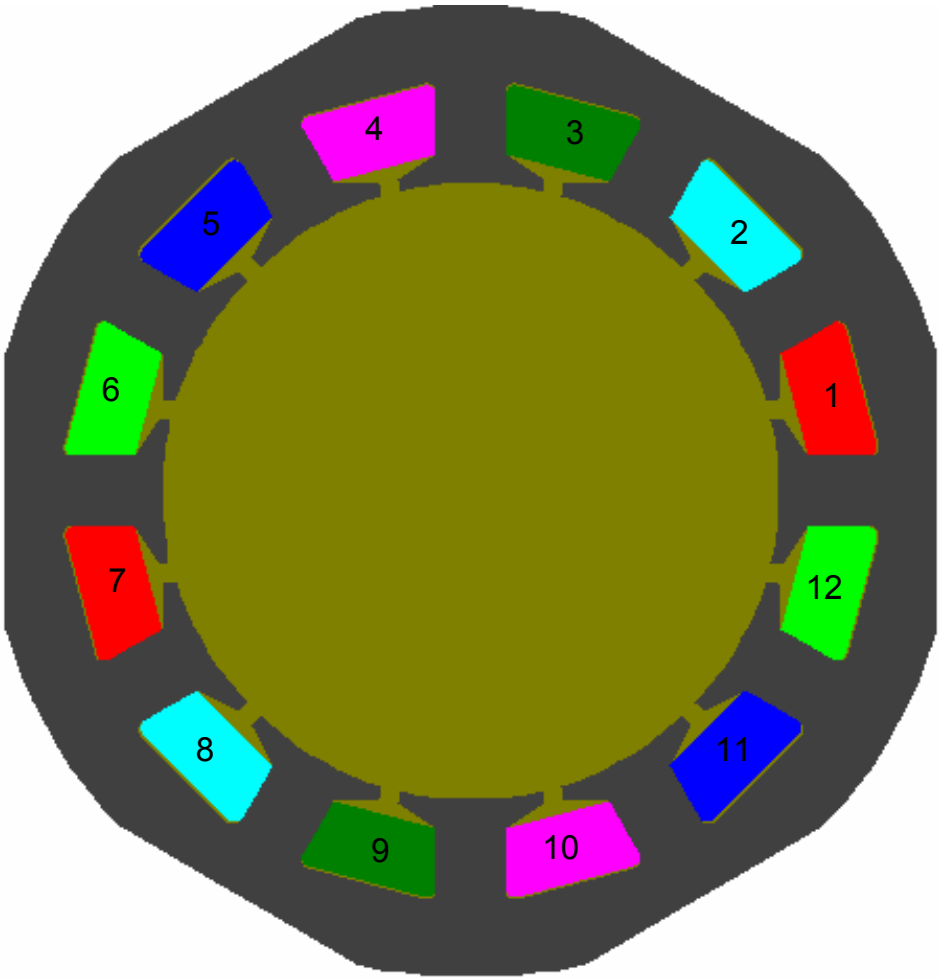

Figure 2- 28 Proposed stator.

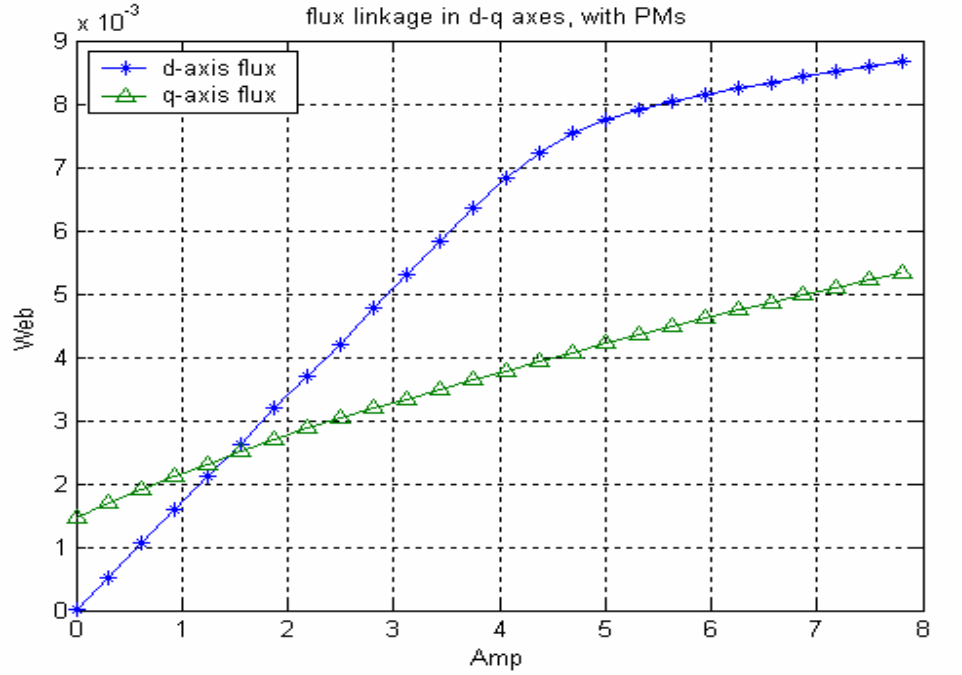

Figure 2- 29 Variation of d-q axes fluxes vs. stator current vector amplitude.

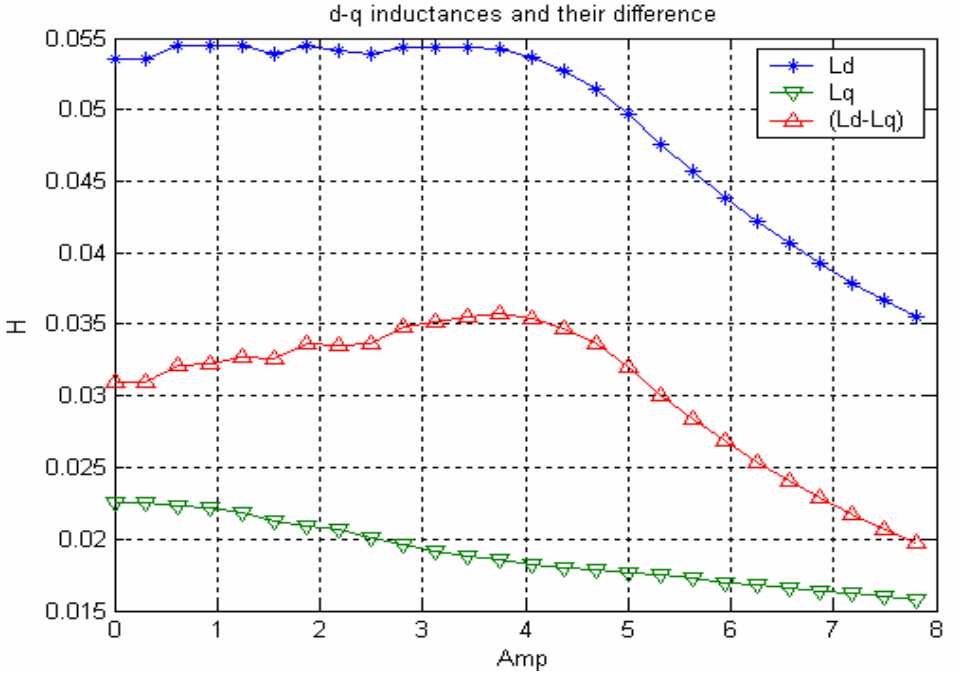

Figure 2- 30 Calculated d-q axes inductances.

Using the measured fluxes, d and q axes inductances can be calculated by use of winding information. Figure 2-30 shows the calculated d-q axes inductances.

The effects of inserted magnets on the d-q inductances and their difference and ratio can be seen by comparing the inductances of the SynRM without PMs in rotor core in Figure 2-31 and 2-32. As it can be inferred by inserting magnets in the rotor, the inductance ratio and their difference have increased which implies increase of power factor and torque density of the motor. These improvements are caused by saturation of the tangential and radial ribs inside the rotor core due to the permanent magnets fluxes. This saturation can be seen in Figure 2-33. As it can be seen, the adjacent tangential ribs are saturated.

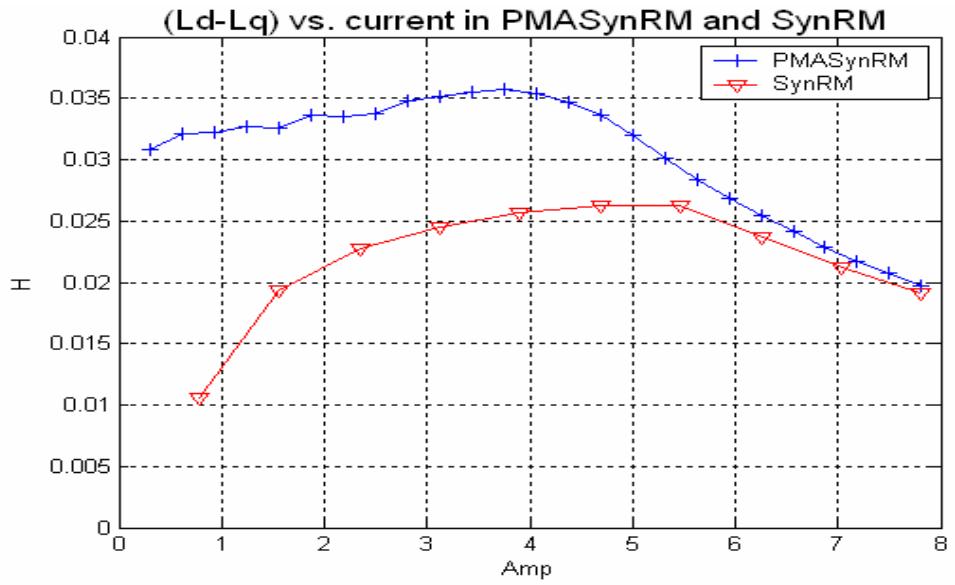

Figure 2- 31 (L_d -L_q) vs. current for PMa-SynRM and SynRM.

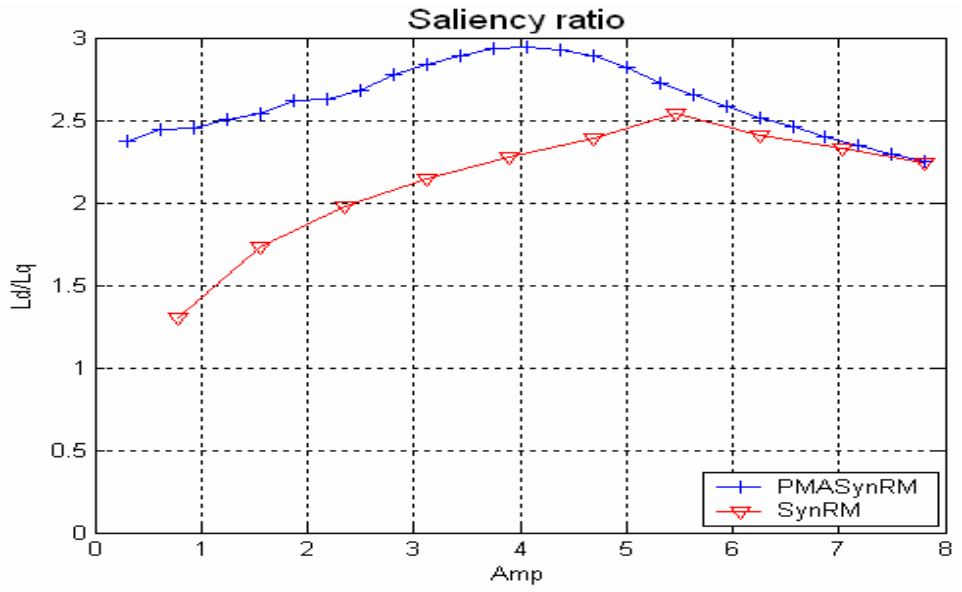

Figure 2- 32 Saliency ratio (L_d / L_q) vs. current.

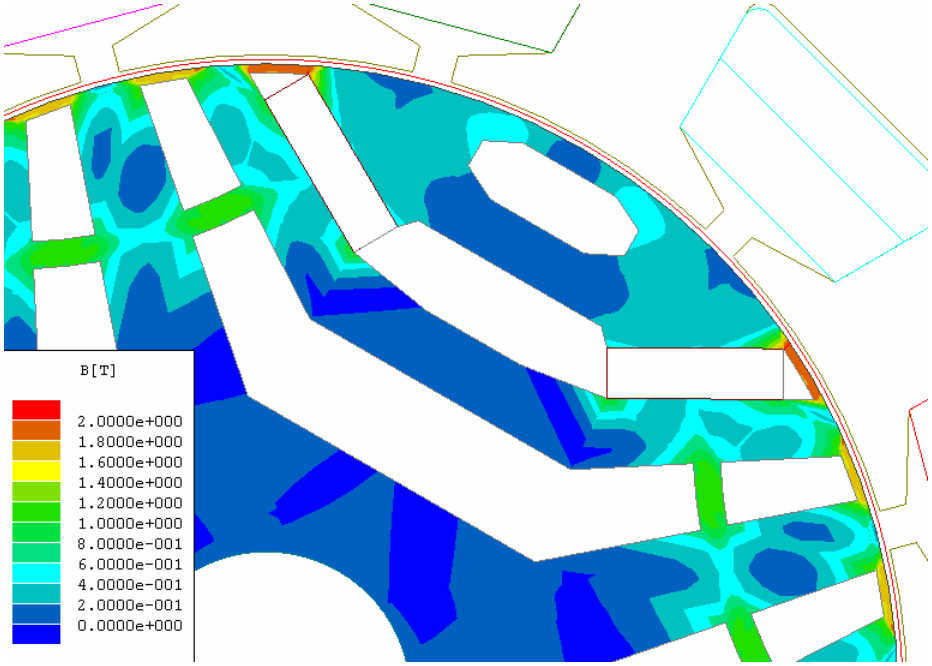

Figure 2- 33 Saturation effect due to the PM of the rotor.

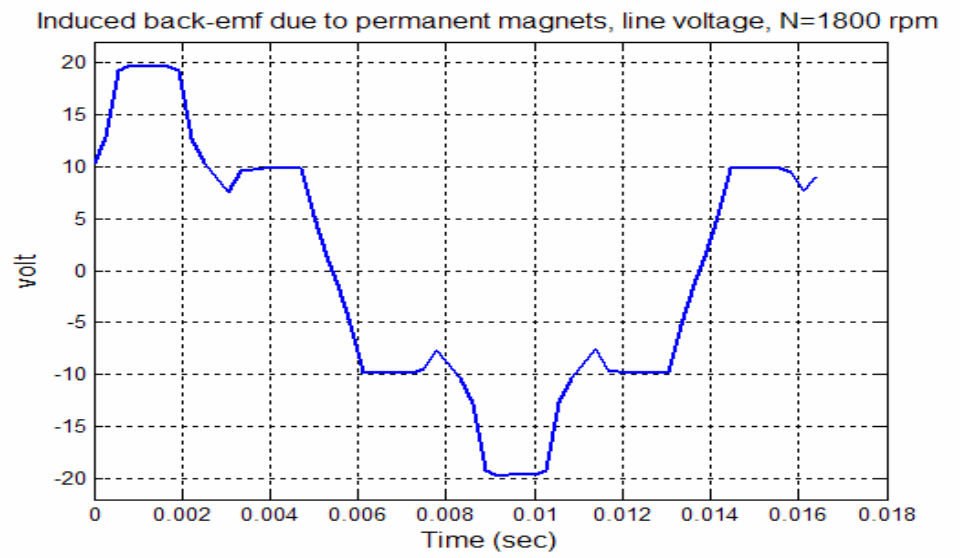

Figure 2- 34 Line-to-line back-EMF in PMa-SynRM.

Another important effect of the magnets is PM back-EMF. Figure 2-34 shows the line-to-line back-EMF at 1800 rpm due to permanent magnet fluxes, calculated in FEM.

The effect of the magnets on output torque also can be shown by comparing the torque-angle curve of SynRM and PMa-SynRM. Figure 2-35 shows the calculated torque angle curve of SynRM and PMa-SynRm.

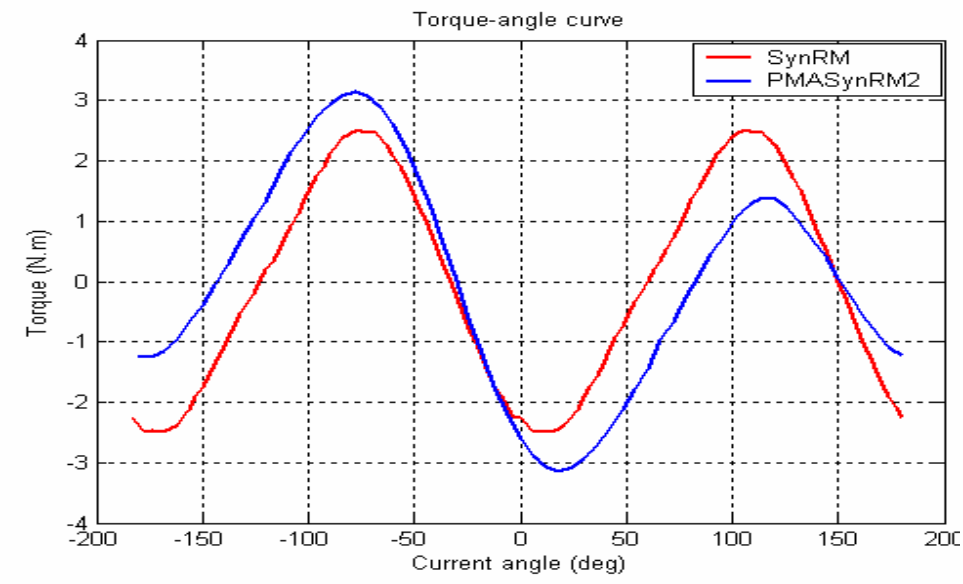

Figure 2- 35 Torque-angle curves of the PMa-SynRM and SynRM.

F. EXPERIMENTAL RESULTS

Figure 2-36 shows the rotor/stator laminations of the 1.5kW prototype motor. The implementation of the control system was carried out using a TMS320LF2407 based controller board. The controller runs the motor on maximum torque per current condition.

Figure 2-37 shows the waveform of the actual line-to-line back-EMF at shaft speed of 1800 rpm. In this test, the effect of non-sinusoidal back-EMF has been ignored in the current controller loop. As it can be seen, the back-EMF due to the permanent magnets flux linkages is in close agreement with the predicted one from simulation shown in Figure 2-34.

Figure 2-38 presents the torque-angle curve of the prototype motor. Since the reluctance torque in this motor is higher than the magnetic one, there are two positive and negative picks in this curve. Here, the knowledge of proper rotor angle is crucial to have the highest possible efficiency. In this case, some methods presented in literature for alignment of the rotor using stator excitation may not work properly. Table 2-2 shows the calculated efficiency of the PMa-SynRM using the FEM package and also from experiment compared with the SynRM motor with the same specs.

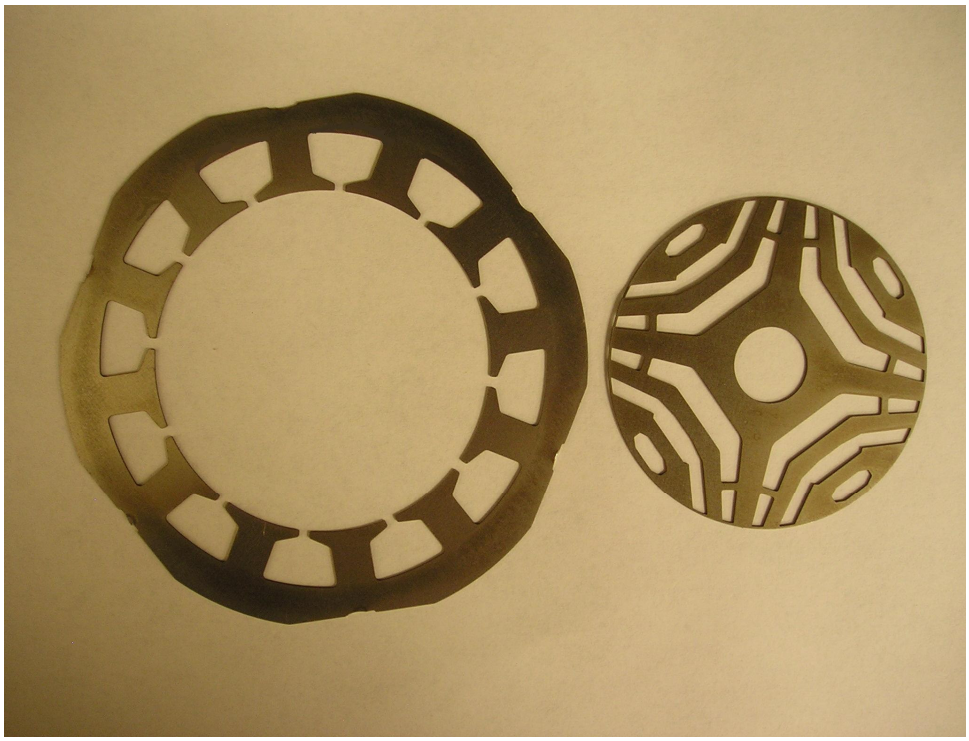

Figure 2- 36 Stator and rotor laminations of the proposed PMa-SynRM.

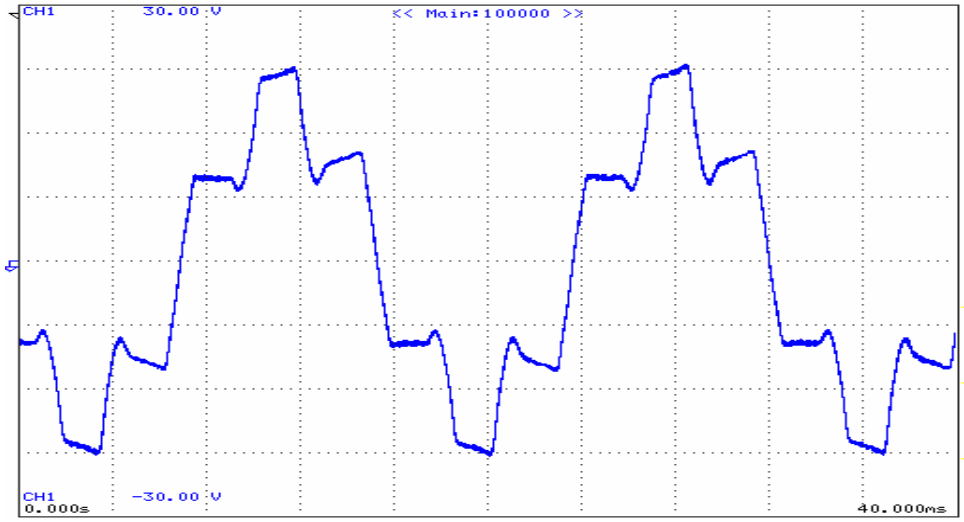

Figure 2- 37 Actual back-EMF line voltage at 1800 rpm.

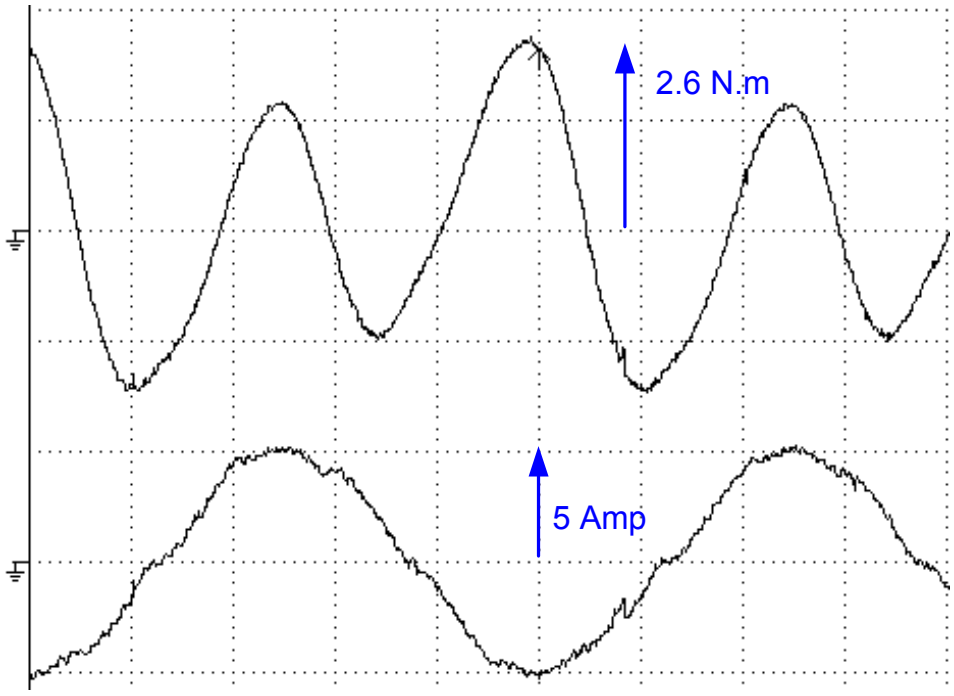

Figure 2- 38 Torque-angle curves of the PMa-SynRM.

Table 2- 2 Efficiency of proposed motor for T_{out}=2.2 N.m

ω_m (rpm)	1800	3600
η % PMa-SynRM (Simulation)	87	91.5
η % PMa-SynRM (Experimental)	84.8	88.8
η % SynRM (Simulation)	81	86

G. CONCLUSION

In this chapter, a FEM approach was performed to analyze the effects of rotor design variables such as the flux barrier width, flux barrier location, insulation ratio, pole span over pole pitch ratio, length of the radial and tangential ribs on SynRM performance. Effects of each variable were shown in the case of a four-pole transversally laminated SynRM.

A systematic procedure was applied to obtain the optimized geometry for rotor flux barriers. An insulation ratio of 0.4-0.6 should be selected to maximize the developed torque. Location of the flux barriers plays an important role in the torque ripple; however, it does not affect the average torque significantly. Minimum air-gap length is limited by the mechanical manufacturing limits. The lengths of tangential and radial ribs are determined by the mechanical stress ruggedness. These two variables affect the developed torque significantly and use of small magnets in the rotor is recommended to saturate these ribs and enhance the performance of the SynRM. Effects of the magnets on d-q inductances were studied and a comparison between output torque of SynRM and

PMa-SynRM was performed. Some experimental results on a 1.5 kW prototype motor were presented to validate the results of simulation studies.

CHAPTER III

ON-LINE PARAMETER ESTIMATION OF PM-ASSISTED SYNCHRONOUS RELUCTANCE MOTOR

A. INTRODUCTION

Interior permanent magnet motors (IPM) can offer high-efficiency motor drives by utilizing both torque productions due to the permanent magnet and the reluctance. It can offer a wide constant power region using the flux-weakening technique. However, drawbacks such as large d-axis current at high-speed during flux weakening region and the uncontrolled generator mode of operation following unexpected inverter shutdowns are restricting widespread applications of this motor. These problems are caused by the uncontrolled flux linkages produced by the permanent magnets. However, they can be eliminated in PMa-SynRM which is very similar to IPM. The amount of magnets and the magnet flux linkages are small in comparison with the conventional IPM and the reluctance torque has the most contribution in the developed torque. With respect to the conventional synchronous reluctance machine, this motor offers better torque capabilities and power factors.

In the most control systems of synchronous reluctance motors, controllers are parameter dependent and their performances rely on the knowledge of motor parameters. For example, the motor operation at maximum torque per ampere or its speed sensorless operation could be considered as the parameter dependent control systems.

Majority of techniques for optimizing torque production are sensitive to machines parameters. Unfortunately, stator resistance and permanent magnet flux vary with motor temperature [82]. The d and q axes total inductance, L_d and L_q, are known to depend on the airgap flux [83]. So in practical applications, on-line parameter estimation for L_d and L_q, are required to achieve maximum torque per ampere control.

Performance of the advanced parameter dependent control strategies can be improved by using the off-line model of the motor parameters. However, this is computationally intensive because of the non-linearity due to iron saturation. Such calculations are usually unreasonable in real time. Moreover, including cross saturation effect is very difficult and intensive in off-line parameter estimation.

In this chapter, a simple and practical method for parameter estimation of PMa-SynRM is introduced. This method is capable of identifying the d and q axes inductances and the permanent magnet back-EMF.

B. PARAMETER IDENTIFICATION ALGORITHMS

In the most of parameter estimation methods, the back-EMF due to permanent magnets is considered as a known sinusoidal waveform with constant amplitude. However, in PMa-SynRMs specially the ones with a low stator slot number; back-EMF is not necessarily sinusoidal. Moreover, permeability or flux linkage of the permanent magnets is affected by the variation of temperature.

Most parameter estimation approaches are dependent on the accurate measurement of the motor input signals. So if an accurate measurement system is not available, the

convergence of estimated parameters to their real value is not guaranteed. To overcome this problem, some of the estimation algorithms have utilized recursive least square (RLS) procedure. Having a persistence excitation condition is necessary in RLS based parameter estimator. This condition can guarantee the convergence of the estimated parameters to their real values. However, in the most of the practical applications, a persistent exciting signal is not presented at the machine operating point.

Several adaptive estimation methods have been proposed in the literature [66, 67, 68, 69]. The most common problem of these estimators is their dependency on accurate measurement and knowledge of the model.

C. PARAMETER ESTIMATION

The voltage and current equations of the PMa-SynRM in terms of machine variables can be obtained from a wound rotor synchronous motor. In this case, there is no winding or damper on the rotor and d-q axes inductances are not equal.

$$v_{abcs} = R_s i_{abcs} + \frac{d}{dt}\lambda_{abcs} \tag{3-1}$$

where

$$\begin{aligned} f_{abcs} &= \begin{bmatrix} f_{as} & f_{bs} & f_{cs} \end{bmatrix} \\ R_s &= diag\begin{bmatrix} r_s & r_s & r_s \end{bmatrix} \end{aligned} \tag{3-2}$$

The flux linkages can be introduced as

$$\lambda_{abcs} = L_s(\theta) i_{abcs} + \lambda_{pm} \tag{3-3}$$

Where $L_s(\theta)$ is the stator inductance matrix and is a function of the rotor position and is defined as (3-4) [70, 84].

$$L_s = \begin{bmatrix} L_{ls} + L_A - L_B\cos 2\theta_r & -\frac{1}{2}L_A - L_B\cos 2(\theta_r - \frac{\pi}{3}) & -\frac{1}{2}L_A - L_B\cos 2(\theta_r + \frac{\pi}{3}) \\ -\frac{1}{2}L_A - L_B\cos 2(\theta_r - \frac{\pi}{3}) & L_{ls} + L_A - L_B\cos 2(\theta_r - \frac{2\pi}{3}) & -\frac{1}{2}L_A - L_B\cos 2(\theta_r + \pi) \\ -\frac{1}{2}L_A - L_B\cos 2(\theta_r + \frac{\pi}{3}) & -\frac{1}{2}L_A - L_B\cos 2(\theta_r + \pi) & L_{ls} + L_A - L_B\cos 2(\theta_r + \frac{2\pi}{3}) \end{bmatrix} \quad (3\text{-}4)$$

L_{ls} is stator leakage inductance and L_A and L_B are defined based on the d-q axes inductances as (3-5).

$$\begin{aligned} L_A &= \frac{1}{3}(L_{md} + L_{mq}) \\ L_B &= \frac{1}{3}(L_{md} - L_{mq}) \end{aligned} \quad (3\text{-}5)$$

λ_{pm} is the flux linkages due to the permanent magnets and can be defined as

$$\lambda_{pm} = \lambda_m \begin{bmatrix} \sin(\theta_r) \\ \sin(\theta_r - \frac{2\pi}{3}) \\ \sin(\theta_r + \frac{2\pi}{3}) \end{bmatrix} \quad (3\text{-}6)$$

Figure 3-1 shows the four pole PMa-SynRM rotor designed and presented in Chapter II with the definition of d-q axes. The stator voltages and flux linkages equations of the PMA-SynRM in the d-q reference frame are expressed as follows.

$$\begin{aligned} v_d &= r_s i_{ds} + \frac{d}{dt}\lambda_{ds} - \omega_r \lambda_{qs} \\ v_q &= r_s i_{qs} + \frac{d}{dt}\lambda_{qs} + \omega_r \lambda_{ds} \end{aligned} \quad (3\text{-}7)$$

$$\begin{aligned} \lambda_{ds} &= L_{ls} i_{ds} + L_{md} i_{ds} = L_{ds} i_{ds} \\ \lambda_{qs} &= L_{ls} i_{qs} + L_{mq} i_{qs} = L_{qs} i_{qs} \end{aligned} \quad (3\text{-}8)$$

Suitable model for efficient and compact parameter estimation can be obtained by neglecting the derivative terms, which are zero at the steady state. Omission of derivative terms also separates the estimation of L_q from that of L_d and reducing the sensitivity of the estimator to the noise. Neglecting the higher order harmonics of the back-EMF, the corresponding model of the parameter estimator in the rotor reference frame can be obtained as,

$$\begin{aligned} v_{ds}^{r} - r_s i_{ds}^{r} - \omega_r \lambda_m &= -L_{qs} \omega_r i_{qs}^{r} \\ v_{qs}^{r} - r_s i_{ds}^{r} &= L_{ds} \omega_r i_{qs}^{r} \end{aligned} \tag{3-9}$$

Using a simple low pass filter and measuring the stator voltages and currents, parameters of the motor can be obtained [85]. Stator resistance and flux linkages are included in these models. In this method of parameter estimation, λ_m is considered to be constant. However, λ_m can vary due to the change of temperature, especially if ferrite magnets are used in the rotor core. Aging of the permanent magnets also can affect the amplitude of λ_m. In ferrite permanent magnets, usually a change of 80°C in temperature can cause almost a deterioration of 25% in permanent magnet flux density. These changes can be seen in Figure 3-2. Of course this demagnetization is reversible as long as the temperature is below 800°F.

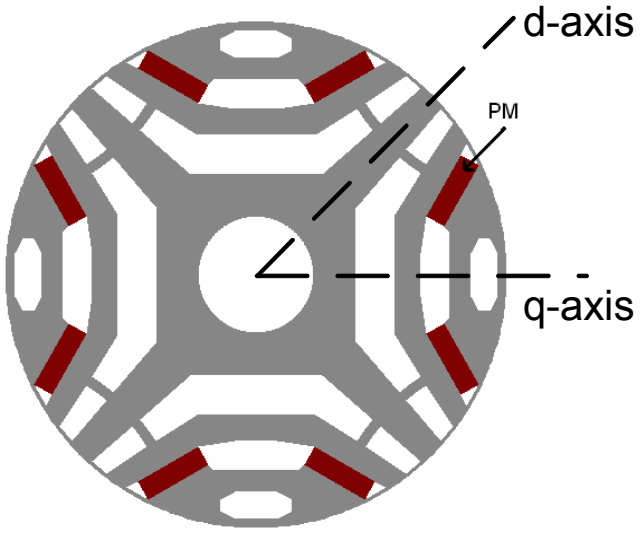

Figure 3- 1 A four pole PMa-SynRM rotor.

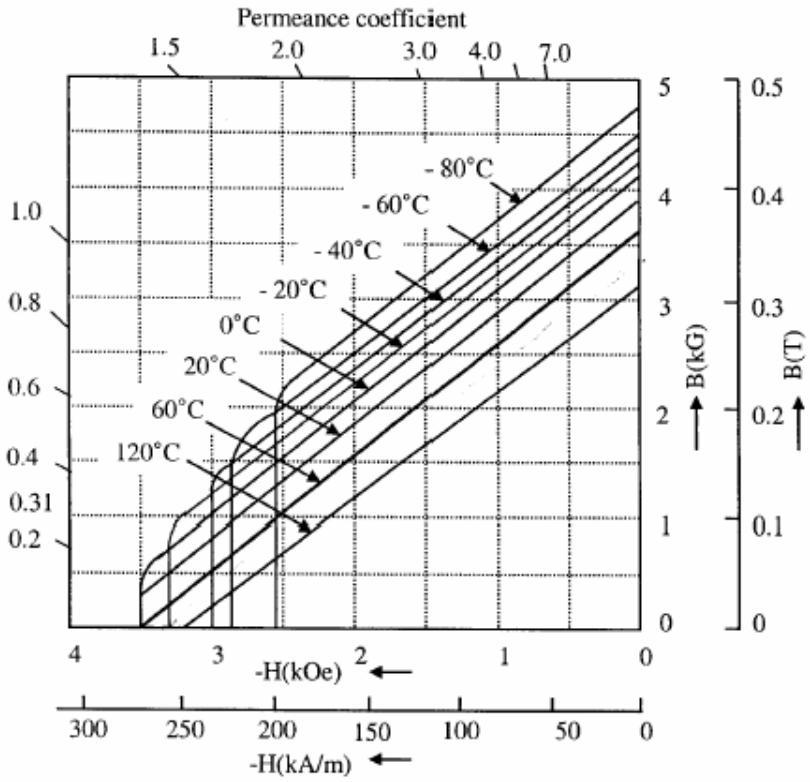

Figure 3- 2 B-H characteristics of ferrite.

Sensitivity of estimated L_{ds} and L_{qs} to change of λ_m and stator resistance r_s can be defined by (3-10) and (3-11).

$$\lambda_m \to \lambda_m \pm \Delta\lambda_m \quad , \quad r_s \to r_s \pm \Delta r_s \tag{3-10}$$

$$\frac{\hat{L}_{qs}}{L_{qs}} = 1 \mp \frac{\Delta\lambda_m}{L_{qs} i_{qs}} \quad , \quad \frac{\hat{L}_{qs}}{L_{qs}} = 1 \mp \frac{\Delta r_s i_{ds}}{\omega L_{qs} i_{qs}} \tag{3-11}$$

$$\frac{\hat{L}_{ds}}{L_{ds}} = 1 \pm \frac{\Delta r_s i_{qs}}{\omega L_{ds} i_{ds}} \tag{3-12}$$

Figure 3-3 and 3-4 show the sensitivity of estimated parameter to the change of permanent magnet flux and stator resistor. As it can be inferred from (3-11), the estimated L_q is very sensitive to λ_m at low torque and high speed due to the dominant back-EMF relative to the resistive voltage drop and cross-coupling $L_q \omega_r i_{qs}^r$ in (3-9). The sensitivity to r_s is relatively small in estimation of L_q and very small in estimation of L_d. To have an accurate estimation of parameters, knowledge of λ_m is also necessary. Moreover, demagnetization of permanent magnets is also another concern during operation of PMa-SynRM which can be avoided by estimation of λ_m.

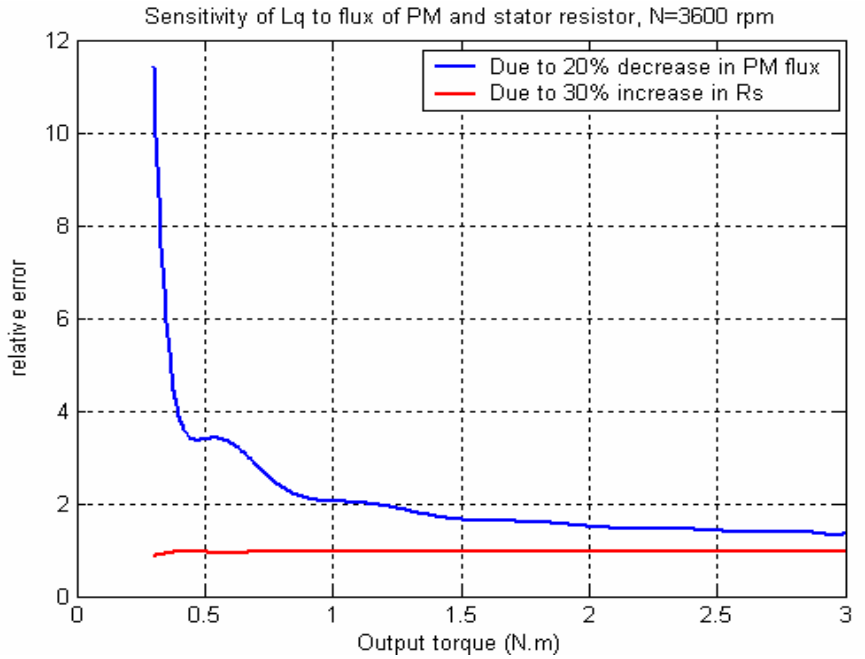

Figure 3- 3 Sensitivity of estimated L_q to the change of PM flux and stator resistor at 3600 rpm.

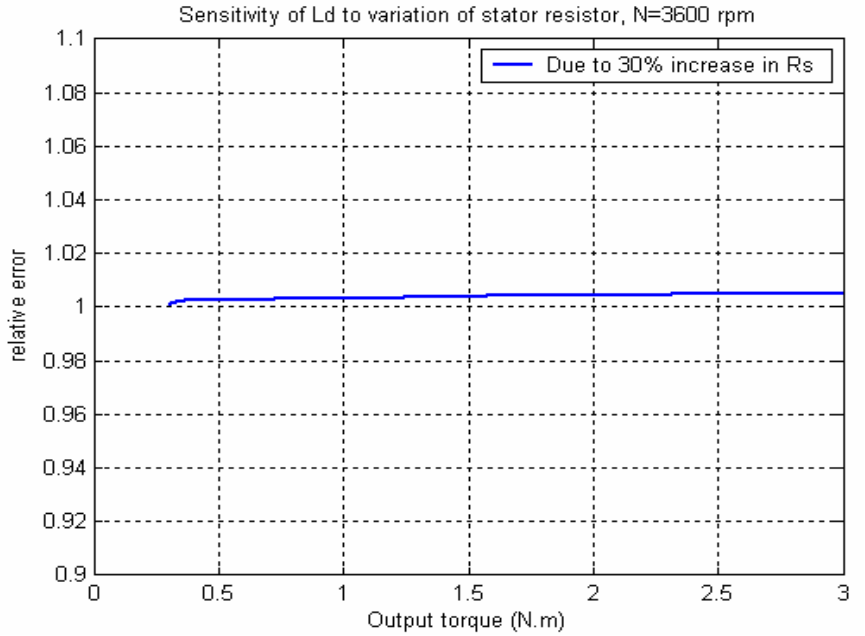

Figure 3- 4 Sensitivity of estimated L_d to the change of stator resistor at 3600 rpm.

So far, it is assumed that the back-EMF is sinusoidal. However, in the most PMa-SynRM due to the shape of flux barriers inside the rotor, the back-EMF is not sinusoidal. Therefore, the d-q model of the motor is valid only for fundamental harmonic of the back-EMF. Using Maxwell software [76], a 2D-FEM simulation has been done on the presented 1.5kW prototype PMa-SynRM. Figure 3-5 and 3-6 show the simulation results of the back-EMF of phase 'A' and its normalized existing harmonics in line voltage, respectively. As it can be seen, the fifth harmonic is the second dominant harmonic existing in the line voltage. In this case λ_{pm} introduced in (3-6) is changed to (3-13).

$$\lambda_{pm} = \lambda_m \cdot \sum_{n=1}^{\infty} K_{2n-1} \begin{bmatrix} \sin((2n-1)\theta_r) \\ \sin((2n-1)(\theta_r - \frac{2\pi}{3})) \\ \sin((2n-1)(\theta_r + \frac{2\pi}{3})) \end{bmatrix} \tag{3-13}$$

The peak strength of the fundamental harmonic of the permanent magnet flux linkage is considered to be constant since it is assumed that no demagnetization is occurring. The coefficient of K_n denotes the normalized magnitude of the n'th component of the permanent magnet flux linkage with respect to the fundamental harmonic. So in this case K_1=1.0.

Dynamic equations describing the motor behavior for higher order harmonics can be used to modify the parameter estimation method. Using multiple reference frame technique, the model of PMa-SynRM with non-sinusoidal back-EMF is obtained.

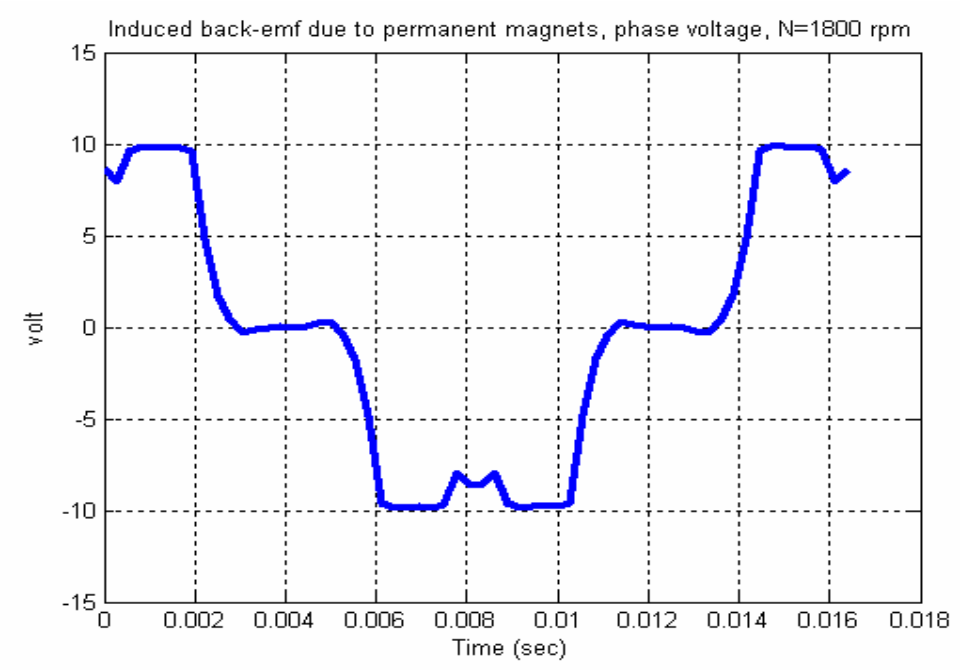

Figure 3- 5 Back-EMF due to permanent magnets in phase A.

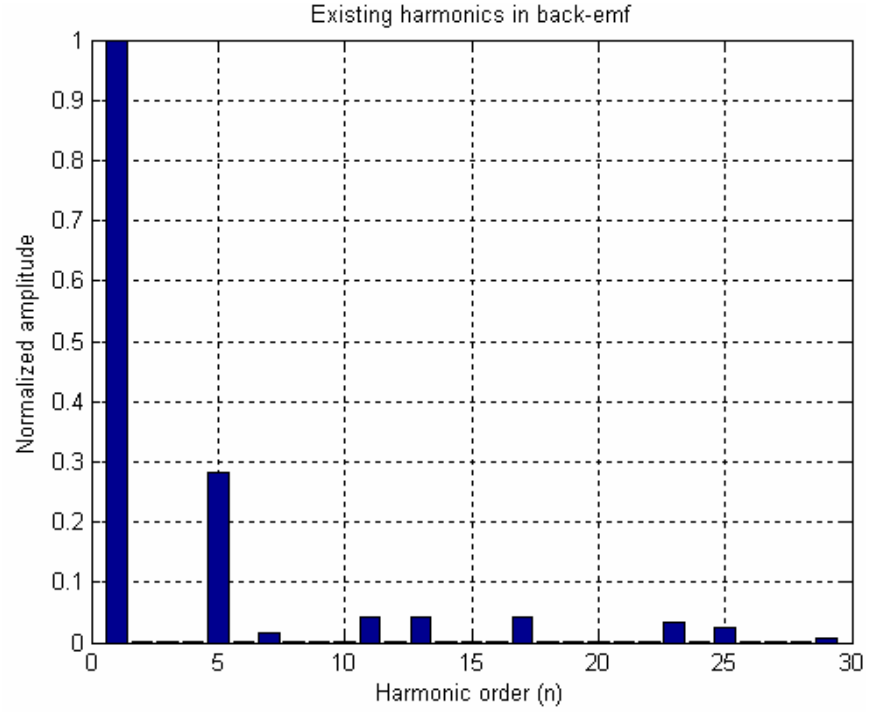

Figure 3- 6 Normalized harmonics of line-line back-EMF due to PMs.

D. MULTIPLE REFERENCE FRAME

In a PMa-SynRM machine with sinusoidal back-EMF considerable simplification is obtained by transforming the abc machine variables to dq model in the rotor reference frame. The transformation is given by:

$$f^{r}_{dq0s} = T.f_{abcs} \tag{3-14}$$

$$T(\theta) = \frac{2}{3}\begin{bmatrix} \cos(\theta) & \cos(\theta - \frac{2\pi}{3}) & \cos(\theta + \frac{2\pi}{3}) \\ \sin(\theta) & \sin(\theta - \frac{2\pi}{3}) & \sin(\theta + \frac{2\pi}{3}) \\ 1/\sqrt{2} & 1/\sqrt{2} & 1/\sqrt{2} \end{bmatrix} \tag{3-15}$$

In (3-14), f might be the stator voltages, flux linkages or currents. In the case of a PMa-SynRM with nonsinosoidal back-EMF, transforming the machine voltages and flux linkages equations to the rotor reference frame yields:

$$v^{r}_{qs} = r_s i^{r}_{qs} + \omega_r \lambda^{r}_{ds} + \frac{d}{dt}\lambda^{r}_{qs} \tag{3-16}$$

$$v^{r}_{ds} = r_s i^{r}_{ds} - \omega_r \lambda^{r}_{qs} + \frac{d}{dt}\lambda^{r}_{ds} \tag{3-17}$$

$$\lambda^{r}_{qs} = L_{qs} i^{r}_{qs} - \lambda_m - \lambda_m \sum_{n=1}^{\infty} (K_{6n-1} + K_{6n+1}) \cos(6n\theta) \tag{3-18}$$

$$\lambda^{r}_{ds} = L_{ds} i^{r}_{ds} - \lambda_m \sum_{n=1}^{\infty} (K_{6n-1} + K_{6n+1}) \sin(6n\theta) \tag{3-19}$$

The required analysis begins by expressing the transformation of the q- and d-axes variables from the rotor reference frame to another reference frame rotating at some multiple of the rotor's electrical speed [86]. In particular,

$$f_{dq}^{xr} = T_S^{xr} . f_{dq}^{r} \tag{3-20}$$

where,

$$T_S^{xr} = (T_S^{xr})^{-1} = \begin{bmatrix} \cos(x\theta_r - \theta_r) & -\sin(x\theta_r - \theta_r) \\ \sin(x\theta_r - \theta_r) & \cos(x\theta_r - \theta_r) \end{bmatrix} \tag{3-21}$$

T_s^{xr} represents the transformation from the rotor reference frame 'r' into the 'xr' reference frame rotating at 'x' times the electrical speed of the rotor. Applying (3-20) to (3-16) and (3-17) yields the voltage equations in the 'xr' reference frame which may be expressed by,

$$\begin{aligned} v_{qs}^{xr} &= r_s i_{qs}^{xr} + x\omega_r \lambda_{ds}^{xr} + \frac{d}{dt}\lambda_{qs}^{xr} \\ v_{ds}^{xr} &= r_s i_{ds}^{xr} - x\omega_r \lambda_{qs}^{xr} + \frac{d}{dt}\lambda_{ds}^{xr} \end{aligned} \tag{3-22}$$

Transforming the d-q rotor reference frame flux linkages (3-18) and (3-19) into the 'xr' reference frame yields,

$$\begin{aligned} \lambda_{qs}^{xr} &= L_{qs} i_{qs}^{xr} - \lambda_m \sum_{n=1}^{\infty} [K_{6n-1} \cos((x-1+6n)\theta_r) + \\ &\quad K_{6n+1} \cos((x-1-6n)\theta_r)] - \lambda_m \cos((x-1)\theta_r) \\ \lambda_{ds}^{xr} &= L_{ds} i_{ds}^{xr} - \lambda_m \sum_{n=1}^{\infty} [K_{6n-1} \sin((x-1+6n)\theta_r) - \\ &\quad K_{6n+1} \sin((x-1-6n)\theta_r)] + \lambda_m \sin((x-1)\theta_r) \end{aligned} \tag{3-23}$$

Note that the voltage equations have the same form as the traditional d-q model (3-16) and (3-17).

E. MODIFIED PARAMETER ESTIMATION METHOD

The most dominant harmonics in the back-EMF of the mentioned motor are the 5th and 7th harmonics. By writing the motor equations in the 5th harmonics reference frame, we have one extra equation for the d-axis voltage. To find out this extra equation in (3-23), n and x should be selected as 1 and -5 respectively. Now by considering (3-9), three equations are available to estimate the L_{ds}, L_{qs} and λ_m. This extra q-axis equation will help us to estimate λ_m. K_i is considered to be a known constant since its value is defined by the shape of back-EMF and not by its amplitude. By knowing λ_m, estimation of the L_{ds} and L_{qs} is possible in a more accurate way.

$$v_{ds}^{r} - r_s i_{ds}^{r} + \omega_r \lambda_m = -L_{qs} \omega_r i_{qs}^{r} \tag{3-24}$$

$$v_{ds}^{5r} - r_s i_{ds}^{5r} = 5\omega_r L_{qs} i_{qs}^{5r} - 5\omega_r K_5 \lambda_m \tag{3-25}$$

$$v_{qs}^{r} - r_s i_{qs}^{r} = L_{ds} \omega_r i_{ds}^{r} \tag{3-26}$$

Use of a low pass filter for both the fundamental harmonic and the 5th harmonics reference frame is necessary to avoid influence of other existing higher order voltage and current harmonics. Figure 3-7 shows the block diagram of the control system along the proposed parameter estimator. Figure 3-8 represent the inside block diagram of the parameter estimator.

1. Low pass filter

In order to reject the high order harmonics from the measured signals in rotating reference frame an Infinite Impulse response (IIR) filter can be used. The form of the low pass filter is as following:

$$y(n) = a.y(n-1) + b.x(n) \tag{3-27}$$

Where y is the output or filtered signal and x is the input or noisy signal. In z domain, the filter has the following transfer function;

$$H(z) = \frac{b}{1 - a.z^{-1}} \tag{3-28}$$

The required filter can be designed in s domain and then transferred to z domain by bilinear method. Because the low pass filter is used in a synchronous reference frame, there is no need for filter to have a variable cut-off frequency. The cut-off frequency should be as small as possible. The amplitude of the filter transfer function and its effect on K_i should be also considered.

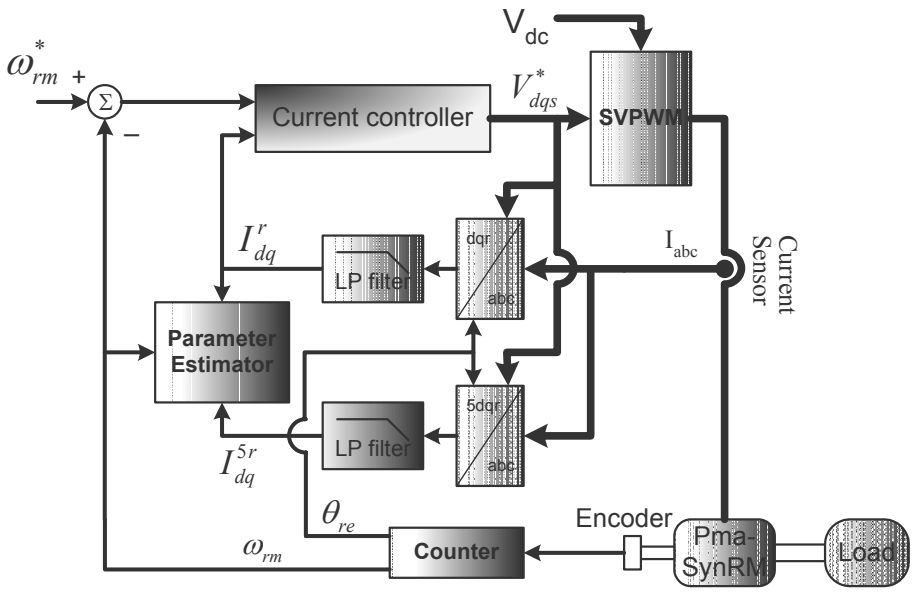

Figure 3- 7 Block diagram of control system along the parameter estimator.

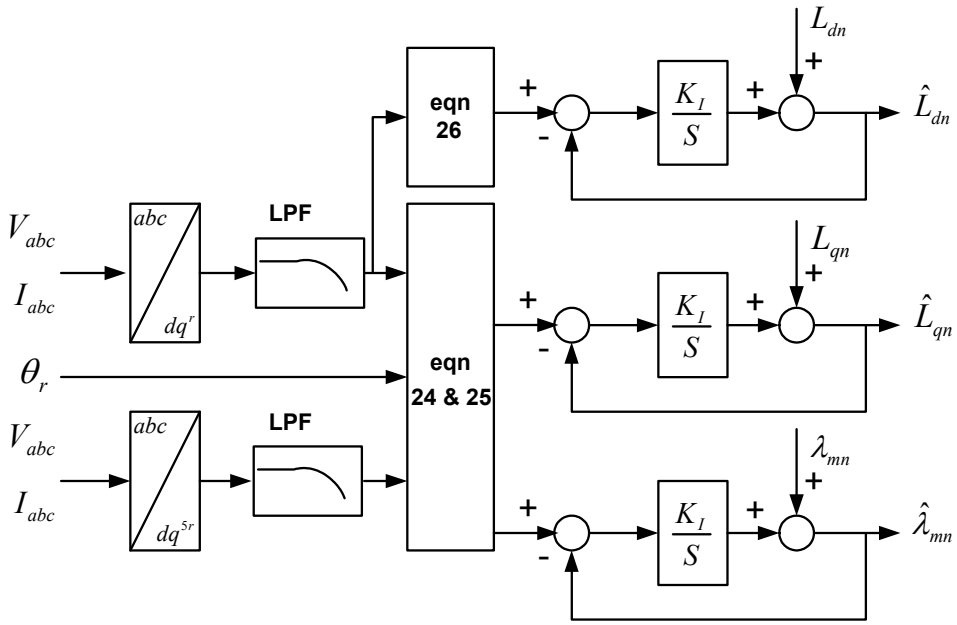

Figure 3- 8 Block diagram of the parameter estimator.

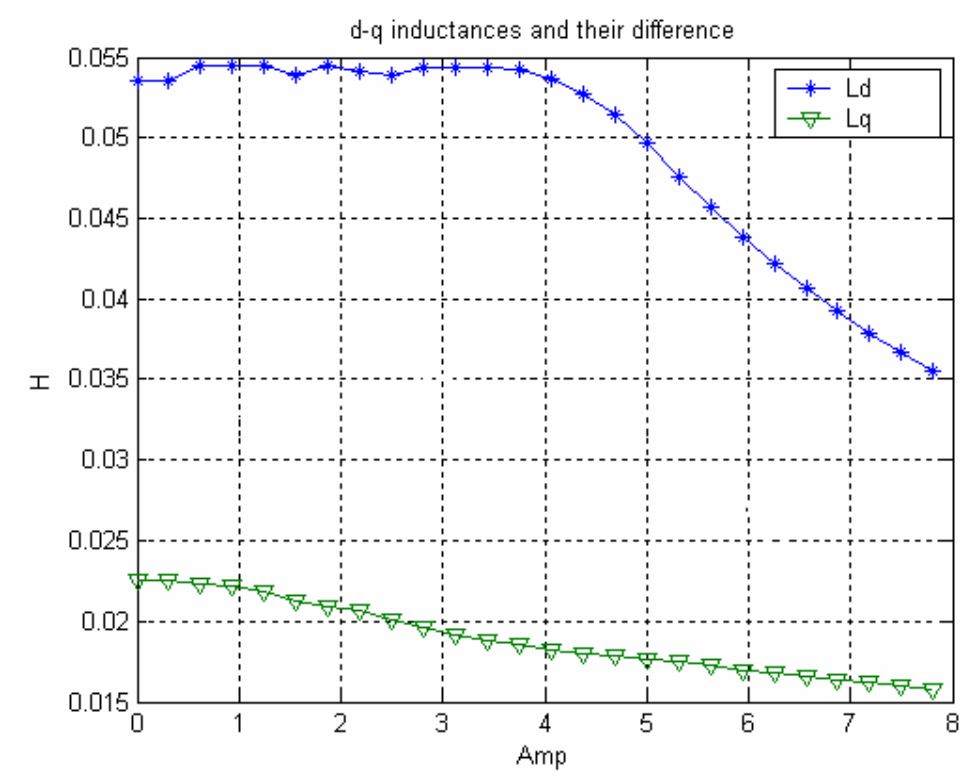

Figure 3- 9 d-q axes inductances and (L_d-L_q) vs. current.

F. SIMULATION AND EXPERIMENTAL RESULTS

The drive system with the proposed control parameter estimator has been simulated extensively prior to the laboratory experimentation. Matlab/Simulink™ has been used to model the PMa-SynRM, the vector control, and the space vector PWM.

The simulation was done using the measured d-q inductances of the prototype 1.5kW PMa-SynRM motor. These inductances and the prototype motor are shown in Figure 3-9. As it can be seen saturation effect has been considered in the simulation study. However, effect of cross saturation has been ignored in the simulation due to the complex model of cross saturation effect. Permanent magnets back-EMF waveform has been approximated by Figure 3-10 and has been used in the simulation.

Existing harmonics of this waveform and their magnitude can be obtained by its Fourier series:

$$\begin{aligned} &Back-EMF=\sum_{n=1}^{\infty} b_n \sin(n\omega t) \\ &n:even, \quad b_n=0 \\ &n:odd, \quad b_n=\frac{4}{\pi}\frac{A}{n}\cos(\frac{1}{2}nu) \end{aligned} \tag{3-29}$$

In the simulation, by varying the command torque currents, the reference current in both d and q axes have been changed. By changing the currents in the d and q axes, the inductances will change. Behavior of the proposed estimator is shown in Figure 3-11. As it can be seen, the estimated d-q inductances converge to real values within a short interval. Figure 3-12 shows behavior of parameter estimator when flux due to the permanent magnet (λ_m) is changed. In this simulation, the amounts of the current in both

d-q axes are kept constant. As it can be seen, the estimated value of λ_m is converging to real value.

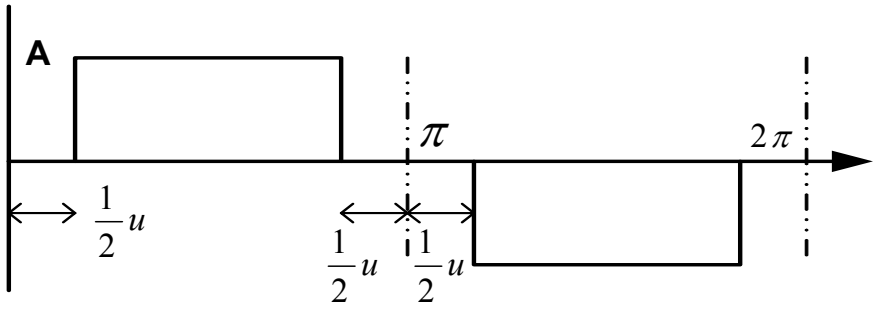

Figure 3- 10 Approximated permanent magnets back-EMF used in the simulations.

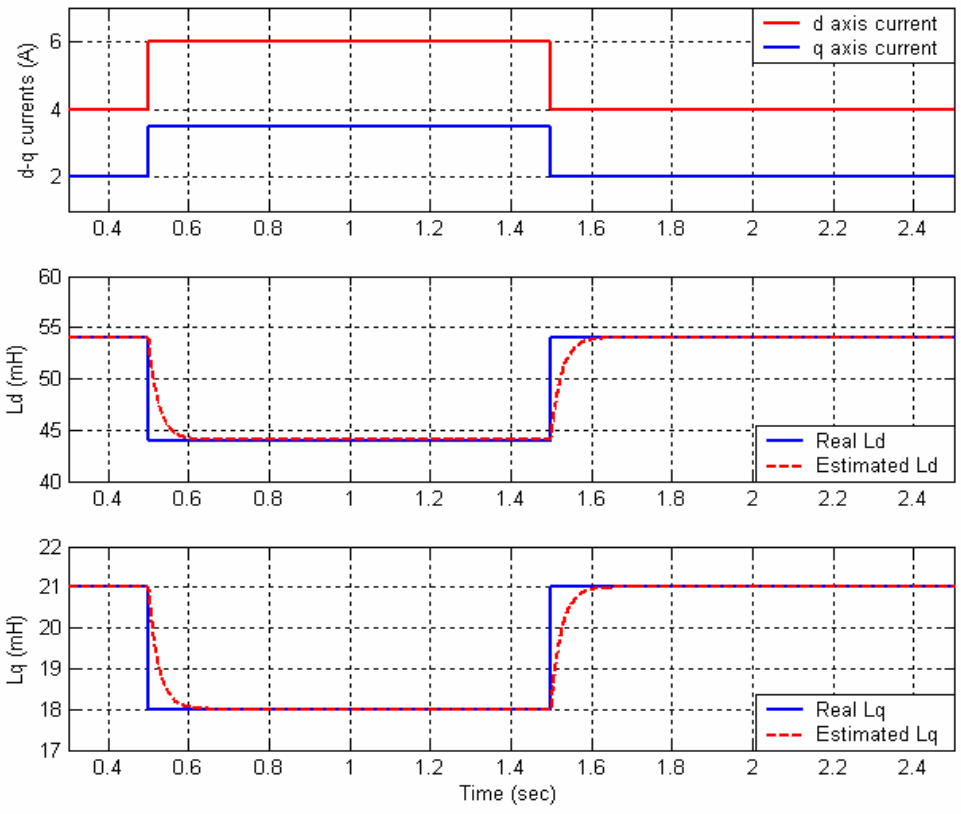

Figure 3- 11 On-line estimated parameters (L_d, L_q).

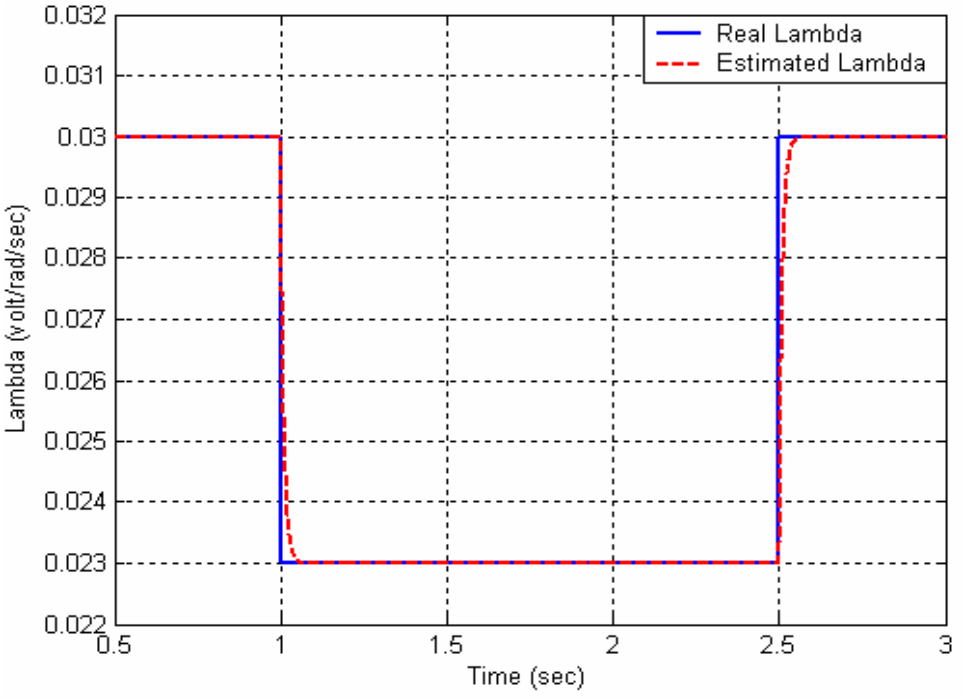

Figure 3- 12 On-line estimated parameters (λ_m).

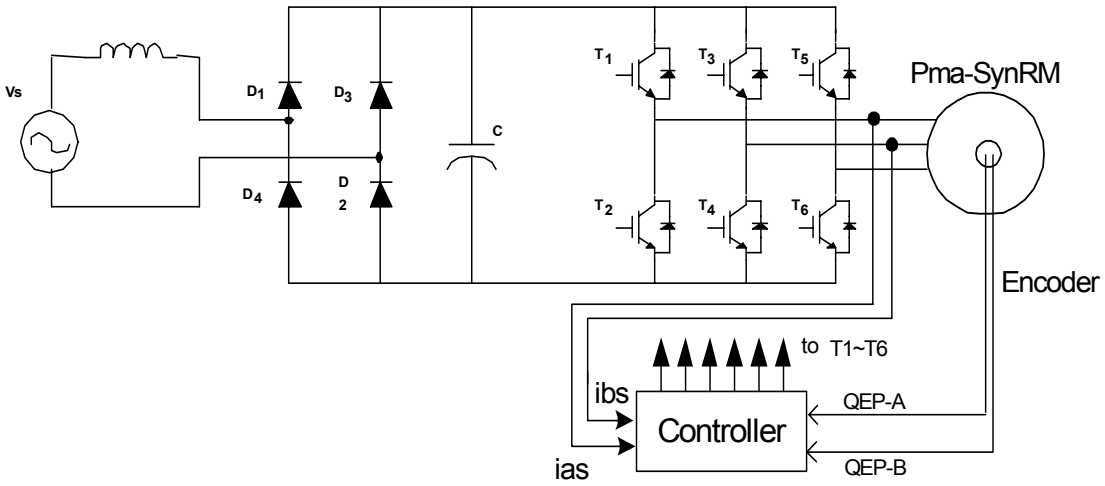

Figure 3- 13 PMa-SynRM speed control system.

The schematic block diagram of the laboratory experimental setup is given in Figure 3-13. Experiments have been performed on the 1.5 kW PMa-SynRM motor, design and presented in Chapter II, using the DSP TMP320F2812 DSK. Figure 3-14 shows the prototype motor used for the test.

The back-EMF of this motor is shown in Figure 3-15 at the shaft speed of 1800 rpm. The peak-to-peak line voltage is almost 22 volts. To detect the rotor position an incremental shaft encoder with resolution of 1024 pulse per revolution was used. In this test, just a simple current controller has been used and the effect of non-sinusoidal back-EMF has not been considered in the design of the current controller. Figure 3-16 shows the measured currents of the d -and q-axes in the rotor reference frame along with the estimated d and q inductances. In this test, only the q-axis current has been changed and the effect of this change on the estimated values of d and q inductances can be seen. Due to the change in the q-axis current, a transient in the d-axis current control loop happened which caused a transient in estimation of the d-axis inductance. Although the d-axis current has been regulated to its previous value, the estimated L_d is different from its values before the change in i_{qs}. This change shows the effect of cross saturation and coupling of the d and q axes inductances. Estimated values of L_d and L_q can be used in a maximum torque per ampere control strategy in order to obtain the maximum efficiency of the drive.

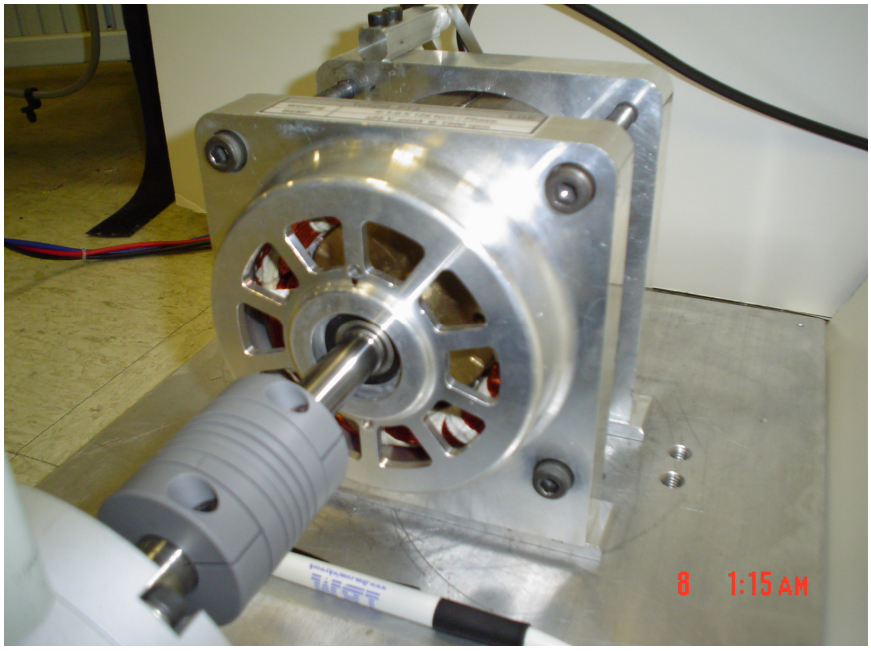

Figure 3- 14 1.5kW prototype PMa-SynRM.

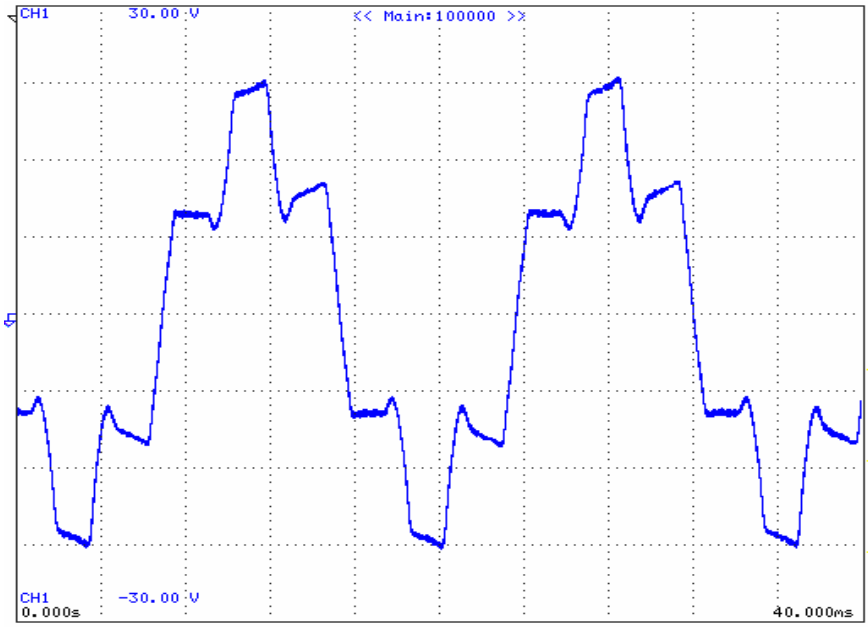

Figure 3- 15 Back-EMF voltage at 1800 rpm.

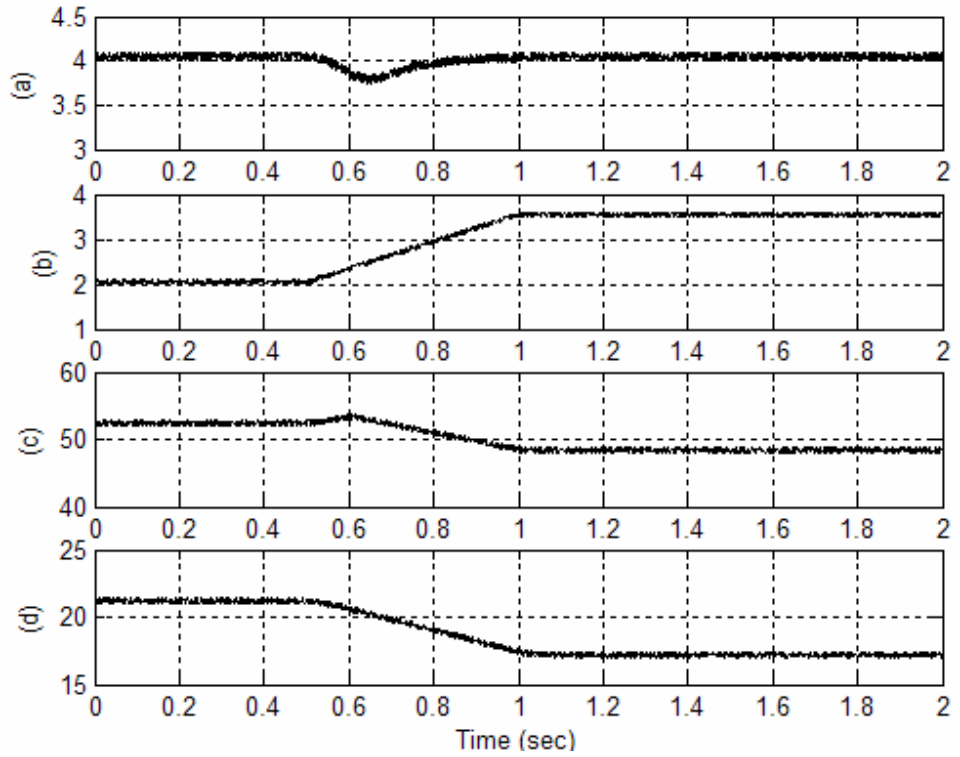

Figure 3- 16 Experimental results of inductance estimation, a) measured i_{ds} b) measured i_{qs} c) estimated L_{ds} d) estimated L_{qs}.

G. CONCLUSION

Synchronous reluctance motor drives have offered better torque capabilities and power factors. However, to utilize the maximum efficiency of the motor, knowledge of the motor parameters is necessary. Variation of the PMa-SynRM parameters was shown and a simple practical method for estimation of the motor parameters was presented. Simulation results of the proposed technique validate the effectiveness of the estimation method and the experimental results were presented to show the feasibility of the proposed method. This method can be used to improve the performance of some other control strategies which are dependent on the knowledge of the motor parameters.

CHAPTER IV

ROBUST MAXIMUM TORQUE PER AMPERE (MTPA) CONTROL OF PM-ASSISTED SYNCHRONOUS RELUCTANCE MOTOR

A. INTRODUCTION

Energy saving has been always an important issue for a motor drive system. Among the electric motors, induction motor is the most popular one in industrial and residential applications. Therefore improvement of energy consumption of induction motor drive has a considerable impact on survival of today energy resources. Several reports have been published on the subject of efficiency improvement of the induction motor drives [67, 68, 69]. Efficiency of the induction motor can be improved by use of reduced voltage operation while a light loads is driven if a fixed frequency drive is available.

It is also known that induction motor losses can be minimized at the partial loads by driving the motor at the optimum slip using an adjustable-frequency drive. In an adjustable-frequency induction motor drive, the voltage and frequency can be controlled independently. Therefore, a specific torque-speed operating point can be obtained through a variety of different voltage frequency pairs.

Each voltage frequency pairing defines a particular motor torque speed characteristic, but motor efficiency may vary widely. Magnetizing current and core losses are large if the applied voltage is high. On the other hand, if the voltage is reduced excessively, then motor currents and copper losses may increase. Consequently, there should be an optimum voltage and frequency in which, efficiency is maximum for a

specified torque and speed. At light loads, maximum efficiency will be achieved with a reduced voltage and increased slip, compared with the usual constant volts per-hertz mode of operation.

The same concept can also be applied to IPM, synchronous reluctance motor and PM assisted synchronous reluctance motor drives. Because of presenting higher efficiency especially in fractional power rates, these motors are considered as the alternative and reasonable replacement for the induction motors. In the field-oriented control of synchronous reluctance motors, d- and q-axis components of the stator current vector can be independently controlled. As a result, a specific torque at any motor speed can be achieved with a variety of different d–q current pairs. Each d–q current pairing defines a particular motor torque characteristic, but motor efficiency may vary widely. If the d-axis current is high, then core losses are high. If the d-axis current is reduced, to maintain the demanded output torque, the q-axis current should increase which results in increase of copper losses. Therefore, there is an optimum operating point in which efficiency or ratio of output torque over amplitude of input current is maximum. This point can be calculated by use of an accurate model of the motor.

One of the most popular methods for saving the energy is to drive the motor with maximum torque per ampere (MTPA) controller. MTPA controller is a parameter dependent controller and its performance relies on the knowledge of motor parameters. Unfortunately, stator resistance and permanent magnet flux linkage vary with motor temperature [70]. The d- and q-axes total inductances, L_{ds} and L_{qs}, are known to depend on the airgap flux [71]. Ferrite, ceramic magnets and Neodymium-Iron-Boron (Nd-Fe-

Br) materials are well known materials used in IPM motors. The flux density of the magnets changes significantly by variation of temperature. The variation of the flux density affects the d- and q-axes inductances and also directly affects the output torque.

For the practical realization of an efficiency-optimized synchronous reluctance motor drive, an optimum-efficiency controller may be accomplished with the aid of a loss model for the drive into which complete parameter values, including inductance saturation, coefficients of iron losses, temperature, and harmonic effects, must be programmed. At any operating point, the controller performs a computation on optimum efficiency operating conditions and adjusts one, or more, variables in the model until the optimum values are found. These optimized values then become the commanded values for the drive regulator. The effectiveness of this approach obviously depends on the accuracy of the model.

In case of using off-line models, the trajectory of reference currents can be obtained to implement maximum torque per ampere condition. However, this is computationally intensive because of the non-linearity due to iron saturation. Such calculations are usually unreasonable in real time. Moreover, including cross saturation effect is very difficult and intensive in off-line parameter estimation.

In this chapter, a practical and innovative maximum torque per ampere controller is introduced. This method is robust against the variation of motor parameters. MTPA condition can be achieved by calculation of the output torque and perturbing one variable while seeking the maximum output torque at the particular operating point. The maximization of the electromagnetic torque might be sensitive to the variation of the

motor parameters. In order to reduce this sensitivity, the on-line parameter estimator, introduced in Chapter III, is used to estimate the motor parameters and calculate the electromagnetic torque more accurately. The overall control strategy for searching the maximum output torque is also discussed. This control strategy was implemented to verify the developed control scheme, and an experimental study was carried out with the implemented drive system.

B. MAXIMUM TORQUE PER AMPERE CONTROL

Figure 4-1 shows the four pole PMa-SynRM rotor, designed and presented in Chapter II, with the definition of d-q axes. In PMa-SynRM, permanent magnets are placed in the q-axis (in IPM they are considered in the d-axis). Therefore, the stator voltages and flux linkages equations in the d-q reference frame are expressed as follows and are different from IPM voltage and flux equations.

$$\begin{aligned} v_d &= r_s i_{ds} + \frac{d}{dt}\lambda_{ds} - \omega_r \lambda_{qs} \\ v_q &= r_s i_{qs} + \frac{d}{dt}\lambda_{qs} + \omega_r \lambda_{ds} \end{aligned} \tag{4-1}$$

$$\begin{aligned} \lambda_{ds} &= L_{ls} i_{ds} + L_{md} i_{ds} = L_{ds} i_{ds} \\ \lambda_{qs} &= L_{ls} i_{qs} + L_{mq} i_{qs} - \lambda_m = L_{qs} i_{qs} - \lambda_m \end{aligned} \tag{4-2}$$

The steady-state d- and q-axis equations of a PMa-SynRM in the rotor reference frame are given in (4-3).

$$\begin{aligned} v_{ds}^r - r_s i_{ds}^r - \omega_r \lambda_m &= -L_{qs} \omega_r i_{qs}^r \\ v_{qs}^r - r_s i_{qs}^r &= L_{ds} \omega_r i_{ds}^r \end{aligned} \tag{4-3}$$

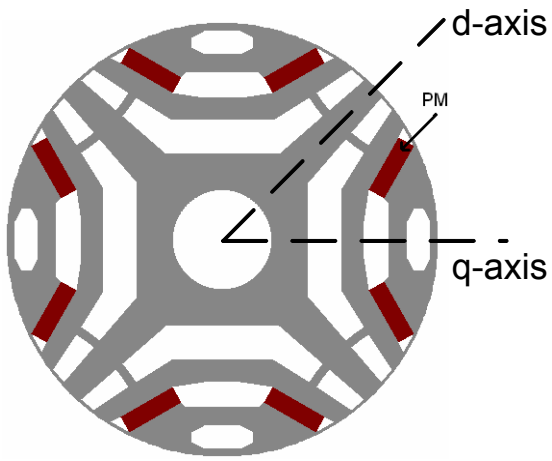

Figure 4- 1 A four pole PMa-SynRM rotor.

Ignoring the leakage inductances, the corresponding generated electromagnetic torque is given by,

$$T = \frac{3}{2}\frac{P}{2}\left((L_{ds} - L_{qs})i_{ds}i_{qs} + \lambda_m i_{ds}\right) \tag{4-4}$$

where P denotes the number of poles. Also, for a practical inverter-fed motor drive, there are two constrains on the output voltages and output currents. Assume that the maximum available phase voltage amplitude and the maximum line current amplitude are V_{SM} and I_{SM} respectively. Then, the feasible operating region is limited by (4-5) and (4-6):

$$i_{ds}^{r2} + i_{qs}^{r2} \le I_{SM}^2 \tag{4-5}$$

$$v_{ds}^{r2} + v_{qs}^{r2} \le V_{SM}^2 \tag{4-6}$$

From (4-4), it can be observed that when the i_{ds} is constant, then the resulting T can be controlled by controlling the i_{qs}. Hence, it is quite simple to implement a high-performance drive as in [87, 88, 89]. However, the magnetic torque of the PMa-SynRM

is not fully utilized. In the case where i_{ds} is not constant, T contains a nonlinear term. Therefore, design of the controller becomes more difficult.

As far as achieving a fast transient response is concerned, the maximum torque per ampere control [90], [91] is rather attractive. For a given torque demand, the line current amplitude, or equivalently $\sqrt{i_{ds}^2 + i_{qs}^2}$, is minimized to achieve the maximum torque. Within the current constraint of (4-5) and by assuming L_{ds} and L_{qs} as the constant parameters, the d- and q-axes stator currents should satisfy (4-7):

$$\frac{dT}{dI_s} = 2(L_{ds} - L_{qs})i_{qs} - \lambda_m + \sqrt{\lambda_m^2 + 4(L_{ds} - L_{qs})^2 i_{ds}^2} = 0 \tag{4-7}$$

In a special case, when the maximum available line current amplitude I_{SM} is considered as:

$$i_{ds}^{r\,2} + i_{qs}^{r\,2} = I_{SM}^2 \tag{4-8}$$

then from (4-7) and (4-8), the maximum available torque can be obtained as (4-9):

$$T = \frac{3}{2}\frac{P}{2}\left((L_{ds} - L_{qs})I_{qsM} + \lambda_m\right)I_{dsM} \tag{4-9}$$

where

$$I_{dsM} \triangleq \frac{\lambda_m - \sqrt{\lambda_m^2 + 8(L_{ds} - L_{qs})^2 I_{SM}^2}}{4(L_{ds} - L_{qs})} \tag{4-10}$$

$$I_{qsM} \triangleq \sqrt{I_{SM}^2 - I_{dsM}^2} \tag{4-11}$$

Also, the corresponding angular speed, namely ω_{rM} can be calculated by substituting (4-3), (4-10) and (4-11) in (4-6):

$$(r_s I_{qsM} + \omega_{rM} L_{ds} I_{dsM})^2 + \left[r_s I_{dsM} - \omega_{rM}(L_{qs} I_{qsM} - \lambda_m)\right]^2 = V_{SM}^2 \tag{4-12}$$

The corresponding generated electromagnetic torque can be introduced based on the current angle as (4-13).

$$T = \frac{3}{2}\frac{P}{2}\left(\frac{1}{2}(L_{ds} - L_{qs})I_s^2 \sin 2\beta + \lambda_m I_s \cos\beta\right) \tag{4-13}$$

where I_s is the current magnitude and is defined by $I_s = \sqrt{i_{ds}^2 + i_{qs}^2}$, and $\beta = \tan^{-1}(i_{qs} / i_{ds})$ is the current phase angle. To achieve MTPA for a given I_s in [92], it has been shown that:

$$\beta = \sin^{-1}\left(\frac{-\lambda_m + \sqrt{\lambda_m^2 + 8(L_{ds} - L_{qs})^2 I_s^2}}{4(L_{ds} - L_{qs})I_s}\right) \tag{4-14}$$

As it was mentioned previously, in all these analytical approaches toward MTPA condition, motor parameters such as L_{ds}, L_{qs} and λ_m are considered constant and independent of the motor operating point. It means that, the effects of saturation and cross saturation on inductances as well as the change of permanent magnets back-EMF due to the temperature change have been ignored.

Variation of d-q axes inductances with change of operating point (i_{ds} and i_{qs}) and also variation of the amount of permanent magnet flux with the change of temperature has been reported in literature. Figure 4-2 shows the d-q axes inductances of a prototype PMa-SynRM. These inductances, especially the d-axis inductance, are functions of the d-q axes currents. In this figure, the effect of the cross saturation has been ignored.

By assuming L_{ds} and L_{qs} as functions of i_{ds} and i_{qs}, the current phase angle obtained in (4-14) is not valid anymore for the MTPA condition. Maximum torque per ampere condition can be achieved by calculation of the output torque and perturbing one variable while seeking the maximum output torque at the particular operating point.

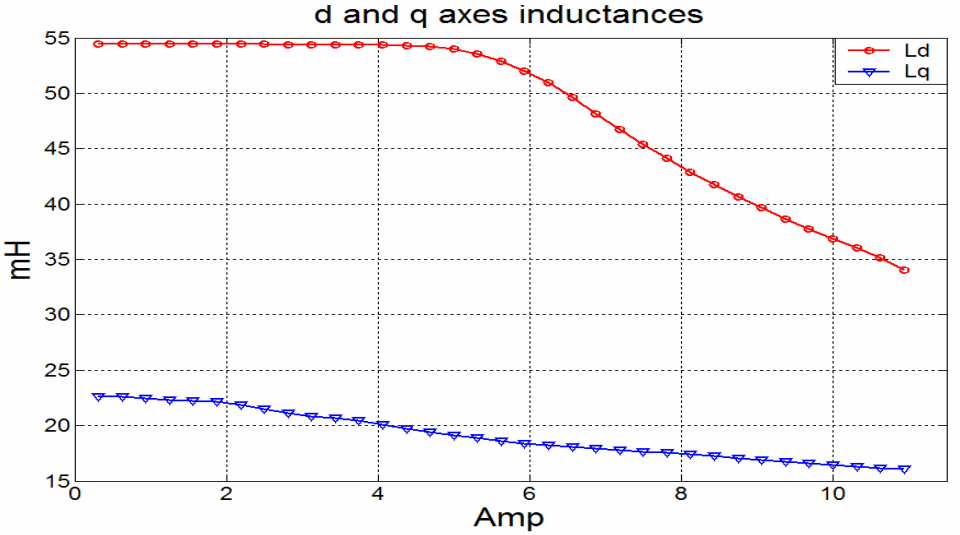

Figure 4- 2 d-q axes inductances vs. current.

To calculate the accurate amount of the electromagnetic torque, accurate values of motor parameters are needed. Therefore, on-line identification of these parameters can be a solution to calculate the output torque and maintain the MTPA condition. In the next step, a simple on-line parameter estimator is introduced and this parameter estimator will be combined with the maximum torque per ampere controller to enhance the overall performance of the drive.

C. MTPA CONTROL SYSTEM

Figure 4-3 shows the block diagram of a high-performance speed control system with the maximum torque control. The magnitude command I_s of the armature current is decided through the speed controller from the difference between the speed command ω_r^* and the detected speed ω_r. The speed command is usually decided from the position controller in the servo drive system, which is not shown in Figure 4-3. Initially, the

current phase command β^* is calculated according to (4-14) based on the motor parameters. However, by increase of I_s from some certain value, this angle starts getting updated through the MTPA controller.

The output torque of PMa-SynRM is a function of motor parameters and two components of the stator current vector as in (4-13). Hence, there exist various combinations of I_s and β (d-q axes currents) which provide a certain amount of motor torque. The objective of the MTPA controller is to seek a current phase angle, β, which provides the demanded torque and minimizes the I_s. To do so, at beginning the controller starts searching for the optimum current phase angle by adding a small amount of perturbation to β. The output torque is calculated at each point using the measured currents and the on-line estimated motor parameters.

Figure 4-4 illustrates the stator current vectors to which small perturbations are superimposed to find a maximum torque per ampere operating point. First, the output torque is calculated at the operating point. Next, stator current, commanded by speed control loop, is kept constant and in two steps, small amount of perturbation, Δβ, is added to and subtracted from β. The torque at two operating points is calculated using (4-13) and is expressed as (4-15) where the quantities with subscripts 1, 2 or 3 denote quantities at each operating point.

$$
\begin{aligned}
T_1 &= \frac{3}{2}\frac{P}{2}\left(\frac{1}{2}(L_{d1}-L_{q1})I_s^2\sin 2\beta + \lambda_{m1}I_s\cos\beta\right)\\
T_2 &= \frac{3}{2}\frac{P}{2}\left(\frac{1}{2}(L_{d2}-L_{q2})I_s^2\sin 2(\beta+\Delta\beta) + \lambda_{m2}I_s\cos(\beta+\Delta\beta)\right)\\
T_3 &= \frac{3}{2}\frac{P}{2}\left(\frac{1}{2}(L_{d3}-L_{q3})I_s^2\sin 2(\beta-\Delta\beta) + \lambda_{m3}I_s\cos(\beta-\Delta\beta)\right)
\end{aligned}
\qquad (4\text{-}15)
$$

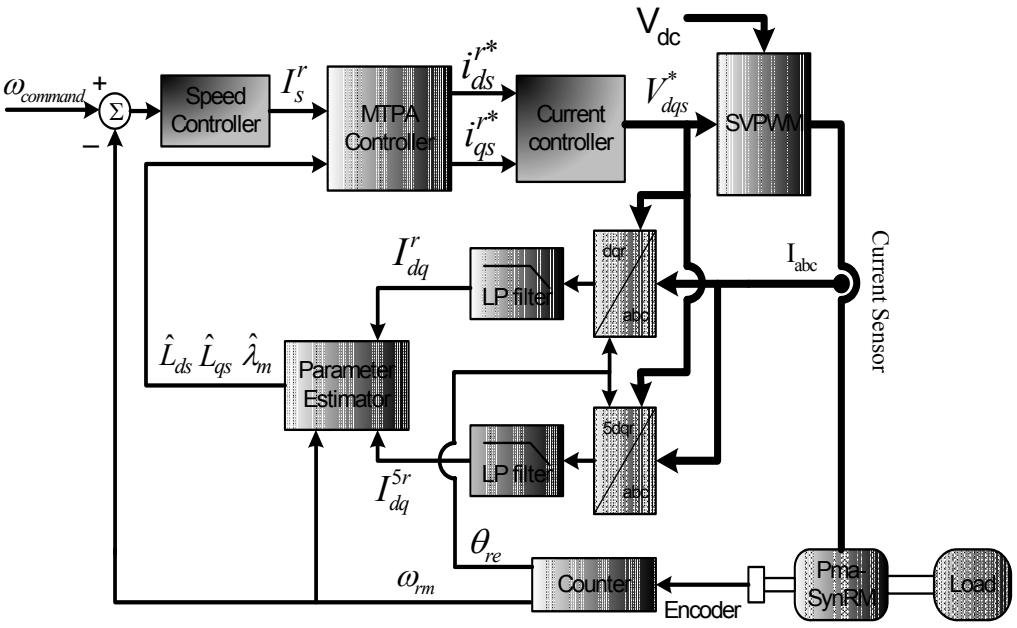

Figure 4- 3 Block diagram of MTPA control system along the parameter estimator.

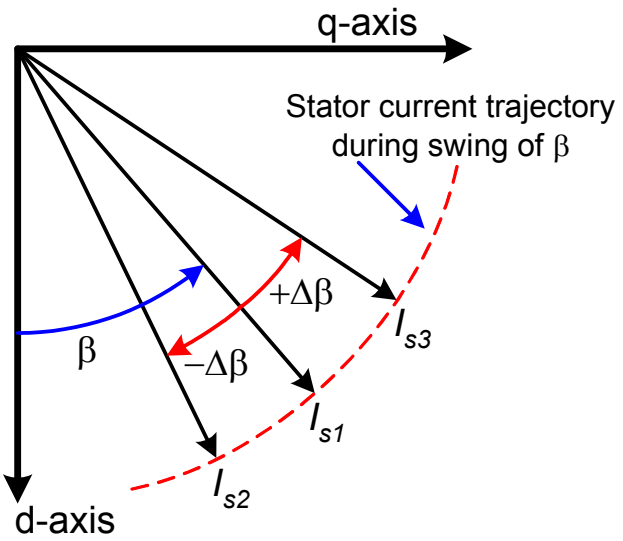

Figure 4- 4 Illustration of current vector swing to find the MTPA operating point.

At this point, there are three operating point that in one of them the calculated torque is higher than the other. MTPA controller updates the value of β to the one which corresponds to the highest torque. At this stage, because the output torque is higher than before, speed goes up. So the MTPA controller allows the speed control loop to updates the amount of the I_s and regulates the speed. This process keeps going until the maximum torque per ampere condition is obtained. To obtain the optimum current phase angle, the MTPA controller calculated the output electromagnetic torque using the estimated motor parameters. So assumption of having a steady state load torque is not necessary and the whole process is not affected by any change in the load torque. More clarification on MTPA control procedure can be obtained using the flowchart of this procedure presented in Figure 4-5.

D. SIMULATION STUDY

The drive system with the proposed MTPA controller has been simulated extensively prior to the laboratory experimentation. Matlab/Simulink™ has been used to model the PMa-SynRM, vector control, and space vector PWM. The simulation was done using the measured parameters of a 4-pole laboratory prototype PMa-SynRM with 1.5 kW nominal power. D-q axes inductances used in the simulation are shown in Figure 4-2. As it can be seen the saturation effect has been considered in the simulation study. However, effect of cross saturation has been ignored in the simulation due to the complex model of cross saturation effect. Permanent magnets back-EMF waveform has been approximated by Figure 4-6 and has been used in the simulation.

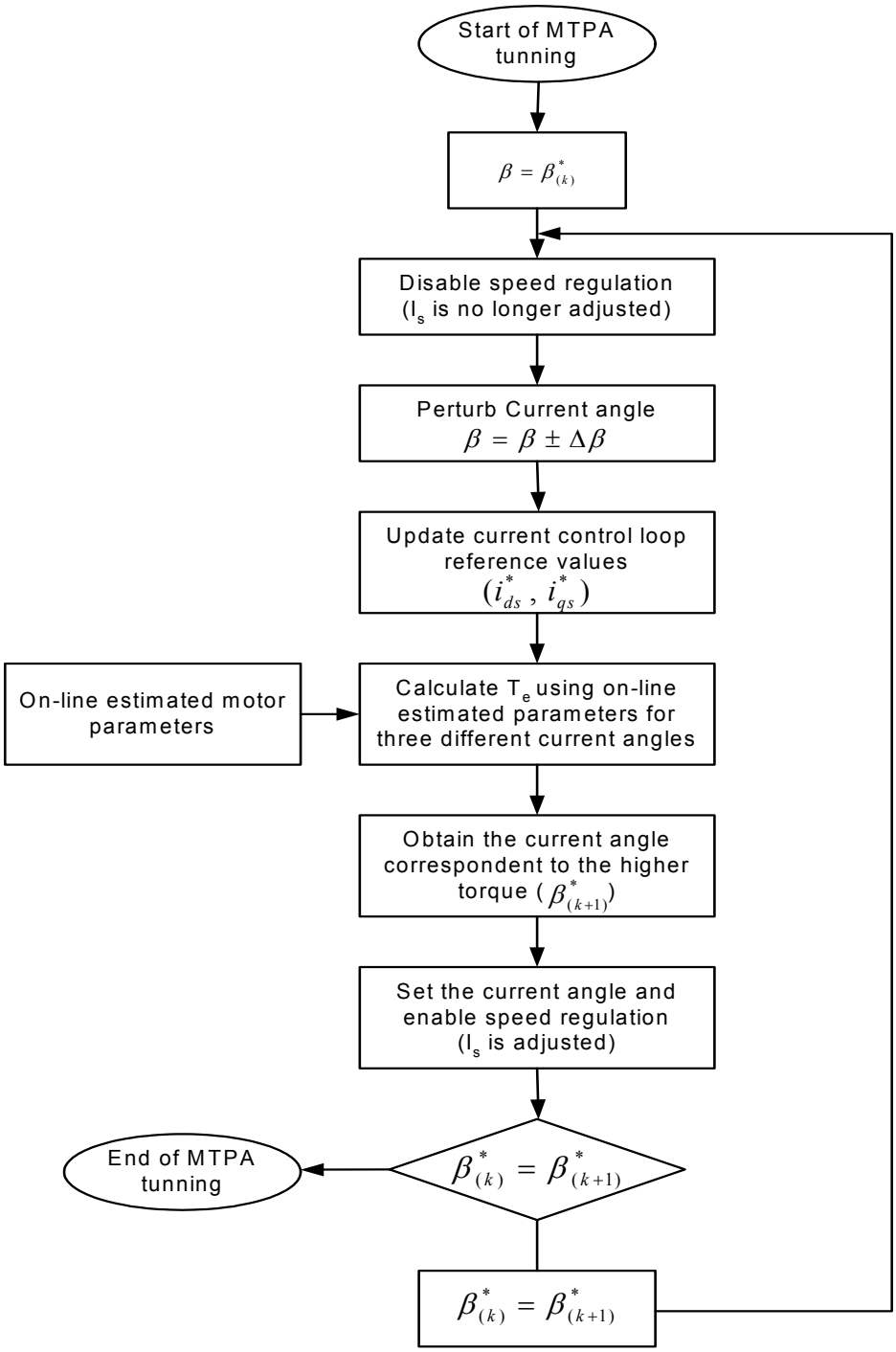

Figure 4-5 Flowchart of MTPA procedure.

Simulation and some experimental results on the parameter identification have been presented in chapter three of this dissertation. Figures 4-7 and 4-8 show the current phase angle, β, and output torque of PMa-SynRM versus stator current amplitude (I_s) in case of using conventional MTPA and introduced MTPA controller with presence of parameter estimator. The produced torque in the PMa-SynRM drive with the proposed MTPA controller equipped with the parameter estimator is higher than the conventional one. Figure 4-9 shows the stator voltage for different values of I_s under MTPA condition. As it can be seen, the required stator voltage in the proposed controller is lower than the required voltage in the conventional control strategy.

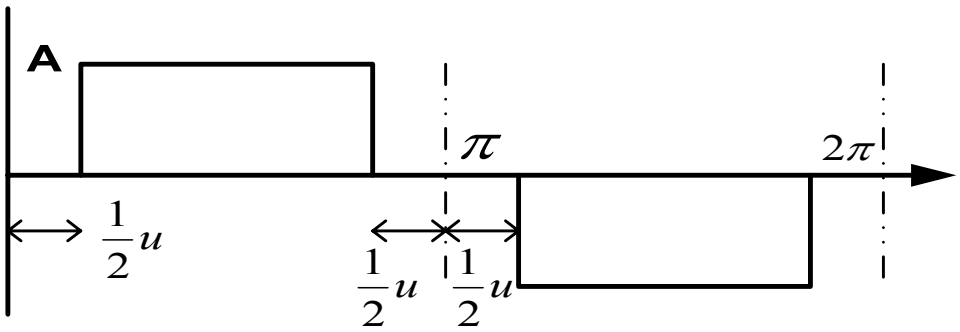

Figure 4- 6 Approximated permanent magnets back-EMF used in the simulations.

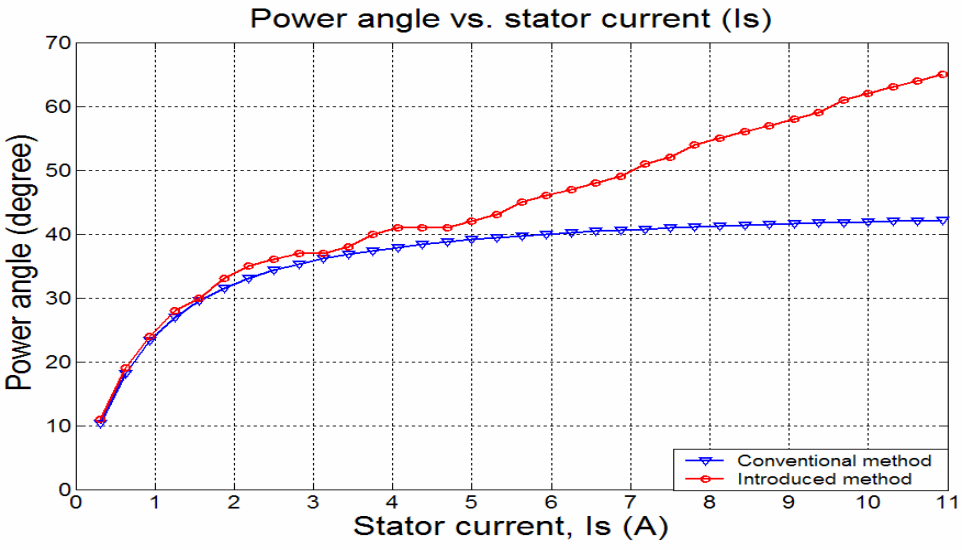

Figure 4- 7 Calculated current phase angle (β) versus amplitude of the stator current vector in order to achieve MTPA.

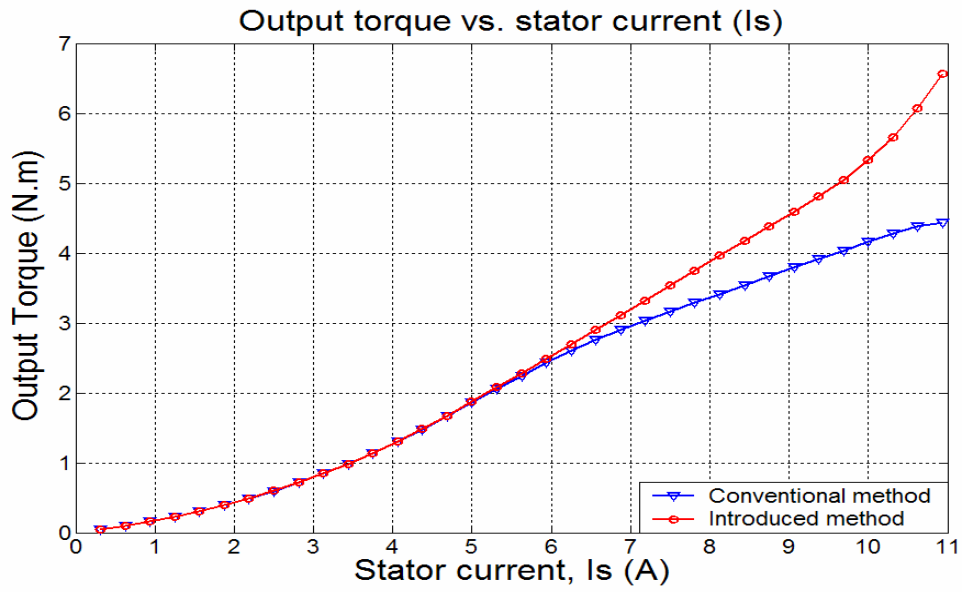

Figure 4- 8 Comparison of the output torque in the conventional MTPA control and the proposed one.

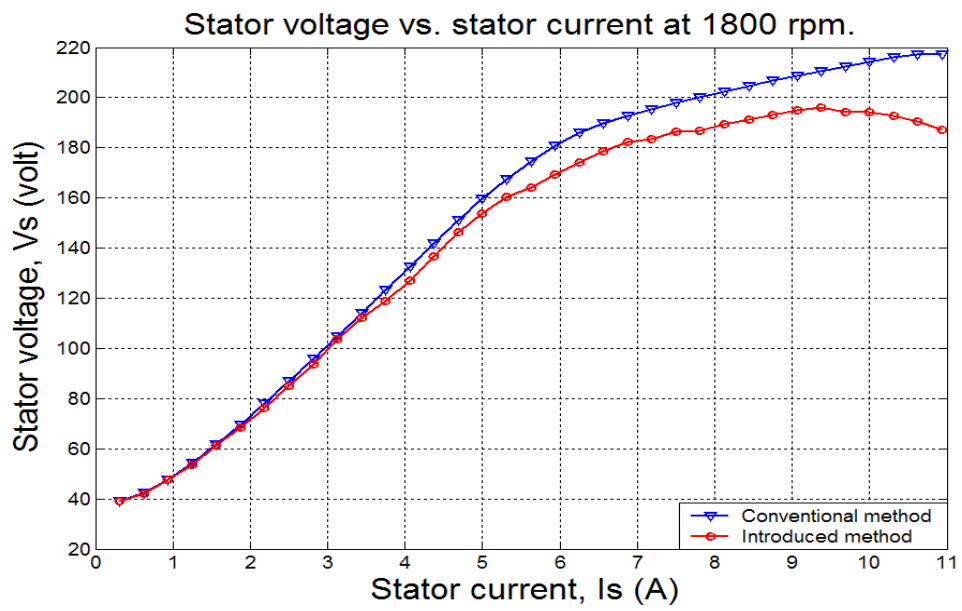

Figure 4- 9 Stator voltage versus stator current at 1800 rpm under the MTPA control.

E. EXPERIMENTAL RESULTS

The schematic block diagram of the laboratory experimental setup is given in Figure 4-10. Experiments have been performed on the 1.5 kW PMa-SynRM motor introduced in Chapter II. MTPA algorithm presented in Figure 4-5 has been implemented using the DSP TMP320F2812 DSK. To detect the rotor position an incremental shaft encoder with resolution of 1024 pulse per revolution was used. Figure 4-11 shows the experimental setup.

Figure 4-12 shows the torque T, the filtered current of phase A, and the rotor d-axis indicator pulse which is generated using encoder pulses. This signal is aligned with the rotor d-axis and comes once in each rotor revolution. To have a better comparison, the current of phase A has been filtered to eliminate the effect of non-sinusoidal back-EMF.

If the magnetic torque is disregarded, theoretically, during the no-load condition the rotor d-axis indicator signal should lag by 90° with respect to the current of phase A. This figure shows the torque and the filtered current of phase A while the d-q inductances as well as the back-EMF due to permanent magnets are considered constant in the MTPA controller. The phase shift between the encoder pulse and the current of phase A is almost 130° which means that the current phase angle or the angle between the stator current vector and the rotor d-axis is almost 40° . The output torque is 3.5 N.m and the phase peak current is 9 A.

Figure 4-13 shows the results of the same test but the controller parameters are getting updated by parameter estimator. As it can be seen, for the same amount of torque, the maximum value of phase current is lower than the previous case (Figure 4-10). The current phase angle can be obtained from the phase shift of the encoder pulse and the phase current. In Fig.14 the phase shift between the encoder pulse and the phase current is almost 144°. So, the current phase angle is equal to 54° degree. The phase peak current is almost 7.7 A.

Presented results clearly prove the ability of the proposed MTPA controller and improvement of the introduced method with respect to the conventional one. As the motor is often operated over the continuous rating, the proposed maximum torque control method is suitable for different vehicle applications of PMa-SynRM.

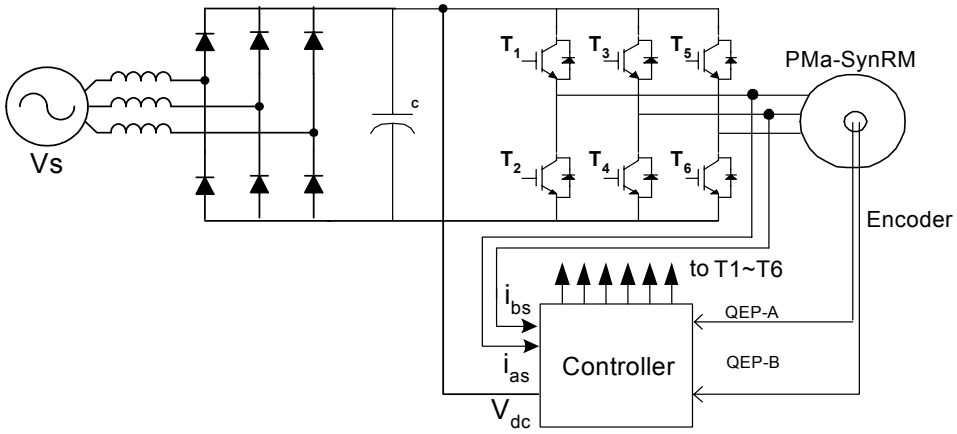

Figure 4- 10 Block diagram of the PMa-SynRM test-bed.

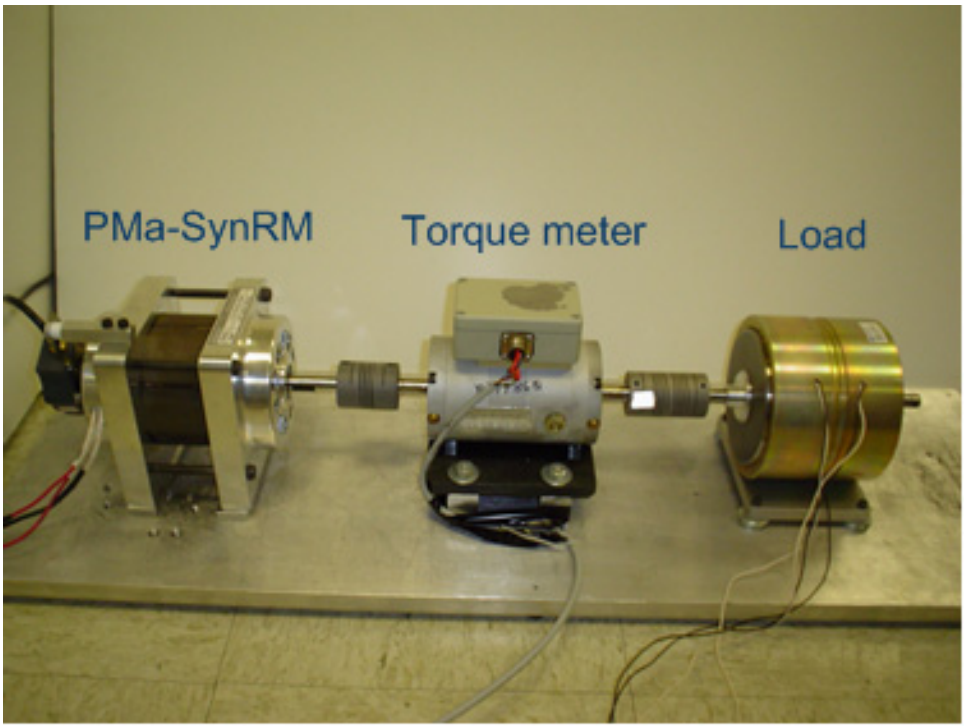

Figure 4- 11 Laboratory experimental setup.

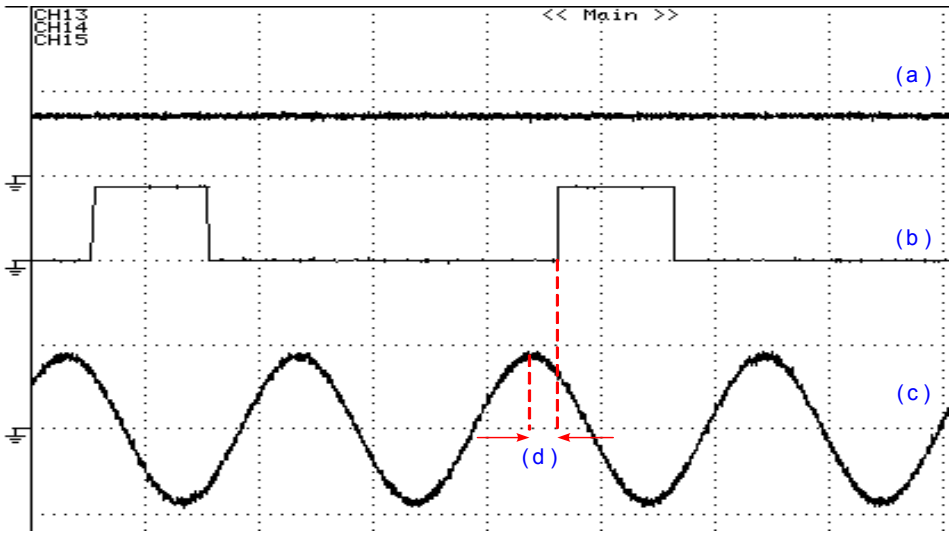

Figure 4- 12 Experimental results of conventional MTPA, a) measured output torque b) encoder pulse indicating rotor d-axis c) filtered current of phase A d) current phase angle (β).

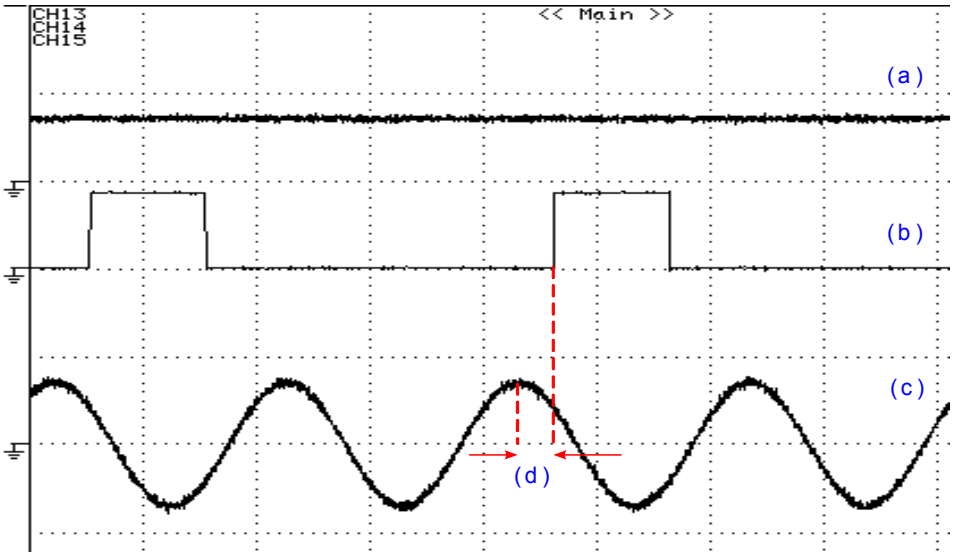

Figure 4- 13 Experimental results of proposed MTPA, a) measured output torque b) encoder pulse indicating rotor d-axis c) filtered current of phase A d) current phase angle (β).

F. CONCLUSION

To utilize the maximum efficiency of the motor and to implement a robust maximum torque per ampere control, knowledge of the motor parameters is necessary. In this chapter, a MTPA control strategy for PMa-SynRM was presented.

In this strategy a small amount of perturbation is added to the current phase angle reference for the purpose of maximizing the output torque. The output torque is calculated using the motor parameters and the measured stator currents.

This assures the robustness of the proposed controller against the variation of the load. The motor parameters are estimated through an on-line procedure. Therefore, calculated output torque is not affected by the effects of the saturation as well as variation of permanent magnets' flux due to the change of temperature. This feature assures the robustness of the MTPA controller against the variations of the motor parameters. Simulation and experimental results of the proposed technique validate the effectiveness of the proposed controller and prove the feasibility of the proposed method.

CHAPTER V

CONCLUSION AND EXTENSION

A. CONCLUSION

Recently, PM assisted SynRMs has been considered as an alternative drive in compare with the IPMs due to utilizing both the permanent magnet and the reluctance torque productions. Some drawbacks such as large d-axis current at high-speed during flux weakening region and the uncontrolled generator mode of operation following unexpected inverter shutdowns in IPMs can be eliminated in PMa-SynRMs. These problems are caused by the uncontrolled flux linkages produced by the permanent magnets in IPMs. The amount of magnets and the magnet flux linkages in PMa-SynRM are small in comparison with the conventional IPM and the reluctance torque has the most contribution in the developed torque. With respect to the conventional synchronous reluctance machine, this motor offers better torque capabilities and power factors.

To obtain a high performance drive, having an optimized motor is necessary. To achieve such this design, Chapter II studied various key points in the rotor design of a low cost permanent magnet assisted synchronous reluctance motor (PMa-SynRM). To optimize the motor design, a reasonably good magnetic design can be obtained without using numerical techniques. However, the finite-element method must be used to consider the nonlinear magnetic behaviors of the materials which play a key role whenever overload performance prediction is essential.

In chapter II, a FEM approach was performed to analyze the effects of rotor design variables such as the flux barrier width, flux barrier location, insulation ratio, pole span over pole pitch ratio, length of the radial and tangential ribs on SynRM performance. Effects of each variable were shown in the case of a four-pole transversally laminated SynRM. A systematic procedure was applied to obtain the optimized geometry for rotor flux barriers. Effects of the magnets on d-q inductances were studied and a comparison between output torque of SynRM and PMa-SynRM was performed. Some experimental results on a 1.5 kW prototype motor were presented to validate the results of simulation studies.

In the most control systems of synchronous reluctance motors, controllers are parameter dependent and their performances rely on the knowledge of motor parameters. For example, the motor operation at maximum torque per ampere or its speed sensorless operation could be considered as the parameter dependent control systems.

Majority of techniques for optimizing torque production are sensitive to machines parameters. Unfortunately, stator resistance and permanent magnet flux vary with motor temperature. The d and q axes total inductance, L_d and L_q, are known to depend on the airgap flux. So in practical applications, on-line parameter estimation for L_d and L_q, are required to achieve maximum torque-per-ampere control.

Performance of the advanced parameter dependent control strategies can be improved by using the off-line model of the motor parameters. However, this is computationally intensive because of the non-linearity due to iron saturation. Such

calculations are usually unreasonable in real time. Moreover, including cross saturation effect is very difficult and intensive in off-line parameter estimation.

In chapter III, a simple and practical method for parameter estimation of PMa-SynRM was introduced. This method is capable of identifying the d and q axes inductances and the permanent magnet back-EMF. Variation of the PMa-SynRM parameters was shown and a simple practical method for estimation of the motor parameters was presented. Simulation results of the proposed technique validate the effectiveness of the estimation method and the experimental results were presented to show the feasibility of the proposed method. This method can be used to improve the performance of some other control strategies which are dependent on the knowledge of the motor parameters.

Efficiency is always an important issue for a motor drive system. In the field-oriented control of synchronous reluctance motors, d- and q-axis components of the stator current vector applied to the motor are independently variable, and a specific torque at any motor speed can be achieved with a variety of different – current component combinations. Each – current component pairing defines a particular motor torque characteristic, but motor efficiency may vary widely. If the d-axis current is high, then core losses are large. If the d-axis current is reduced excessively, then motor currents and copper losses must increase. Consequently, there is an optimum current vector which gives a specified torque with maximum efficiency at every operating point.

Maximum torque per ampere controller, known as one of the high efficiency controllers, is parameter dependent and its performance relies on the knowledge of

motor parameters. Unfortunately, stator resistance and permanent magnet flux linkage vary with motor temperature. The d- and q-axes total inductances, L_{ds} and L_{qs}, are known to depend on the airgap flux. Ferrite, ceramic magnets and Neodymium-Iron-Boron (Nd-Fe-Br) materials are well known materials used in IPM motors. The flux density of the magnets changes significantly by variation of temperature. The variation of the flux density affects the d- and q-axes inductances and also directly affects the output torque.

For the practical realization of an efficiency-optimized synchronous reluctance motor drive, an optimum-efficiency controller may be accomplished with the aid of a loss model for the drive into which complete parameter values, including inductance saturation, coefficients of iron losses, temperature, and harmonic effects, must be programmed. At any operating point, the controller performs a computation on optimum efficiency operating conditions and adjusts one, or more, variables in the model until the optimum values are found. These optimized values then become the commanded values for the drive regulator. The effectiveness of this approach obviously depends on the accuracy of the model.

In case of using off-line models, the trajectory of reference currents can be obtained to implement maximum torque per ampere condition. However, this is computationally intensive because of the non-linearity due to iron saturation. Such calculations are usually unreasonable in real time. Moreover, including cross saturation effect is very difficult and intensive in off-line parameter estimation.

To utilize the maximum efficiency of the motor and to implement a robust maximum torque per ampere control, knowledge of the motor parameters is necessary. In chater IV, a MTPA control strategy for PMa-SynRM was presented.

In this strategy a small amount of perturbation is added to the current phase angle reference for the purpose of maximizing the output torque. The output torque is calculated using the motor parameters and the measured stator currents.

This assures the robustness of the proposed controller against the variation of the load. The motor parameters are estimated through an on-line procedure. Therefore, calculated output torque is not affected by the effects of the saturation as well as variation of permanent magnets' flux due to the change of temperature. This feature assures the robustness of the MTPA controller against the variations of the motor parameters. Simulation and experimental results of the proposed technique validate the effectiveness of the proposed controller and prove the feasibility of the proposed method.

B. SUGGESTIONS AND EXTENSIONS

A 2D finite element based design procedure was introduced in chapter II. This procedure was performed in order to optimize the PMa-SynRM rotor geometry. Implementation of the 3D FEM based design through the same procedure is proposed for the future work. In the presented work, effect of each parameter was study independent of the other existing parameters. Use of a design procedure which includes the mutual

effects of different parameters is suggested in order to achieve a global optimized rotor geometry.

To improve the efficiency of the drive, on-line identification of the motor parameters is necessary. In this work, based on the new model of the motor, a simple parameter estimator was introduced. In this estimator, transient response of the model has been ignored in order to achieve a simple estimator. Use of some advance estimator based on the introduced model of the motor is proposed for the future research. In these estimators, the transient response can be considered and therefore a faster estimation can be obtained.

Synchronous PI current regulators are commonly used for AC machines. When the AC machine model in the stationary frame is transformed into a synchronous frame, unwanted cross-coupling is produced. In order to decouple the cross-coupling, accurate parameter estimation is required. The inherent cross-coupling is a function of current, rotor velocity, and motor parameters, L_d and L_q, which vary with operating conditions due to magnetic saturation. A cross-coupling decoupling current regulator along with the introduced on-line parameter estimator is proposed for future work.

In case of using a fast parameter estimator, behavior of the current regulator can be more improved. Also some of model based sensorless algorithms rely on the knowledge of motor parameters. Performance study of the sensorless control of PMa-SynRM in presence of the parameter estimator is suggested for the future work.

REFERENCES

[1] J. K. Kostko, "Polyphase reaction synchronous motors," *J. Amer. Inst. Elec. Ing.*, vol. 42, pp. 1162–1168, Nov. 1923.

[2] R. E. Betz, "Control of synchronous reluctance machines," *Proc. IEEE-IAS Annual Meeting*, Detroit, pp. 456–462, Sept 1991.

[3] R. E. Betz, "Theoretical aspects of control of synchronous reluctance machines," *IEE Proceedings-B*, vol. 139, no. 4, pp. 355–364, 1992.

[4] A. Chiba and T. Fukao, "A closed-loop operation of super high-speed reluctance motor for quick torque response," *IEEE Transactions on Industry Applications*, vol. 28, no. 3, pp. 600–606, 1992.

[5] D. A. Staton, T. J. E. Miller, and S. E. Wood, "Maximizing the saliency ratio of the synchronous reluctance motor," *IEE Proceedings-B*, vol. 140, no. 4, pp. 249–259, 1993.

[6] T. Matsuo and T .A. Lipo, "Rotor design optimization of synchronous reluctance machine," *IEEE Transactions on Energy Conversion*, vol. 9, no. 2, pp. 359–365, 1994.

[7] T. A. Lipo, A. Vagati, L. Malesani, and T. Fukao, "Synchronous reluctance motors and drives-a new alternative," *IEEE-IAS Annual Meeting Tutorial*, October 1992.

[8] P. J. Lawrenson and L. A. Agu, "Theory and performance of polyphase reluctance machines," *IEE Proceedings*, vol. 111, no. 8, pp. 1435–1445, 1964.

[9] A. J. O. Cruickshank, A. F. Anderson, and R. W. Menzies, "Theory and performance of reluctance motors with axially laminated anisotropic rotors," *IEE Proceedings*, vol. 118, no. 7, pp. 887–894, 1971.

[10] V. B. Honsinger, "Steady-state performance of reluctance machines," *IEEE Transactions on Power Apparatus and Systems*, vol. PAS-90, no. 1, pp. 305–317, 1971.

[11] B. J. Chalmers and A. S. Mulki, "New reluctance motors with unlaminated rotors," *IEE Proceedings.* vol. 117, no. 12, pp. 2271–2272, 1970.

[12] B. J. Chalmers and A. S. Mulki, "Design and performance of reluctance motors with unlaminated rotors," *IEEE Transactions on Power Apparatus and Systems*, vol. PAS-91, pp. 1562–1569, 1972.

[13] W. Fong and J. S. C. Htsui, “New type of reluctance motor,” *IEE Proceedings*, vol. 117, no. 3, pp. 545–551, 1970.

[14] P. J. Lawrenson, “Two-speed operation of salient-pole reluctance machines,” *IEE Proceedings*, vol. 112, no. 12, pp. 2311–2316, 1965.

[15] W. Fong, “Change-speed reluctance motors,” *IEE Proceedings*, vol. 114, no. 6, pp. 797–801, 1967.

[16] S. A. Hassan, A. M. F. Osheiba, and A. L. Mohamadein, “Performance of different types of reluctance motors, experimental comparative study,” *Electric machines and Electromechanics*, no. 5, pp. 225–236, 1980.

[17] A.L.Mohamadein, Y.H.A.Rahim, and A.S.Al-Khalaf, “Steady-state performance of self-excited reluctance generators,” *IEE Proceedings*, Pt.B, vol. 137, no. 5, pp. 293–298, 1990.

[18] H. A. Toliyat, L. Xu, and T. A. Lipo, “A five-phase reluctance motor with high specific torque,” *IEEE Transactions on Industry Applications*, vol. 28, no. 3, pp. 659–667, 1992.

[19] T. Fukao, A. Chiba, and M. Matsui, “Test results on a super-high-speed amorphous iron reluctance motor,” *IEEE Transactions on Industry Applications*, vol. 25, no. 1, pp. 119–125, 1989.

[20] A. Chiba, F. Nakamura, T. Fukao, and M. A. Rahman, “Inductances of cageless reluctance-synchronous machines having nonsinusoidal space distributions,” *IEEE Transactions on Industry Applications*, vol. 27, no. 1, pp. 44–51, 1991.

[21] P.J.Lawrenson and L.A.Agu, “A new unexcited synchronous machine,” *IEE Proceedings*, vol. 110, no. 7, p. 1275, 1963.

[22] P. J. Lawrenson and L. A. Agu, “Low-inertia reluctance machines,” *IEE Proceedings*, vol. 111, no. 12, pp. 2017–2025, 1964.

[23] P. J. Lawrenson and S. K. Gupta, “Developments in the performance and theory of segmental-rotor reluctance motors,” *IEE Proceedings*, vol. 114, no. 5, pp. 645–653, 1967.

[24] P. J. Lawrenson, S. K. Gupta, and S. R. M. Vamaraju, “Multispeed performance of segmental-rotor reluctance machines,” *IEE Proceedings*, vol. 115, no. 5, pp. 695–702, 1968.

[25] P. J. Lawrenson and L. A. Agu, "Low-inertia reluctance machines," *IEE Proceedings*, vol. 111, no. 12, pp. 2017–2025, 1964.

[26] S. C. Rao, "Dynamic performance of reluctance motors with magnetically anisotropic rotors," *IEEE Transactions on Power Apparatus and Systems*, vol. PAS-95, no. 4, pp. 1369–1376, 1976.

[27] M. Ramamoorty and P. J. Rao, "Optimization of polyphase segmented rotor reluctance motor design: A nonlinear programming approach," *IEEE Transactions on Power Apparatus and Systems*, vol. PAS-98, no. 2, pp. 527–535, 1979.

[28] V. B. Honsinger, "The inductances L_d and L_q of reluctance machines," *IEEE Transactions on Power Apparatus and Systems*, vol. PAS-90, no. 1, pp. 298–304, 1971.

[29] V. B. Honsinger, "Inherently stable reluctance motors having improved performance," *IEEE Transactions on Power Apparatus and Systems*, vol. PAS-91, pp. 1544–1554, 1972.

[30] E. A. Klingshirn, "Dc standstill torque used to measure L_q of reluctance and synchronous machines," *IEEE Transactions on Power Apparatus and Systems*, vol. PAS-97, no. 5, pp. 1862–1869, 1978.

[31] P. Y. P. Wung and H. B. Puttgen, "Synchronous reluctance motor operating point dependent parameter determination," *IEEE Transactions on Industry Applications*, vol. 28, no. 2, pp. 358–363, 1992.

[32] M. J. Kamper and A. F. Volschenk, "Effect of rotor dimensions and cross magnetization on L_d and L_q inductances of reluctance synchronous machine with cageless flux barrier rotor," *IEE Proceedings on Electric Power Application*, vol. 141, no. 4, pp. 213–220, 1994.

[33] T. M. Jahns, G. B. Kliman, and T. W. Neumann, "Interior magnet synchronous motors for adjustable-speed drives," *IEEE Transactions on Industry Applications*, vol. 22, pp. 738–747, 1986.

[34] T. J. E. Miller, *Brushless permanent-magnet and reluctance motor drives*. New York: Oxford University Press, 1989.

[35] T. J. E. Miller, A. Hutton, C. Cossar, and D. A. Staton, "Design of a synchronous reluctance motor drive," *IEEE Transactions on Industry Applications*, vol. 27, no. 4, pp. 741–749, 1991.

[36] A. J. O. Cruickshank, R. W. Menzies, and A. F. Anderson, "Axially laminated anisotropic rotors for reluctance motors," *IEE Proceedings*, vol. 113, no. 12, pp. 2058–2060, 1966.

[37] R. W. Menzies, "Theory and operation of reluctance motors with magnetically anisotropic rotors i- analysis," *IEEE Transactions on Power Apparatus and Systems*, vol. PAS-91, pp. 35–41, 1972.

[38] R.W.Menzies, R.M.Mathur, and H.W.Lee, "Theory and operation of reluctance motors with magnetically anisotropic rotors ii - synchronous performance," *IEEE Transactions on Power Apparatus and Systems*, vol. PAS-91, pp. 42–45, 1972.

[39] I. Boldea, Z. X. Fu, and S. A. Nasar, "High-performance reluctance generator," *IEE Proceedings*, vol. 140, no. 2, pp. 124–130, 1993.

[40] D. Platt, "Reluctance motor with strong rotor anisotropy," *IEEE Transactions on Industry Applications*, vol. 28, no. 3, pp. 652–658, 1992.

[41] I. Boldea, N. Muntean, S. Deaconu, S. A. Nasar, and Z. Fu, "Distributed anisotropy rotor synchronous (darsyn) drives - motor identification and performance," *Proc. ICEM*, pp. 542–546, 1992.

[42] I. Boldea, Z. X. Fu, and S. A. Nasar, "Performance evaluation of axially-laminated anisotropic (ala) rotor reluctance synchronous motors," *IEEE Transactions on Industry Applications*, vol. 30, no. 4, pp. 977–985, 1994.

[43] W. L. Soong and T. J. E. Miller, "Field-weakening performance of brushless synchronous ac motor drives," *IEE Proceedings on Electric Power Application*, vol. 141, no. 6, pp. 331–340, 1994.

[44] W. L. Soong, D. A. Staton, and T. J. E. Miller, "Design of a new axially-laminated interior permanent magnet motor," *IEEE Transactions on Industry Applications*, vol. 31, no. 2, pp. 358–367, March/April 1995.

[45] B. K. Bose, *Power Electronics and AC Drives*. Upper Saddle River, New Jersey: Prentice-Hall, 1986.

[46] J. M. D. Murphy and F. G. Turnbull, *Power Electronic Control of AC Motors*. New York: Pergamon Press, 1988.

[47] W. Leonhard, *Control of Electrical Drives*. Berlin: Springer-Verlag, 1985.

[48] I. Boldea and S. A. Nasar, "Torque vector control (tvc) of axially-laminated anisotropic (ala) rotor reluctance synchronous motors," *Electric Machines and Power Systems*, vol. 19, pp. 381–398, 1991.

[49] R. Lagerquist, R. B. Betz, and T. J. E. Miller, "Dsp96002 based high performance digital vector controller for synchronous reluctance motors," Manchester: *ICEM Proceedings*, Sept 1992.

[50] L. Xu, X. Xu, T. A. Lipo, and D. W. Novotny, "Vector control of a synchronous reluctance motor including saturation and iron loss," *IEEE Transactions on Industry Applications*, vol. 27, no. 5, pp. 977–985, 1991.

[51] A. Fratta and A. Vagati, "A reluctance motor drive for high dynamic performance applications," *IEEE Transactions on Industry Applications*, vol. 28, no. 4, pp. 873–879, 1992.

[52] L. Xu and J. Yao, "A compensated vector control scheme of a synchronous reluctance motor including saturation and iron losses," *IEEE Transactions on Industry Applications*, vol. 28, no. 6, pp. 1330–1338, 1992.

[53] I. Boldea, N. Muntean, and S. A. Nasar, "Robust low-cost implementation of vector control for reluctance synchronous machines," *IEE Proceedings on Electric Power Application*, vol. 141, no. 1, pp. 1–6, 1994.

[54] K. Uezato, T. Senjyu, and Y. Tomori, "Modeling and vector control of synchronous reluctance motors including stator iron loss," *IEEE Transactions on Industry Applications*, vol. 30, no. 4, pp. 971–976, 1994.

[55] T. A. Lipo and P. C. Krause, "Stability analysis of a reluctance synchronous machine," *IEEE Trans.*, vol. PAS-86, pp. 825–834, 1967.

[56] P. J. Lawrenson and S. R. Bowes, "Stability of reluctance machines," *IEE Proceedings*, vol. 118, no. 2, pp. 356–369, 1971.

[57] A. Vagati, A. Canova, M. Chiampi, M. Pastorelli and M. Repetto, "Design refinement of synchronous reluctance motors through finite-element analysis," *IEEE Transactions on Industry Application*, vol. 36, no. 4, pp. 1094-1102, July/August 2000.

[58] C. E. G. Martins and P. Kuo-Peng, "Design of synchronous reluctance motor with flux barriers using 2D-FEM," *IEEE International Electric Machines and Drives Conference*, vol.3, pp. 1669-1674, June 2003.

[59] Jr. F. Reiter and T. Stuart, "Composite powder metal synchronous reluctance machine," *IEEE International Electric Machines and Drives Conference*, vol.3, pp. 523-527, June 2003.

[60] E. Schmidt and W. Brandl, "Comparative finite element analysis of synchronous reluctance machines with internal rotor flux barriers," *IEEE International Electric Machines and Drives Conference*, vol.3, pp. 831-837, 2001.

[61] A. Vagati, M. Pastorelli, F. Scapino, G. Franceschini, "Impact of cross saturation in synchronous reluctance motor of the transverse-laminated type," *IEEE Transactions on Industry Application*, vol. 36, no. 4, pp. 1039-1046, July/August 2000.

[62] J. H. Lee, J. C. Kim and D. S. Hyun, "Effect analysis of magnet on L_d and L_q inductance of permanent magnet assisted synchronous reluctance motor using finite element method," *IEEE Transactions on Magnetic*, vol. 35, no. 3, pp. 1199-1202, May 1999.

[63] S. Morimoto, M. Sanada, Y. Takeda, "Performance of PM assisted synchronous reluctance motor for high efficiency and wide constant power operation," *IEEE Transactions on Industry Applications,* vol. 37, no. 5, pp. 1234-1240, September/October 2001.

[64] I. Boldea, L. Tutelea, C. I. Pitic, "PM-Assisted reluctance synchronous motor/generator (PM-RSM) for mild hybrid vehicle: electromagnetic Design," *IEEE Transactions on Industry Application*, vol. 40, no. 2, pp. 492-498, March/April 2004.

[65] M. G. Jovanovic and R. Betz, "Maximum torque control of a sensorless synchronous reluctance motor drive," *IEEE Industry Application Society Conference*, Annual Meeting, vol. 1, pp. 637-644, October 1997.

[66] H. Kubota, K. Matsuse, T. Nakano, "DSP-based speed adaptive flux observer of induction motor", *IEEE Transactions on Industry Application*, vol. 29, no. 2, pp. 344-348, Mar./Apr. 1993.

[67] H. Sugimoto, S. Tamai, "Secondary resistance identification of an induction-motor applied model reference adaptive system and its characteristics", *IEEE Transactions on Industry Application*, vol. 23, no. 2, pp. 296-303, Mar./Apr. 1987.

[68] R.D. Lorenz, D.B. Lawson, "A simplified approach to continuous on-line tuning of field oriented induction machine drives", *IEEE Transactions on Industry Application*, vol. 26, no. 3, pp. 420-425, May/June 1990.

[69] P.Y. Chung, M. Dolen, H. Kim, R.D. Lorenz, "A continuous-time observer to estimate electrical parameters of induction machines", *Industry Application Society Conference*, pp. 259-265, September/October 2001.

[70] I. Boldea, *Reluctance Synchronous Machines and Drives*, Oxford: Clarendon Press, 1996.

[71] W. L. Soong, D.A. Staton and T. J. Miller, "Design of a new axially-laminated interior permanent magnet motor," *IEEE Transactions on Industry Application*, vol. 31, no. 2, pp. 358-367, March/April 1995.

[72] T.A. Lipo, A. Vagati, L. Malesani, and T. Fukao, "Synchronous reluctance motors and drives-a new alternative," *IEEE-IAS Annual Meeting Tutorial*, October 1992.

[73] A. Vegati, A. Canova, and M. Pastorelli, "Design and control of high performance synchronous reluctance motor with multiple flux-barrier rotor," *IPEC 2000*, Tokyo, Japan.

[74] M.G. Jovanovic, R.E. Betz, and D. Platt, "Sensorless vector controller for a synchronous reluctance motor," *IEEE Transactions on Industry Applications*, vol. 34, no. 2, March-April 1998.

[75] N. Bianchi, S. Bolognani, "Interior PM synchronous motor for high performance applications," *Proceedings of Power Conversion Conference*, vol. 1, pp. 148-153, April 2002.

[76] Maxwell, Electrical Engineering Simulation Software, Copyright 1984-2003, Ansoft Corporation, Four Station Square, Suite 200, Pittsburgh, PA 15219.

[77] Stratton, J. A., *Electromagnetic Theory*, New York: McGraw-Hill, 1941, pp. 131-132.

[78] Brauer, J. R., "Saturated magnetic energy functional for finite element analysis of electric machines," *IEEE Power Engineering Society Meeting*, January 1975.

[79] Desai, C. S. and J. F. Abel, *Introduction to the Finite Element Method*, New York: Van Nostrand Reinhold, 1972.

[80] J. R. Brauer, L. A. L. A. Larkin, B. E. MacNeal and J. J. Ruehl, "New nonlinear algorithms for finite element analysis of 2D and 3D magnetic fields," *Journal of Applied Physics*, Vol. 69, pp. 5044-5046, Apr. 1991.

[81] R. J. Brauer, "Improvements in finite element analysis of magnetic devices," *IEEE International Magnetics Conference*, Los Angeles, CA. 1977.

[82] T. Sebastian, "Temperature effects on torque production and efficiency of PM motors using NdFeB magnets", *IEEE Transactions on Industry Application*, vol. 31, pp. 353-357, March/April 1995.

[83] B. Sneyers, D. W. Novotny, T. A. Lipo, "Field-weakening in buried permanent magnet AC motor drives", *IEEE Transactions on Industry Application*, vol. IA-21, pp. 398-407, March/April 1991.

[84] Paul C. Krause, Oleg Wasynczuk, Scott D. Sudhoff, *Analysis of Electric Machinery*, New York: IEEE Press, 1995.

[86] H. Kim, R. D. Lorenz, "Using on-line parameter estimation to improve efficiency of IPM machine drives," *IEEE 33rd Annual of Power Electronics Specialists Conference*, vol. 2, pp. 23-27 June 2002.

[87] M. A. Rahman and M. A. Hoque, "On-line adaptive artificial neural network based vector control of permanent magnet synchronous motors," *IEEE Transactions on Energy Conversions*, vol. 13, no. 4, pp. 311–318, Dec. 1998.

[88] M. A. Rahman, D. M. Vilathgamuwa, M. N. Uddin, and K. J. Tseng, "Nonlinear control of interior permanent-magnet synchronous motor," *IEEE Transactions on Industry Applications*, vol. 39, no. 2, pp. 408–416, Mar./Apr. 2003.

[89] Y. Yi, D. M. Vilathgamuwa, and M. A. Rahman, "Implementation of an artificial-neural-network-based real-time adaptive controller for an interior permanent-magnet motor drive," *IEEE Transactions on Industry Applications*, vol. 39, no. 1, pp. 96–104, January/February 2003.

[90] T. M. Jahns, G. B. Kliman, and T. W. Neumann, "Interior permanent magnet synchronous motors for adjustable-speed drives," *IEEE Transactions on Industry Applications*, vol. 22, no. 4, pp. 738–747, July/August 1986.

[91] S. Morimoto, M. Sanada, and Y. Takeda, "Wide-speed operation of interior permanent magnet synchronous motors with high-performance current regulator," *IEEE Transactions on Industry Applications*, vol. 30, no. 4, pp. 920–926, July/August 1994.

[92] S. Morimoto, K. Hantanaka, Y. Tong, Y. Takeda, T. Hirasa, "Servo drive system and control characteristics of salient pole permanent magnet synchronous," *IEEE Transactions on Industry Applications*, vol. 29, pp. 338-343, March/April 1993.

VITA

Peyman Niazi received his B.S. degree in power engineering from Isfahan University of Technology, Isfahan, Iran, and his M.S. degree in control system engineering from Khaje Nassir Toosi (K. N. T.) University of Technology, Tehran, Iran, in 1996 and 1999, respectively. From September 1999 to August 2001, he was with the Niroo Research Institute (NRI), Tehran, Iran, as a research engineer and was involved with several national projects. On September 2001, he joined the doctoral program of the Department of Electrical and Computer Engineering at Texas A&M University and received his Ph.D. on December 2005. His research interests include analysis and design of the special electric machines, control system design, robust adjustable speed motor drives, power electronics and DSP applications. He can be reached c/o Prof. Hamid A. Toliyat, Advanced Electric Machines and Power Electronics Lab., Department of Electrical and Computer Engineering, Texas A&M University, College Station, Texas 77843 - 3128.